2014

AIR-SEA MOMENTUM FLUX IN A COUPLED OCEAN-WAVE MODEL AND ITS IMPACT ON THE OCEAN RESPONSE TO A HURRICANE

Colin J. Hughes
University of Rhode Island, colin_hughes@my.uri.edu

AIR-SEA MOMENTUM FLUX IN A COUPLED OCEAN-WAVE MODEL AND ITS IMPACT ON THE OCEAN RESPONSE TO A HURRICANE

BY

COLIN J. HUGHES

A THESIS SUBMITTED IN PARTIAL FULFILLMENT OF THE

REQUIREMENTS FOR THE DEGREE OF

MASTER OF SCIENCE

IN

PHYSICAL OCEANOGRAPHY

UNIVERSITY OF RHODE ISLAND

2014

MASTER OF SCIENCE THESIS

OF

COLIN J. HUGHES

APPROVED:

Thesis Committee:

Major Professor Isaac Ginis
Tetsu Hara
Alex Meyerovich
Nasser H. Zawia
DEAN OF THE GRADUATE SCHOOL

UNIVERSITY OF RHODE ISLAND

2014

ABSTRACT

The ocean temperature (especially the Sea Surface Temperature (SST)) is very important to the formation and development of tropical cyclones. Warm water from the sea surface evaporates and provides energy to drive hurricanes. As a tropical cyclone passes over the ocean, the SST behind it becomes significantly cooler than what it was prior to the hurricane's arrival. The surface temperature declines as a result of turbulent mixing as well as upwelling following a divergence of surface currents. This cooling (hereafter the "cold wake") is important to understand in order to develop better tropical cyclone models. The key to modeling this is the momentum flux budget at the air-sea interface.

Current models assume that the momentum flux into the ocean currents is equal to the wind stress. However, this does not take into account momentum lost to or gained from a growing or decaying surface wave field or from wave-induced Coriolis-Stokes forcing. This study seeks to develop a fully coupled ocean-wave model to enhance understanding of the air-sea momentum flux budget in tropical cyclones and as a result improve models of the cold wake. The ocean model component used is the Princeton Ocean Model (POM) with a 1/12 degree resolution and 23 half sigma levels. It calculates the ocean temperature and currents driven by a prescribed wind stress interpolated from hurricane message files generated by the National Hurricane Center. The wave model used is Wave Watch 3.14 and also has a 1/12 degree resolution. It uses a prescribed wind speed based on the same hurricane message file and calculates the momentum flux lost to or gained from a growing or decaying wave field and the momentum flux lost to or gained from Coriolis-Stokes forcing. In the coupled model, the ocean currents are used in the wind stress calculations and in the wave model component.

Results of idealized and real hurricane simulations demonstrate clearly that

the altered wind stress (by including the ocean current effect), wave momentum flux budget, and Coriolis-Stokes forcing significantly alter the momentum flux into the ocean currents and in turn the cold wake. While the wave momentum flux budget and reduced wind stress decrease the surface cooling, the Coriolis-Stokes forcing may lead to increased surface cooling. It is also shown that these three effects can alter the latent heat flux that fuels hurricanes.

ACKNOWLEDGMENTS

My research was funded by the State of Rhode Island through a State Assistantship and by NOAA as part of its Hurricane Forecast Improvement Program (HFIP).

First, I would like to express my appreciation and gratitude for my advisor Dr. Isaac Ginis for all of his help and support. Dr. Tetsu Hara's insight was crucial to the direction of my research. I would like to thank Dr. Alexander Meyerovich as well, who was also part of my thesis committee.

Also, I would like to thank other members of the Hurricane Modeling Group. I could never have gotten the Coupled Model off the ground without the help of Dr. Biju Thomas and Brandon Reichl. Michael Bueti and Dr. Richard Yablonsky also provided very helpful and timely technical assistance throughout the duration of my studies.

My parents helped me stay focused and kept my spirits high on difficult occasions. For this, I am extremely grateful.

TABLE OF CONTENTS

Page

LIST OF TABLES

LIST OF FIGURES

Figure **Page**

Figure **Page**

CHAPTER 1

Introduction

The ocean temperature is of critical importance to the formation and maintenance of hurricanes. This includes both the sea surface temperature (SST) and the upper mixed layer thickness. Following the passage of a hurricane over the ocean, there is a marked cooling in the SST known as the cold wake. The cold wake exists due to storm-induced turbulent mixing and upwelling.

Several numerical studies have shown that the air-sea momentum flux during hurricanes is very important to the SST response (Price, 1981; Ginis and Dikinov, 1989; Jacob et al., 2000; Morey et al., 2006; Fan et al., 2009). The NOAA operational Geophysical Fluid Dynamics Laboratory (GFDL) hurricane forecast system uses primitive equations and movable nested mesh grids to represent the interior structure of tropical cyclones (Kurihara et al., 1998). It is coupled to the Princeton Ocean Model (Bender et al., 2007). In the coupled system, wind stress, heat, moisture, and radiative fluxes are passed to the ocean model, which calculates the SST changes. The new SST is then used in the atmospheric model over the next time step. Another NOAA operational model, Hurricane Weather Research and Forecasting system (HWRF), became operational in 2007. It consists of WRF model software infrastructure, the Non-Hydrostatic Mesoscale Model (NMM) dynamic core, the Princeton Ocean Model (POM) as an ocean model, and the NCEP coupler (Tallapragada et al., 2013).

Neither one of these operational hurricane models is coupled to a wave model. Thus, they do not include explicitly the impact of waves on the air-sea momentum flux or on the ocean response and assume that the momentum flux into the ocean subsurface currents is equal to the wind stress. Waves affect the air-sea momentum

flux through wave breaking, sea spray, adjusting the albedo, increasing or decreasing momentum through a growing or decaying wave field and the Coriolis-Stokes force. This study seeks to investigate the role that two effects of waves on the air-sea momentum flux: 1) the growing/decaying wave field and 2) the Coriolis-Stokes forcing have on the air-sea momentum flux and the SST. The following questions are addressed: What is the relevant contribution of each of the two wave effects? Does either significantly alter the magnitude and spatial distribution of the SST in the cold wake? Does the translation speed of the tropical cyclone alter the impact of the waves on the air-sea momentum flux? How do ocean currents affect wave-related fluxes?

CHAPTER 2

Methodology

2.1 Wave Model

The coupled ocean-wave model used for this study consists of the Princeton Ocean Model (POM), and Wave Watch 3.14 (WWIII). Wave Watch 3.14, developed and operated by NOAA/NCEP, is used to calculate the wave field and wave-wave interactions and solves the spectral action density balance equation for wavenumber-direction spectra (Tolman, 2009):

$$\frac{\partial N}{\partial t} + \nabla_x \cdot [(\vec{U}_\lambda + \vec{C}_g)N] - \frac{\partial}{\partial k}(\vec{k} \cdot \frac{\partial \vec{U}_\lambda}{\partial s}N) + \frac{\partial}{\partial \theta}(\frac{1}{k}\vec{k} \cdot \frac{\partial \vec{U}_\lambda}{\partial m}N) = F \qquad (1)$$

where $N = \psi(k,\theta)/\omega$ is the wave action spectrum, $\psi(k,\theta)$ is the directional wave spectrum, $\vec{U}_\lambda$ are the currents at depth $L/(4 * \pi)$ (where L is the mean wavelength), $\vec{C}_g$ is the group velocity, $\vec{k}$ is the wavenumber vector, θ is the wave direction, s is a coordinate in the direction of the waves, m is a coordinate perpendicular to the waves, and F stands for all of the forcing terms. Note: the currents at depth ($\vec{U}_\lambda$) are not passed to the wave equation in every hurricane experiment. The impact of the ocean currents on the wave evolution will be investigated in special experiments described below.

The spectrum is discretized by wavenumber and wave direction and broken down into two parts: a peak frequency spectrum, and a spectral tail. The peak frequency spectrum is discretized using 40 frequencies from 0.0285 Hz to 1.1726 Hz and the spectral tail is an additional 22 frequencies from 1.2899 Hz to 9.5455 Hz where each frequency is calculated $f_{n+1} = 1.1 * f_n$. The wavenumbers are calculated from these intrinsic frequencies using the dispersion relationship for deep-water waves $\omega = \sqrt{gk}$ where $\omega = 2\pi f$. There are 24 different wave directions from 0 to 6.0214 radians with $\pi/2$ radian increments. The significant wave height

(H_s) is calculated by Wave Watch III and defined as:

$$H_s = 4\sqrt{E} = 4\sqrt{\iint \psi(f,\theta)\ \mathrm{d}\theta \mathrm{d}f} \tag{2}$$

where the relationship with the wave spectrum $\psi(k,\theta)$ is:

$$\psi(f,\theta) = \frac{\partial k}{\partial f}\psi(k,\theta) = \frac{2\pi}{c_g}\psi(k,\theta) \tag{3}$$

The wave model has a resolution of 1/12 degree and has meridional boundaries at 10 and 43 degrees North latitude. Its zonal range is from -108 to -60 degrees East longitude for the idealized hurricane experiments and -98 to -50 degrees East longitude for the real hurricane experiments. The idealized wave domain is on an f-plane centered at $22.4°N$, while the Coriolis parameter in the wave grid ($f = 2\Omega \sin\theta$) varies with latitude (θ) in the real hurricane experiments.

2.2 Ocean Model

The Princeton Ocean Model (POM) is a 3D, primitive equation, numerical ocean model that uses sigma and curvilinear orthogonal coordinates and an Arakawa C differencing scheme (Mellor, 2004). It consists of 23 different vertical half sigma levels that are fixed and extend from a depth of 2.5 m to 2500 m for the idealized hurricanes, but fluctuate with the bathymetry for the real hurricanes. POM is used to calculate the ocean temperature and current response to the momentum flux. It is initialized with a horizontally uniform ocean temperature and salinity as well as a vertical temperature profile based on Gulf of Mexico Common Water from the late summer or early autumn in the idealized hurricane experiments (Figure 1). For real hurricane experiments, the temperature and salinity vary with geography and there are background ocean currents including the Gulf Stream. The output ocean temperature and current response for real hurricanes are interpolated onto 23 defined half sigma levels extending from a depth of 5 m to 5500 m.

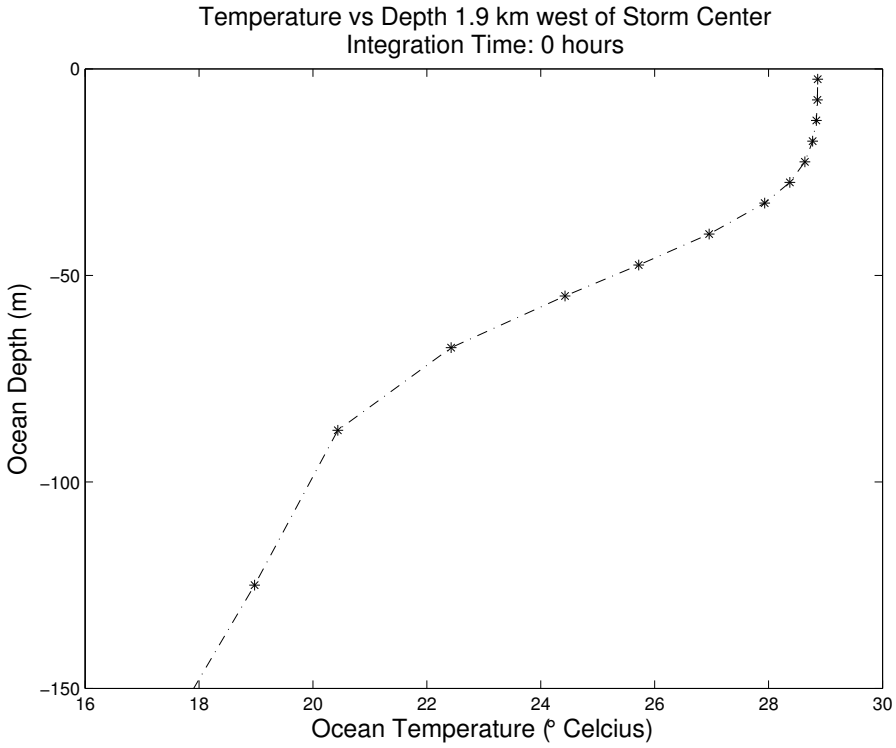

Figure 1: Initial vertical temperature profile in Princeton Ocean Model used in idealized hurricane experiments.

The ocean model resolution is nearly, but not exactly 1/12 degree. Its meridional domain ranges from 10 to 47.5 degrees North latitude, and its zonal domain ranges from -108.5 to -60 degrees East longitude for idealized hurricane experiments and -98.5 to -50 degrees East longitude for real hurricane experiments. As with the wave grid, the idealized ocean domain is on an f-plane centered at $22.4°N$, while the Coriolis parameter in the ocean grid ($f = 2\Omega \sin\theta$) varies with latitude (θ) in the real hurricane experiments.

2.3 Coupled Model

2.3.1 Air-Sea Momentum Flux

The coupled ocean-wave model is used to investigate the effect of waves during tropical cyclones via air-sea momentum flux calculations. There are different

momentum flux parameterizations available, including sea state dependent surface momentum flux parameterizations. In this study, we will use the theoretical framework described in (Fan et al., 2010). The momentum flux at the sea surface is expressed as

$$\vec{\tau}_c = \vec{\tau}_{air} - \vec{\tau}_{diff} - \vec{\tau}_{cor} \tag{4}$$

where $\vec{\tau}_{air}$ is the wind stress, $\vec{\tau}_c$ is the momentum flux into subsurface ocean currents, $\vec{\tau}_{diff}$ is the wave momentum flux budget and $\vec{\tau}_{cor}$ is the Coriolis-Stokes force, as described below.

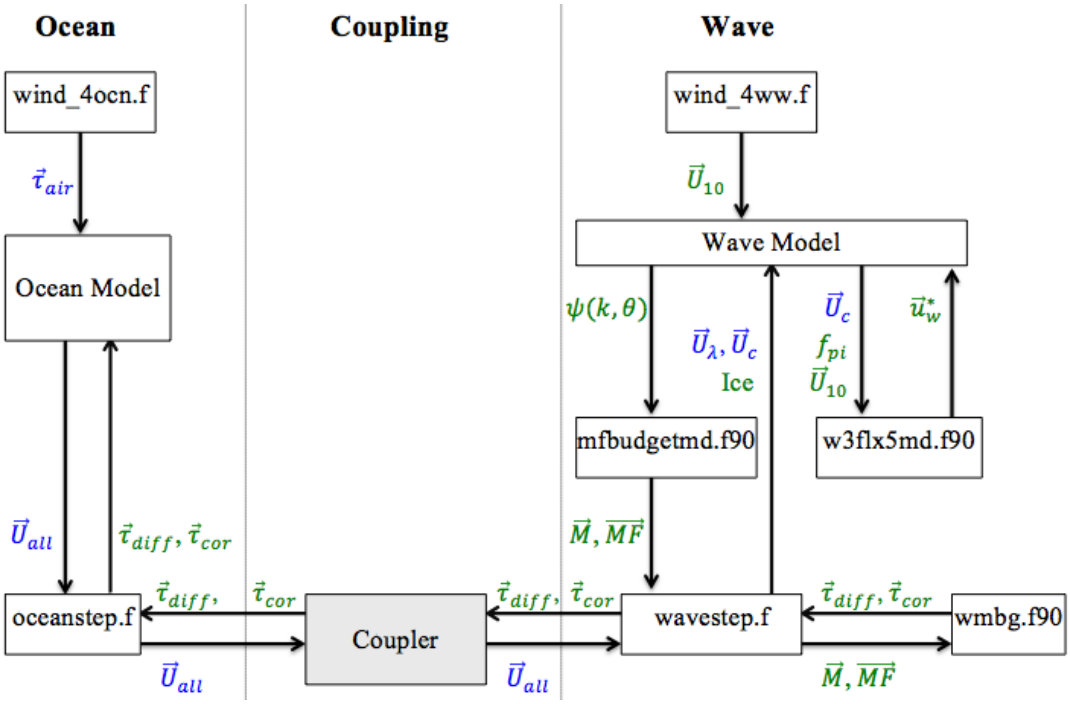

Figure 2: Diagram of the coupled ocean-wave model. Wind subroutines drive both models, with the ocean model requiring an input wind stress and the wave model requiring an input wind speed, blue font indicates ocean model variables, green font indicates wave model variables; Note: wind_4ocn.f and wind_4ww.f are the wind subroutines for the ocean and wave models respectfully, w3flx5md.f90 is a module that calculates the frictional velocity in the wave model, mfbudgetmf.f90 is a module that calculates the momentum budget and energy budget terms and wmbg.f90 is a module that calculates the momentum flux budget based on the local wave field using temporal and spatial derivatives

Table 1: Description of symbols in Figure 2.

Symbol	Explanation
$\vec{U}_{all}$	Ocean currents at all depths
$\vec{U}_c$	Surface ocean currents
$\vec{U}_\lambda$	Ocean currents at $z = L/(4 * \pi)$
$\vec{\tau}_{air}$	Wind stress
$\vec{\tau}_c$	Mom. flux into currents (calculated in ocean model)
$\psi(k, \theta)$	Wave spectrum
$\vec{U}_{10}$	Wind speed at 10 meter height
$\vec{\tau}_{diff}$	Momentum flux into wave field
$\vec{\tau}_{cor}$	Coriolis-Stokes forcing
$\vec{u}^*_w$	Friction velocity in the wave model
f_{pi}	Input peak frequency
$\vec{M}/\vec{MF}$	Total momentum/momentum flux in the wave field

Some of the momentum from the wind is lost to surface waves in the form of wave momentum when the wave field is not fully developed. Growing or decaying wave fields gain or lose momentum and thus lead to either more or less momentum reaching the subsurface currents than the wind stress (Fan et al., 2009). As tropical cyclones have very high winds and generate a complex wave field, it is necessary to account for both momentum changes in time and in spatial dimensions. In addition to the momentum from the air being lost due to a changing wave field, some momentum is also lost to the Coriolis-Stokes force. The Coriolis-Stokes force is a force in a rotating fluid due to the interaction of the Coriolis effect and Stokes drift.

The diagram of the interaction between POM and WWIII is shown in Figure 2. POM is driven by the momentum flux from the wind (or wind stress) ($\vec{\tau}_{air}$), which

can be modified by the surface ocean currents ($\vec{U}_c$):

$$\vec{\tau}_{air} = \rho_{air} C_D |\vec{U}_{10} - \vec{U}_c| * (\vec{U}_{10} - \vec{U}_c) \tag{5}$$

and WWIII is driven by the wind speed 10 meters above the ocean surface ($\vec{U}_{10}$) that can also be altered by the surface currents:

$$\vec{U}_{10} = \vec{U}_{10} - \vec{U}_c \tag{6}$$

As the two models fully interact with each other, the ocean currents are passed into the wave model and interact with the waves, and the two momentum flux components of the waves ($\vec{\tau}_{diff}$ and $\vec{\tau}_{cor}$) are passed into the ocean model.

The currents affect the coupled model in three different ways. In the first, they modify the wind stress driving the ocean model when wind speeds are calculated relative to current speeds. In another couple of affects, the currents are passed to the wave model. The surface currents also reduce the wind driving the wave model ($\vec{U}_{10}$) if they are in the same direction as the wind. They add to the wind forcing if they are in the opposite direction. Finally, currents at a depth of $L/(4 * \pi)$ are passed into the wave equation. Currents at a depth $L/(4 * \pi)$ are passed to the wave equation instead of surface currents because these currents modify the apparent phase speed of the wave train [please refer to (Fan et al., 2009) for a detailed explanation].

2.3.2 Wave Momentum Flux Budget

The wave momentum is decomposed into two horizontal components and is calculated from the directional wave spectrum $\psi(k, \theta)$ (Figure 3) where k is the wavenumber and θ is the wave direction.

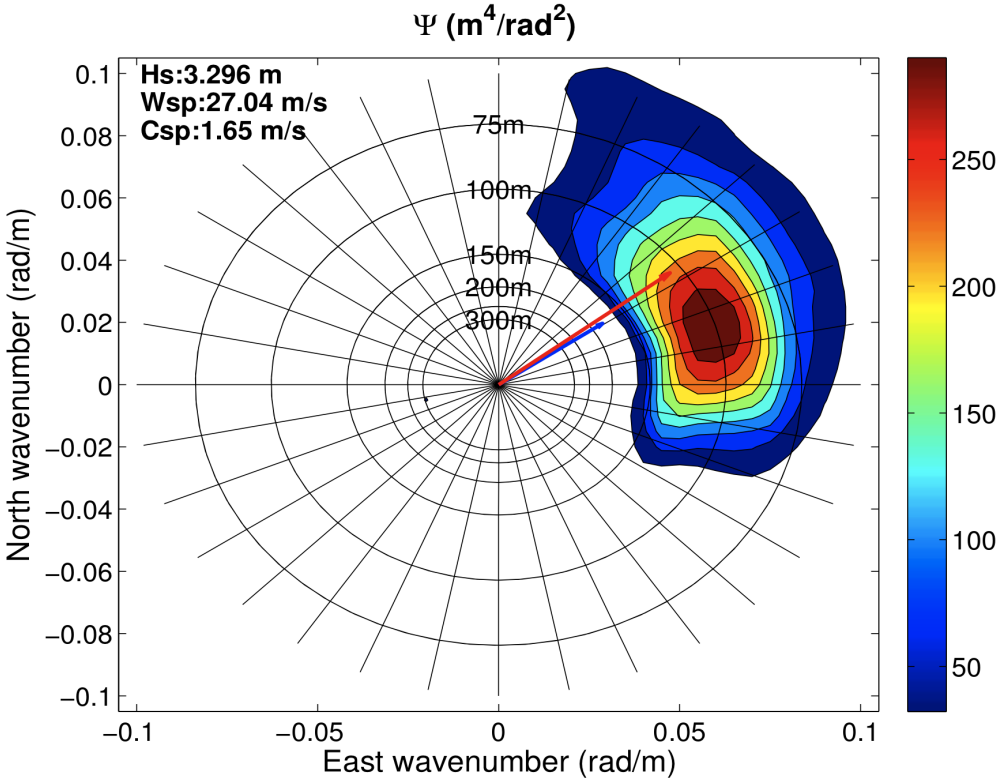

Figure 3: Example of the directional wave spectrum in a hurricane, based on a model simulation.

$$M_x = \iint \rho_w \psi(k,\theta) \cos\theta \sqrt{gk}\ \mathrm{d}\theta \mathrm{d}k \tag{7}$$

$$M_y = \iint \rho_w \psi(k,\theta) \sin\theta \sqrt{gk}\ \mathrm{d}\theta \mathrm{d}k \tag{8}$$

The horizontal fluxes of M_x and M_y are calculated:

$$MF_{xx} = \iint \rho_w \psi(k,\theta) C_g \cos^2\theta \sqrt{gk}\ \mathrm{d}\theta \mathrm{d}k \tag{9}$$

$$MF_{xy} = \iint \rho_w \psi(k,\theta) C_g \cos\theta \sin\theta \sqrt{gk}\ \mathrm{d}\theta \mathrm{d}k \tag{10}$$

$$MF_{yx} = \iint \rho_w \psi(k,\theta) C_g \sin\theta \cos\theta \sqrt{gk}\ \mathrm{d}\theta \mathrm{d}k \tag{11}$$

$$MF_{yy} = \iint \rho_w \psi(k,\theta) C_g \sin^2\theta \sqrt{gk}\ \mathrm{d}\theta \mathrm{d}k \tag{12}$$

where the x and y fluxes of M_x are MF_{xx} and MF_{xy} respectively, and the x and y fluxes of M_y are MF_{yx} and MF_{yy} respectively. Other terms included in the calculations are the angular velocity (which in deep water is $\omega = \sqrt{gk}$), the

density of water ρ_w, and for the momentum fluxes, the velocity with which the wave energy propagates (or group velocity $\vec{C}_g$). The momentum flux gained or lost by growing or decaying wave fields respectively is calculated:

$$\tau_{diff_x} = \frac{\partial M_x}{\partial t} + \frac{\partial MF_{xx}}{\partial x} + \frac{\partial MF_{xy}}{\partial y} \tag{13}$$

$$\tau_{diff_y} = \frac{\partial M_y}{\partial t} + \frac{\partial MF_{yx}}{\partial x} + \frac{\partial MF_{yy}}{\partial y} \tag{14}$$

where the first term is the local time derivative of momentum in waves, and the other two terms are the horizontal divergence of the horizontal momentum flux. This set of terms is referred to as $\vec{\tau}_{diff}$ because of the work of Fan et al. 2009 and Fan et al. 2010 where it described the difference between the wind stress $\vec{\tau}_{air}$ and the momentum flux into the currents $\vec{\tau}_c$.

2.3.3 Coriolis-Stokes Forcing

The Stokes drift is the average Lagrangian transport due to waves (Phillips, 1977; Polton et al., 2005). For instance, a particle floating at the free surface of water waves, experiences a net Stokes drift velocity in the direction of wave propagation. For an inviscid fluid in a rotating frame, there is no net mass transport from Stokes drift (Pollard, 1970), but for a fluid with viscosity of any size there is always a non-zero net mass transport (Hasselmann, 1970). The relationship between planetary vorticity and Stokes Drift results in a force present in the Eulerian Momentum balance $\vec{f} \times \vec{u}_s$ (Hasselmann, 1970) that Polton (2005) referred to as the Coriolis-Stokes force. Polton (2005) gave two different explanations of this. The first is that there is a vortex force on the flow resulting from the Stokes drift trying to tilt and stretch planetary vorticity in the horizontal. Another perspective he presents is the divergence of wave-induced stress. There are two components of the Eulerian velocity: mean velocity u and highly varying wave orbital velocity ũ. The Coriolis acceleration tilts the plane of the orbital ve-

locity along the wave crest direction (perpendicular to the wave direction), which introduces a new orbital component $\tilde{v}$ (also perpendicular to the wave direction). As this velocity is correlated with the vertical term $\tilde{w}$, there is a wave stress $\rho\tilde{v}\tilde{w}$ whose divergence is perpendicular to the wave direction (Figure 4).

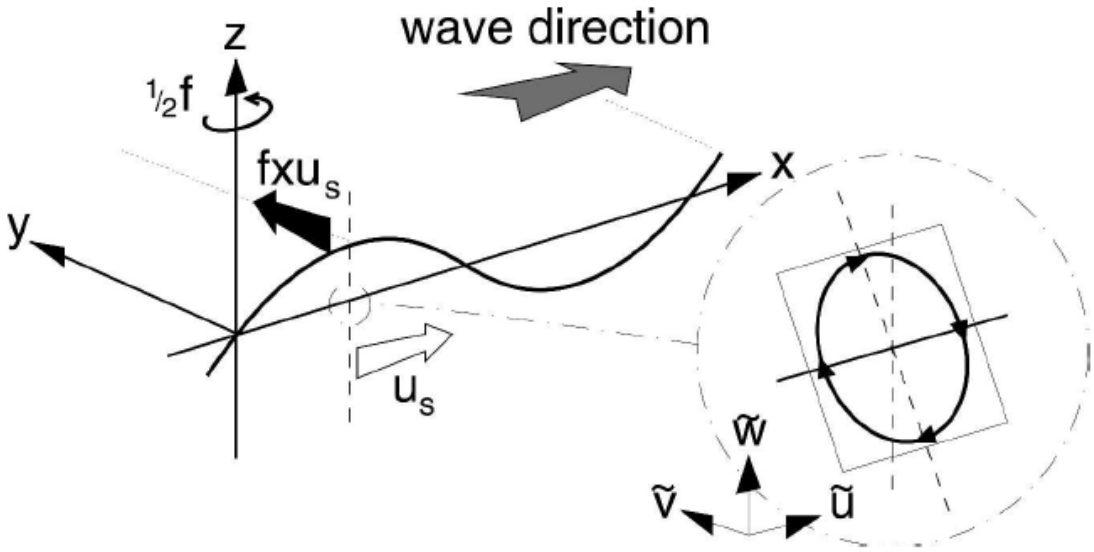

Figure 4: Schematic illustrating the orbital path for a particle under a wave is tilted, by planetary rotation, in the along-wave crest direction. The new $\tilde{v}$ component orbital velocity correlates with the $\tilde{w}$ component to produce a nonzero stress. The divergence of this stress can be written as (Hasselmann, 1970) $-\rho\vec{f}\times\vec{u}_s$ (Polton et al., 2005)

Stokes drift for a single wave is defined with a wavenumber k, wave amplitude a, and phase speed c as:

$$u_s = c(ak)^2 \; e^{2kz} \tag{15}$$

and the Coriolis-Stokes forcing is calculated as (Polton et al., 2005):

$$\vec{\tau}_w(0) = -\int_{-\infty}^{0} \rho_w \vec{f} \times \vec{u}_s \mathrm{d}z \tag{16}$$

Since the Coriolis-Stokes force is subtracted from the wind stress ($\vec{\tau}_{air}$) to get the momentum flux into the ocean currents ($\vec{\tau}_c$), it is defined in this paper as a negative version of what Polton has:

$$\vec{\tau}_{cor} = -\vec{\tau}_w(0) = \int_{-\infty}^{0} \rho_w \vec{f} \times \vec{u}_s \mathrm{d}z \tag{17}$$

Substituting the Stokes Drift (equation 15) and the phase speed $c = \omega/k$ along with the dispersion relation $\omega = \sqrt{gk}$ into equation 17 yields:

$$\vec{\tau}_{cor} = \rho_w \vec{f} \times \int_{-\infty}^{0} a^2 k \sqrt{gk} e^{2kz} \mathrm{d}z = -\rho_w \vec{f} \times a^2 \sqrt{g} \int_{-\infty}^{0} k^{3/2} e^{2kz} \mathrm{d}z \tag{18}$$

Integrating equation 18 gives an equation for the Coriolis-Stokes forcing for a single wave:

$$\vec{\tau}_{cor} = \vec{f} \times \frac{1}{2} a^2 \rho_w \sqrt{gk} \tag{19}$$

For a wave field, the mean square displacement $\overline{\zeta^2}$ is equal to the integrated wave spectrum:

$$\overline{\zeta^2} = \frac{1}{2} \, |a^2| \tag{20}$$

$$\frac{1}{2} \, |a^2| = \iint \psi(k, \theta) \, \mathrm{d}\theta \mathrm{d}k \tag{21}$$

$$\overline{\zeta^2} = \iint \psi(k, \theta) \, \mathrm{d}\theta \mathrm{d}k \tag{22}$$

Substituting for the mean square displacement (equation 21) into the defined Coriolis-Stokes (equation 19) forcing leaves:

$$\vec{\tau}_{cor} = \vec{f} \times \iint \rho_w \psi(k, \theta) \sqrt{gk} \, \mathrm{d}\theta \mathrm{d}k \tag{23}$$

The vertically integrated Stokes Drift is the same as the wave momentum:

$$\vec{M} = \iint \rho_w \psi(k, \theta) \sqrt{gk} \, \mathrm{d}\theta \mathrm{d}k \tag{24}$$

Thus, the Coriolis-Stokes forcing can be defined in terms of the wave momentum:

$$\vec{\tau}_{cor} = \vec{f} \times \vec{M} \tag{25}$$

The Coriolis-Stokes forcing can then be broken down into x and y components:

$$\tau_{cor_x} = -f * M_y \tag{26}$$

$$\tau_{cor_y} = f * M_x \tag{27}$$

2.3.4 Hurricane Wind Specification

For the idealized hurricanes, the axisymmetric wind field distribution is based on the wind field derived from an analytic Holland profile (Holland, 1980), with a central pressure of 950 hPa, environmental pressure of 1013 hPa, maximum wind speed (MWS) of 45 m/s, radius of maximum wind (RMW) of 70 km, air density of 1.28 kg/m^3, and exponential decay parameter (B) defined as $V_m^2 e\rho_a/(p_n - p_c)$, where $e = 2.718$. For moving idealized experiments, $\vec{U}_T/2$, is added to the axisymmetric wind, where $\vec{U}_T$ is the hurricane translation speed vector.

For real hurricane simulations, the wind field is specified based the NCEP Tropical Cyclone Vitals Database (TCVitals) provided at 6-hour increments. The wind field is angular dependent and calculated using the RMW, MWS, and the radii at which the sustained winds reach 18 m/s (R_{18}) and 26 m/s (R_{26}) in all four quadrants of the storm (Moon et al., 2003). For more details on the TCVitals for Hurricane Irene (2011) please refer to Chapter 4, and for Hurricane Sandy (2012) please refer to Chapter 5.

2.3.5 Experimental Design

Our experiments are designed to investigate the importance of each term in the momentum flux budget in real hurricane cases in addition to the idealized ones. The experiments are described in Table 2. In the control case, the momentum flux into the ocean currents is equal to the wind stress: $\vec{\tau}_c = \vec{\tau}_{air}$. The fully coupled case includes all momentum flux components: ($\vec{\tau}_c = \vec{\tau}_{air} - \vec{\tau}_{diff} - \vec{\tau}_{cor}$). Other experiments exclude the Coriolis-Stokes term ($\vec{\tau}_{cor}$), the wave momentum term ($\vec{\tau}_{diff}$) only, or both. Another model experiment includes all of the terms ($\vec{\tau}_c = \vec{\tau}_{air} - \vec{\tau}_{diff} - \vec{\tau}_{cor}$), but does not pass the ocean currents to the wave model.

While the ocean model runs over its entire domain, the wave model runs with a 6 by 6 degree grid around the storm center and ice covering the remaining

domain for the moving hurricanes because of computational limitations, including a tendency of Wave Watch III to produce a wave field with an unrealistic "sprinkler" effect after a larger distance from the storm center. The "sprinkler" effect refers to a computational wave field with uneven regions with many local minima and maxima when in reality the wave field should be continuous.

Table 2: Description of hurricane coupled model experiments.

Experiment	Explanation
1	$(\vec{\tau}_c = \vec{\tau}_{air})$ Control
2	$(\vec{\tau}_c = \vec{\tau}_{air})$ Wind stress forcing ocean model modified by surface currents
3	$(\vec{\tau}_c = \vec{\tau}_{air})$ Currents $z = (L/(4 * \pi))$ passed to wave equation
4	$(\vec{\tau}_c = \vec{\tau}_{air})$ Wind forcing wave model modified by surface currents
5	$(\vec{\tau}_c = \vec{\tau}_{air})$ Combination of 3 and 4
6	$(\vec{\tau}_c = \vec{\tau}_{air})$ Combination of 2 and 5
7	$(\vec{\tau}_c = \vec{\tau}_{air} - \vec{\tau}_{diff})$ Currents not passed to wave model or to wind stress forcing ocean model
8	$(\vec{\tau}_c = \vec{\tau}_{air} - \vec{\tau}_{cor})$ Currents not passed to wave model or to wind stress forcing ocean model
9	$(\vec{\tau}_c = \vec{\tau}_{air} - \vec{\tau}_{diff} - \vec{\tau}_{cor})$ Currents not passed to wave model or to wind stress forcing ocean model
10	$(\vec{\tau}_c = \vec{\tau}_{air} - \vec{\tau}_{diff} - \vec{\tau}_{cor})$ Fully Coupled

An important part of the study is the analysis of the different experiments. This entails comparing the momentum flux into the currents for different experiments, as well as the SST and current comparisons. It also involves examining both idealized hurricanes and real hurricane cases.

CHAPTER 3

Idealized Experiments

Three different sets of idealized hurricane experiments driven by wind based on the Holland wind model are examined. The first is an axisymmetric, stationary hurricane. In the other two, the hurricane moves westward along a constant latitude at different translation speeds (4.8 m/s and 9.6 m/s). In all of these experiments, the hurricane has tangential wind with no inflow angle, a maximum wind speed (MWS) = 45 m/s and a radius of maximum wind (RMW) = 70 km.

3.1 Stationary Hurricane

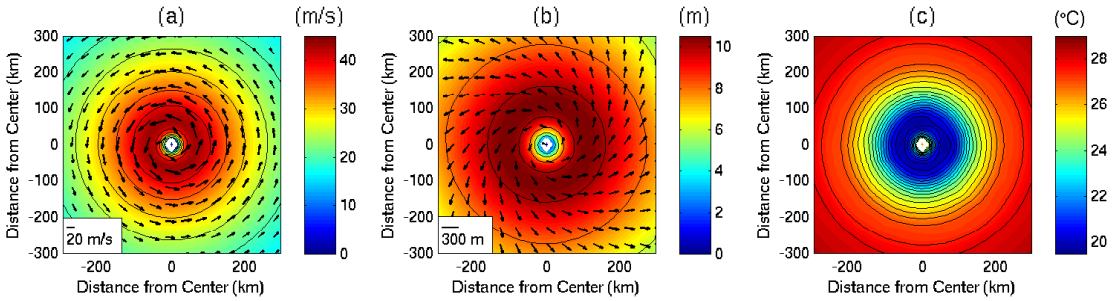

Figure 5: (a) Axisymmetric wind field (contours every 5 m/s), (b) significant wave height (contours every 2 m), (c) SST (contours every 0.5°C) for the stationary hurricane Control Experiment after 24 hours

Each of the stationary hurricane experiments has an axisymmetric wind, wave field, and temperature distribution similar to that of the Control Experiment 1 seen in Figure 5. We will thus review the results of these experiments along the radial direction only.

The significant wave height (H_s), surface currents ($\vec{U}_c$), change in sea surface temperature (δSST), and momentum flux into the ocean ($\vec{\tau}_c$) are compared to evaluate the impact of different effects on the coupled model. Only the experiments in which either the ocean currents at a depth of $L/(4 * \pi)$ are passed to the wave

equation and/or the wind ($\vec{U}_{10}$) is modified by the surface currents is there a reduced significant wave height (H_s) (Figure 6a).

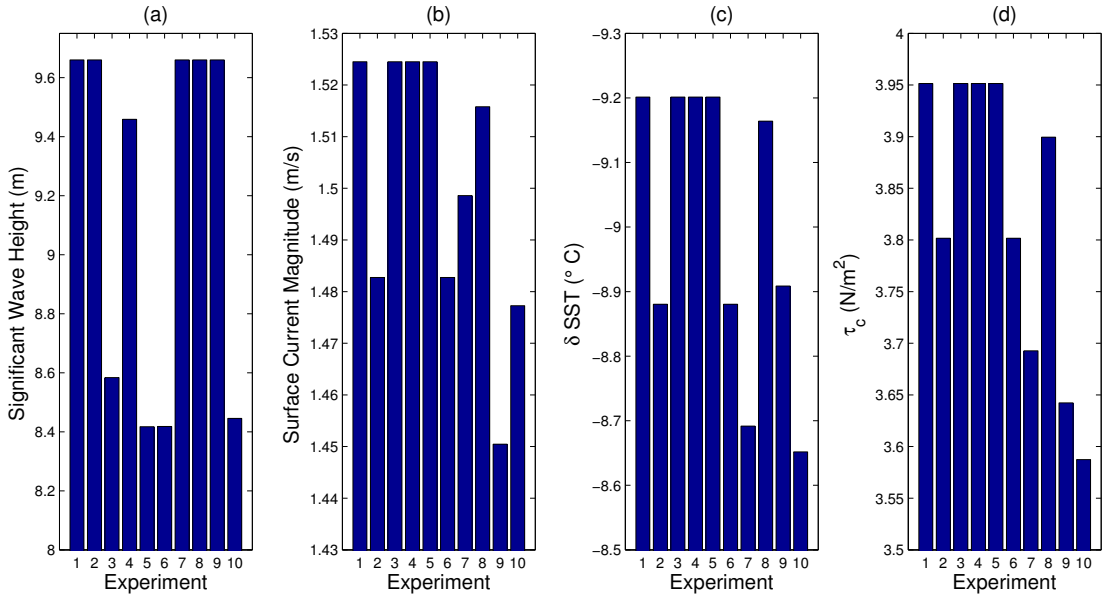

Figure 6: Results for the stationary axisymmetric hurricane near the radius of maximum wind (RMW) after 24 hours: (a) significant wave height (m), (b) surface current magnitude (m/s), (c) change in sea surface temperature ($^{\circ}C$), (d) magnitude of the momentum flux into the ocean (N/m^2)

Experiments 5 and 6 are not substantially different from Experiment 3 or Experiment 10. Experiment 4 also has a reduced significant wave height (H_s), but the remaining sensitivity experiments are consistent with the control experiment (Figure 6a). Thus, the radial plots shown in Figure 7 focus on Experiments 1, 3, 4, and 10.

The significant wave height is reduced between 0 and 3 RMW, but the reduction is most obvious after the wave height stops increasing exponentially and before the wave height decreases (between 0.5-2.0 RMW) (Figure 7). Passing currents at depth to the wave equation reduces the significant wave height more than reducing the wind forcing with the surface currents. This is not surprising given the relatively strong wind forcing (maximum wind speed: 45 m/s).

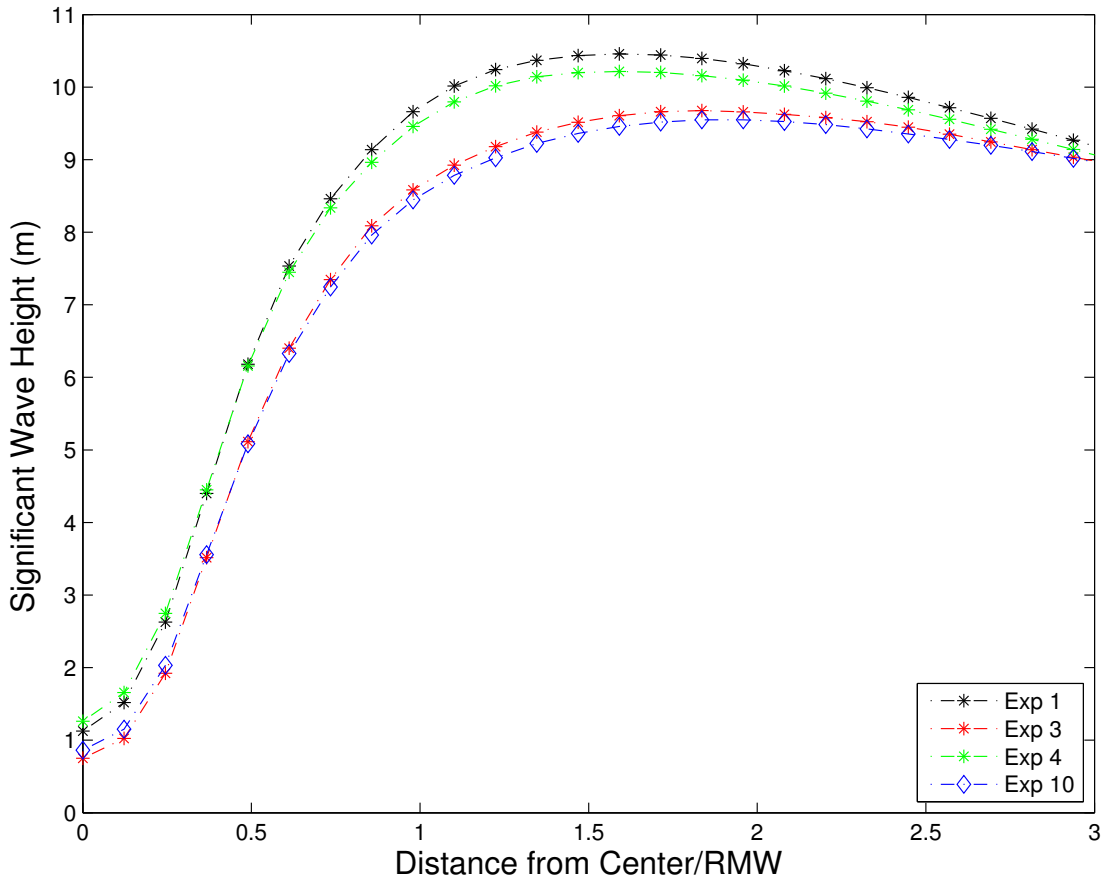

Figure 7: Significant wave height (m) for the stationary axisymmetric hurricane after 24 hours

For the stationary hurricane, Experiment 3 is more important to the significant wave height than Experiment 4. The combined effect (seen in the fully coupled Experiment 10) is much more similar to Experiment 3 than to Experiment 4 (Figure 7).

The individual components from the sensitivity experiments that alter the cooling from the control experiment are: the surface current is subtracted from the wind in the wind stress calculation ($\vec{U}_c$ to $\vec{\tau}_{air}$), the wave momentum flux budget is subtracted from the wind stress in the calculation of the momentum flux into the ocean, and the Coriolis-Stokes forcing is subtracted from the wind stress in the calculation of the momentum flux into the ocean (Figure 8a). Experiment 9 clearly

differs from Experiments 7 and 8 as well as the Fully Coupled Experiment 10. It reduces the cooling less than Experiments 7 and 10, but more than Experiment 8. Passing the ocean currents to the wave model has no effect on the cooling if that is not combined with a modification of the momentum flux into the currents through either adjusting the wind stress or including one or both of the wave momentum terms in the $\vec{\tau}_c$ calculation.

In contrast to the wave field (Figure 7), the changes in the SST anomalies (δSST) are sensitive to the changes of the surface currents and momentum fluxes into the ocean (Figure 8 a, b, and c).

A key aspect of cooling relates to the ocean currents. As surface currents increase in magnitude, vertical current shear also increases. This gives rise to turbulent mixing, which in turn leads to an entrainment of cooler water to the ocean surface that simultaneously increases the subsurface ocean temperature. In the experiments in which the ocean currents are the same as the control experiment, the SST is the same (Figure 6 b and c). However, when the ocean currents are modified (Figure 8b), the change in SST over the 24-hour integration time is different from the control experiment (Figure 8a). Of the individual components, the Coriolis-Stokes forcing modifies the currents over the largest area, but the wave momentum flux budget reduces the currents by the largest magnitude. These differences can be explained as follows. The Coriolis-Stokes forcing shifts the current direction to the right (in the same direction as the Coriolis force) while the wave momentum flux budget has a larger impact on the current magnitude. Another reason is that $\vec{\tau}_{diff}$ is large but more concentrated because the wave field grows or decays the most close to the RMW, while $\vec{\tau}_{cor}$ more closely follows the overall wave field (thus having a broader impact but a smaller maximum magnitude).

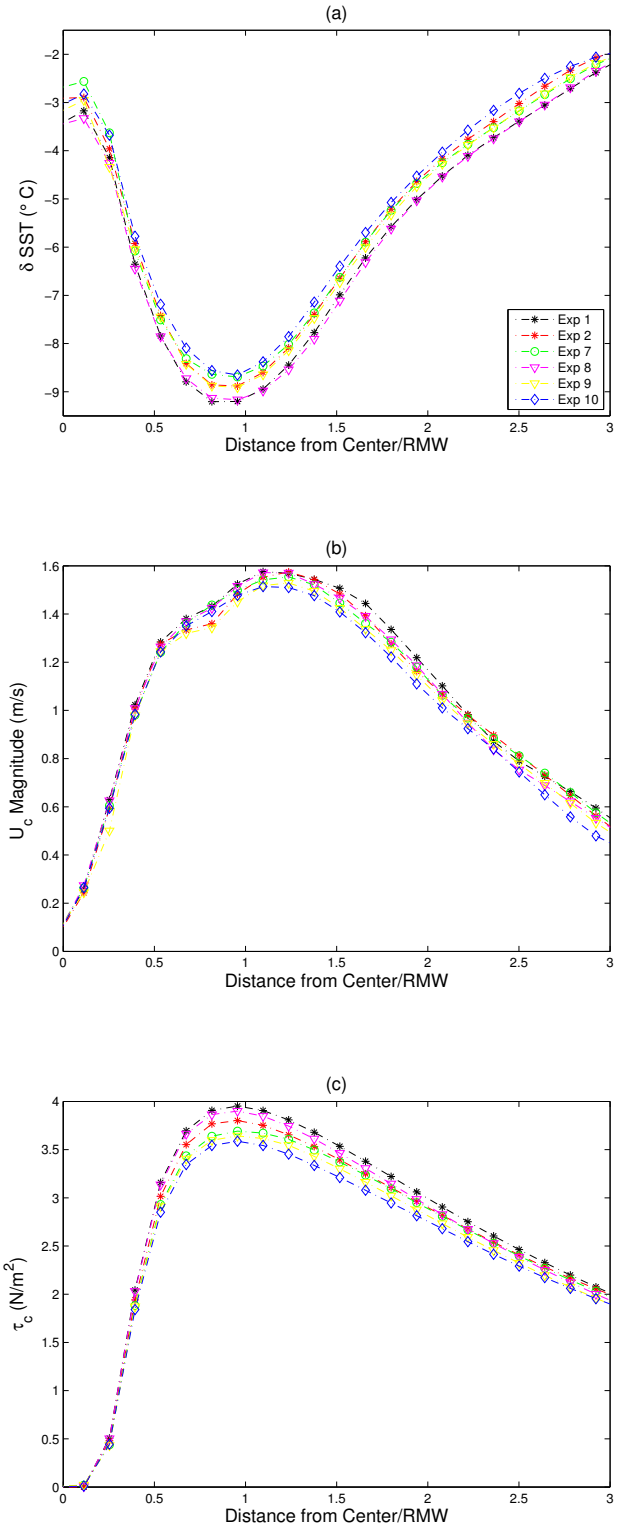

Figure 8: Results for the stationary hurricane after 24 hours: (a) δSST ($^{\circ}C$), (b) surface current magnitude ($\vec{U}_c$) (m/s), (c) magnitude of momentum flux into ocean ($|\vec{\tau}_c|$) (N/m^2)

Near the radius of maximum wind (RMW), Experiment 7 reduces the cooling more than Experiments 2 and 8 do (Figure 6c) and (Figure 8a). However, Experiment 2 reduces the cooling over the largest area. This is reflected in the momentum flux into the ocean currents ($\vec{\tau}_c$) (Figure 8c). Experiment 7 reduces the momentum flux into the ocean currents ($\vec{\tau}_c$) more than Experiments 2 or 8 do near the RMW, but the difference is much smaller close to the storm center and even farther away from it. Including the Coriolis-Stokes forcing ($\vec{\tau}_{cor}$) in the calculation of the momentum flux into the ocean ($\vec{\tau}_c = \vec{\tau}_{air} - \vec{\tau}_{cor}$) leads to the cooling actually increasing in some areas despite a reduction in magnitude of the momentum flux into the currents. This result can be explained as follows. In addition to turbulent mixing, the hurricane generates upwelling (upward advection of colder thermocline water) near the storm center, which is caused by the divergence of the ocean currents in the upper ocean. This upwelling leads to an increase of the turbulent mixing and the SST cooling (Price, 1981; Yablonsky and Ginis, 2009). Since the Coriolis-Stokes forcing shifts the currents to the right, it enhances the current divergence and upwelling (Figure 9). As a result, the SST cooling is increased.

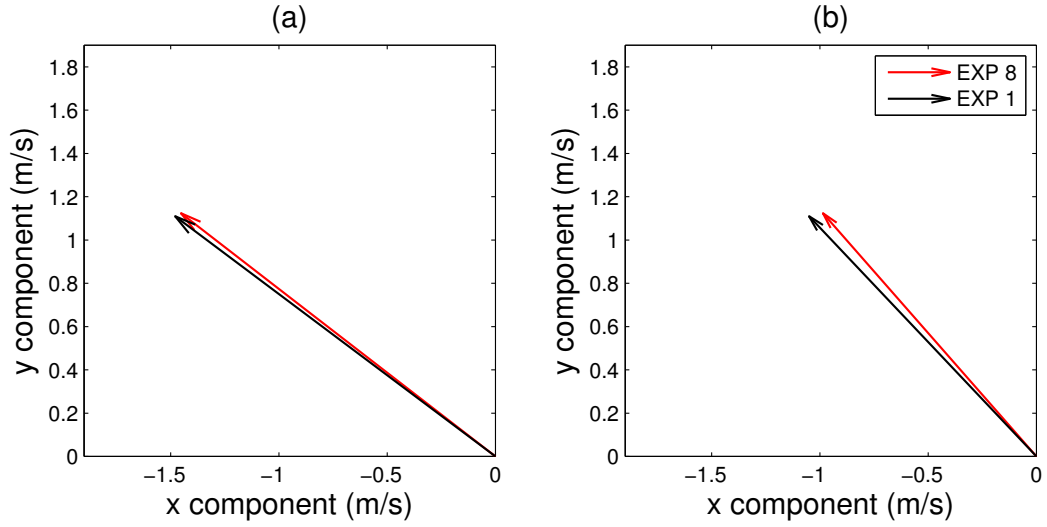

Figure 9: Surface current vectors (m/s) after (a) 6 hours and (b) 24 hours for a stationary, axisymmetric TC 1.93 km west of and 101.1 km north of storm center

Near the RMW and close to the storm center, the cooling in Experiment 10 is very similar to that of Experiment 7 (Figure 8a). However, as the distance from the eye increases, Experiment 10 clearly has less cooling than the other experiments until it converges with Experiment 2 (around 3 RMW). This is somewhat consistent with the momentum flux into the ocean currents for Experiment 10 (Figure 8c). While the momentum flux into the ocean currents ($\vec{\tau}_c$) is smallest in Experiment 10 along almost the entire radial profile, the difference between it and the other experiments is more pronounced between (0.5 and 2 RMW). Between 1.5 and 2 RMW, Experiment 1 clearly has the largest surface current magnitude. The Experiment 9 momentum flux into the ocean profile resembles a combined effect of the two individual wave momentum components of Experiments 7 and 8 (Figure 8c). In fact, the difference between Experiments 7 and 9 is similar to the difference between Experiment 8 and Control Experiment 1. However, the Experiment 9 δSST profile resembles an average between Experiments 7 and 8 (Figure 8a). The Experiment 8 δSST radial profile is also closer to the Control Experiment 1 profile than any other sensitivity experiment is. However, it is not identical and the cooling actually slightly increases due to the Coriolis-Stokes forcing.

3.2 Moving Hurricane

Two sets of idealized moving hurricane experiments were conducted. In both, the hurricane moved along a constant latitude of $22.4°N$ with a constant translation speed ($4.8\ m/s$ and $9.6\ m/s$) to the west. This led to larger significant wave heights, as well as larger differences between the various momentum budget experiments and the control experiment (Figures 13 and 15) compared to the stationary hurricane experiments.

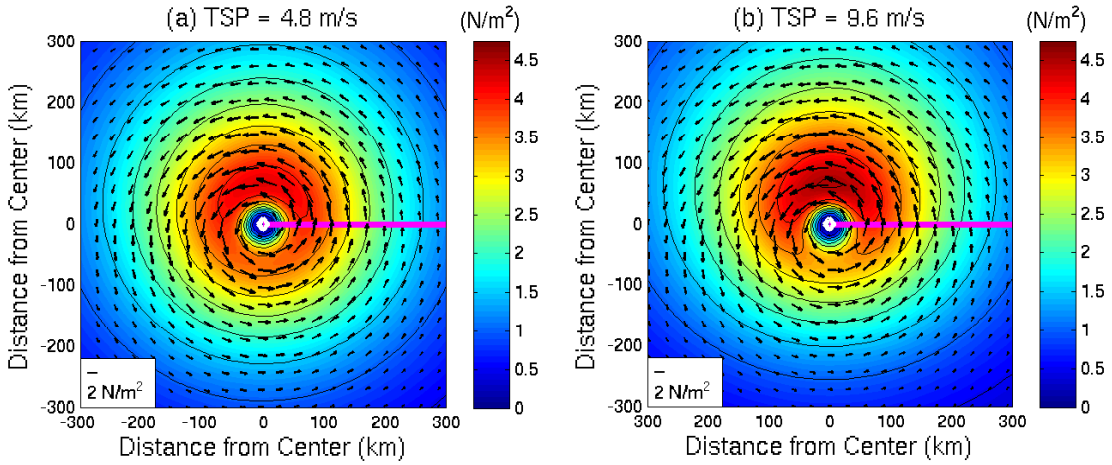

Figure 10: Control Experiment momentum flux into the ocean ($\vec{\tau_c}$) (contours every 0.5 N/m^2) after 72 hours for moving TC with TSP= (a) 4.8 m/s and (b) 9.6 m/s;

The momentum flux into the ocean for the control experiments is simply the wind stress. It is continuous and larger to the right of the storm track due to the translation speed being in the same direction there (Figure 10). Differences between the momentum flux into the ocean for each experiment and the Control Experiment 1 also are continuous (Figure 11). Experiment 7 and Experiment 8 both alter the wind stress by a greater vector magnitude difference than Experiment 2. However, Experiment 7 modifies the vector flux into the ocean over the smallest geographic range. The 9.6 m/s version of Experiment 7 differs from the other individual component sensitivity experiments in that it has a second region with an altered flux into the ocean in the left rear quadrant that is reflected in Experiment 9 and in the fully coupled Experiment 10.

Experiment 2 reduces the air-sea momentum flux to the right of the storm track for both moving idealized tropical cyclones, although the magnitude and range of the reduction are both smaller for the 4.8 m/s translating hurricane than its 9.6 m/s counterpart (Figure 12 a and b). The air-sea momentum flux is reduced by a larger magnitude during Experiment 7 than Experiment 2, but the reduction is confined to a smaller region (Figure 12 c and d). For the 4.8 m/s translating

hurricane, this change is mostly confined to the rear right quadrant, but not far from the storm center. However, for the 9.6 m/s translating hurricane, one region of smaller momentum flux is located just inside of the front right quadrant, while there is a second region of reduction to the left of the storm track. Experiment 8 actually increases the air-sea momentum flux, but in the rear right quadrant, but slightly reduces it in the front left quadrant (Figure 12 e and f). The two different versions of Experiment 9 vary considerably: the 4.8 m/s momentum flux is reduced to the right of the storm track and slightly more behind than even with the storm center, but the 9.6 m/s momentum flux is reduced more in front of the storm, while it is increased in the rear right quadrant (Figure 12 g and h). Experiment 10 leads to values of $|\vec{\tau_c}|$ differing the most from the control for both hurricanes, and the same discrepancies between the 4.8 and 9.6 m/s hurricanes, except there is no increased flux in the rear right quadrant this time (Figure 12 i and j).

As expected, the wave fields are largest in the front right quadrant due to the large fetch, wind duration and the direction of the translation speed of the storm (Figure 13). This is consistent with other numerical hurricane experiments (Young, 1988; Moon et al., 2003; Young, 2003; Fan et al., 2009; Fan et al., 2010) and observations (Young and Burchell, 1996; Wright et al., 2001). The maximum significant wave height (H_s) is increased from 15.6 m to 20.9 m as the translation speed is increased from 4.8 m/s to 9.6 m/s. For both translating hurricanes, the significant wave height is reduced by passing currents to the wave equation and by subtracting the surface currents from the wind driving the wave model (Figure 15). Consistent with the stationary hurricane, passing the currents at depth $z = L/(4 * \pi)$ to the wave equation (Figure 15 a and b) reduces the wave heights more than modifying the wind (Figure 15 c and d).

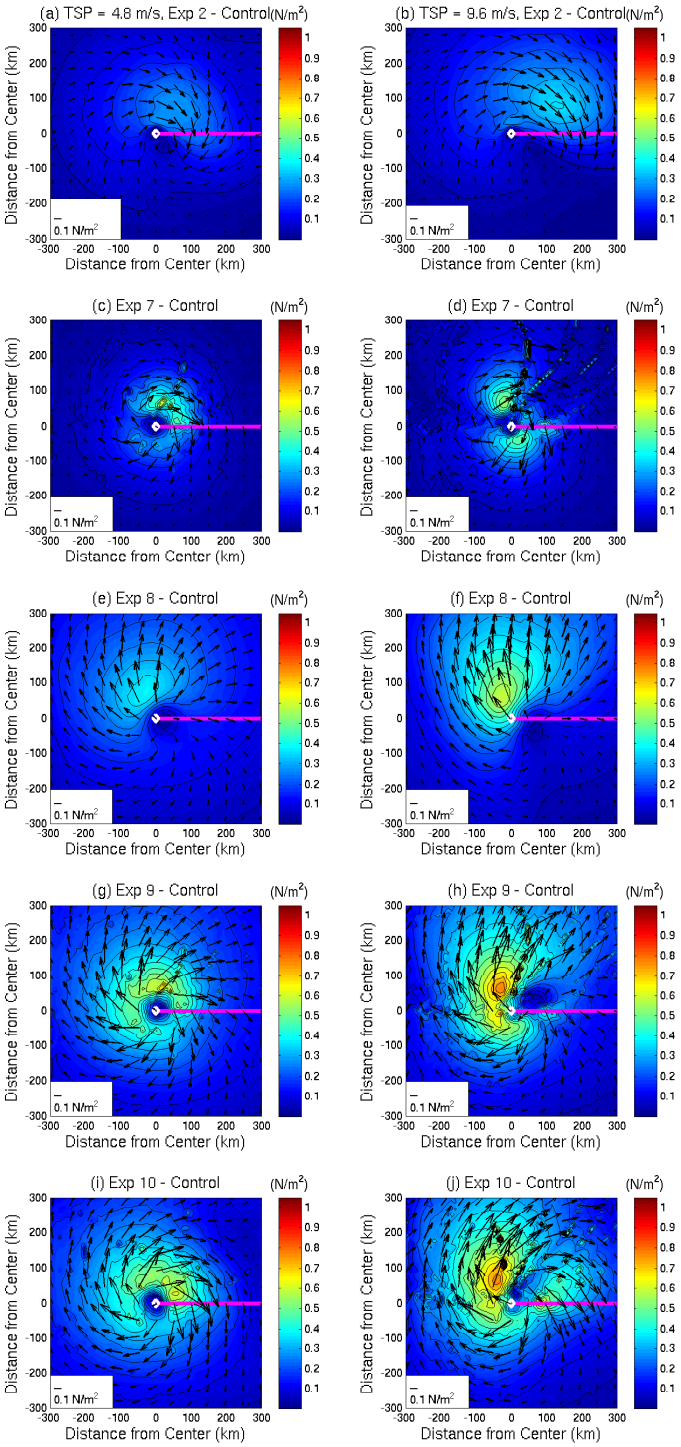

Figure 11: Momentum flux into the ocean ($\vec{\tau_c}$) differences (Current Experiment - Control) (contours every 0.05 N/m^2) for moving TCs with TSP = 4.8 m/s (left column) and 9.6 m/s (right column): Experiment 2 (a) and (b); Experiment 7 (c) and (d); Experiment 8 (e) and (f); Experiment 9 (g) and (h); Experiment 10 (i) and (j)

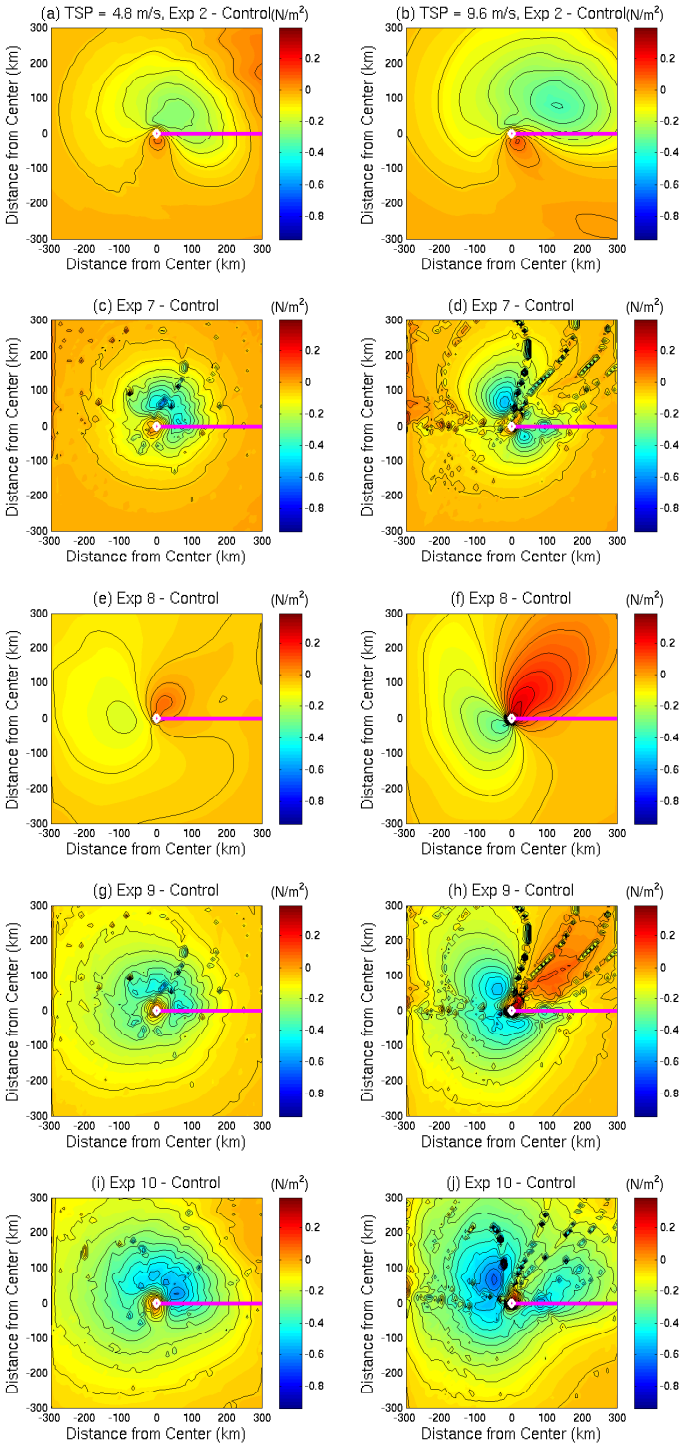

Figure 12: Momentum flux into the ocean ($\vec{\tau_c}$) magnitude differences (Current Experiment - Control) (contours every 0.05 N/m^2) for moving TCs with TSP = 4.8 m/s (left column) and 9.6 m/s (right column): Experiment 2 (a) and (b); Experiment 7 (c) and (d); Experiment 8 (e) and (f); Experiment 9 (g) and (h); Experiment 10 (i) and (j)

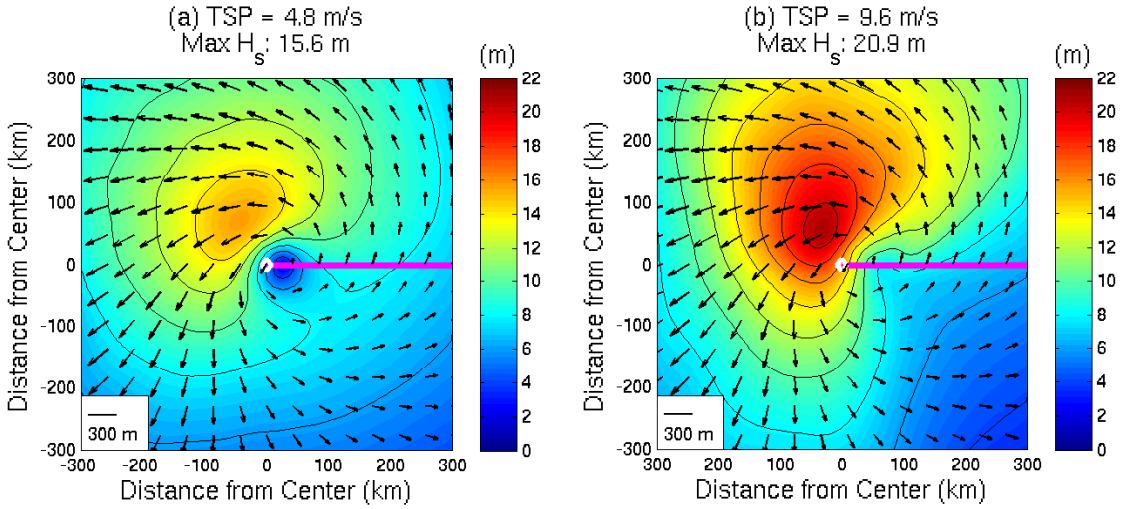

Figure 13: Control Experiment significant wave height (m) (contours every 2 m) after 72 hours for moving TC with TSP= (a) 4.8 m/s and (b) 9.6 m/s

For the 9.6 m/s translating hurricane, Experiment 3 has a second large difference region well behind the storm center and away from the largest section of the wave field. This second area of major wave height reduction for the 9.6 m/s translating hurricane is probably due to an increase of the region of the largest waves and the different ocean current structure in comparison with the 4.8 m/s translating hurricane (Figure 14).

While the influence of the currents modifying the wave equation is larger than the reduced wind forcing on the significant wave height, the fully coupled experiment clearly has a wave field with a greater difference from the control experiments for both the 4.8 m/s and 9.6 m/s translating hurricanes (Figure 15 e and f). The change is the largest in the region of the highest waves. Both the area and the magnitude of the difference are larger for the fully coupled experiment than either of the other two difference experiments. As is the case for Experiment 3 for the 9.6 m/s translating hurricane, Experiment 10 has a second large difference region behind and to the right of the storm center. The magnitude and size of this region are slightly larger in the fully coupled experiment than Experiment 3,

which can be attributed to the effect of reducing the wind forcing and the slightly different resulting ocean currents that modify the wave equation.

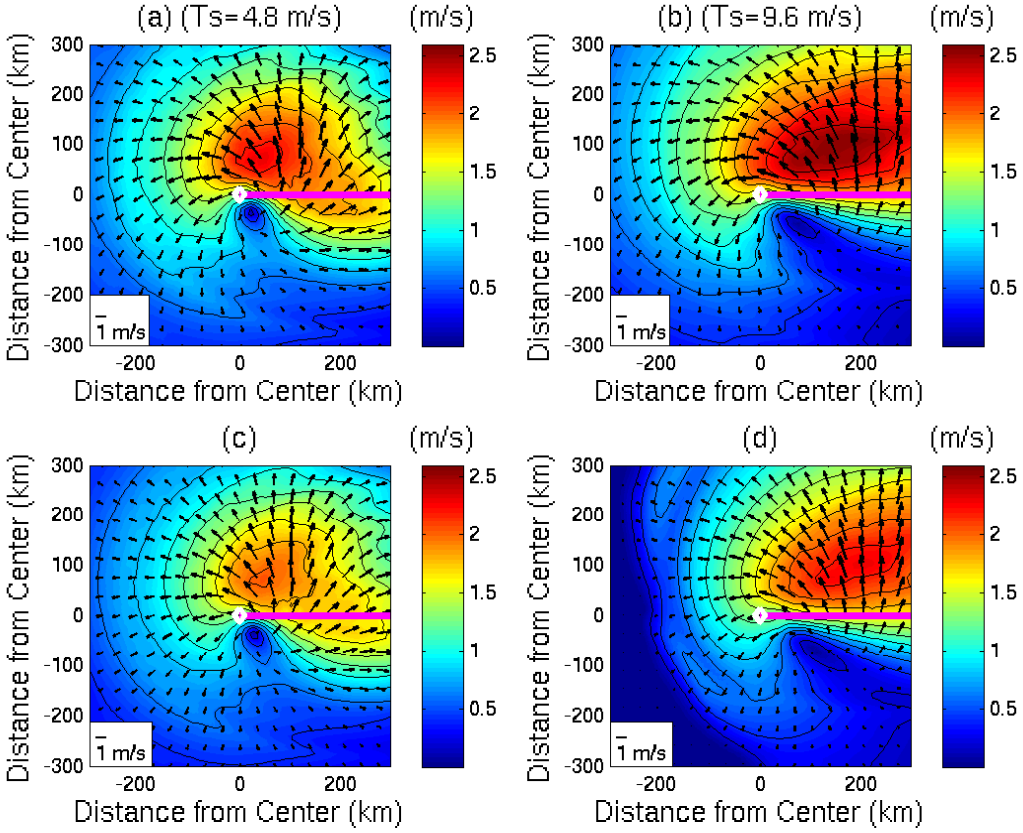

Figure 14: Control Experiment ocean currents (m/s) (contours every 0.2 m/s) after 72 hours for moving TC with TSP= 4.8 m/s (left column) and 9.6 m/s (right column), top row are surface currents, bottom row are currents at depth $L/(4 * \pi)$

The cold wake is clearly visible behind the storm center, especially to the right of the storm track (Figure 16 a and b). There is less cooling to the left of the storm track due to weaker currents and in turn less turbulent mixing (Figure 14 a and b). The currents are larger to the right of the storm due to the resonance effect between the moving hurricane and the inertial rotation of the currents. To the right of the storm track, at any given location, the wind direction rotates to the right as the hurricane passes, while to the left of the storm track, the wind rotates to the left (Figure 17).

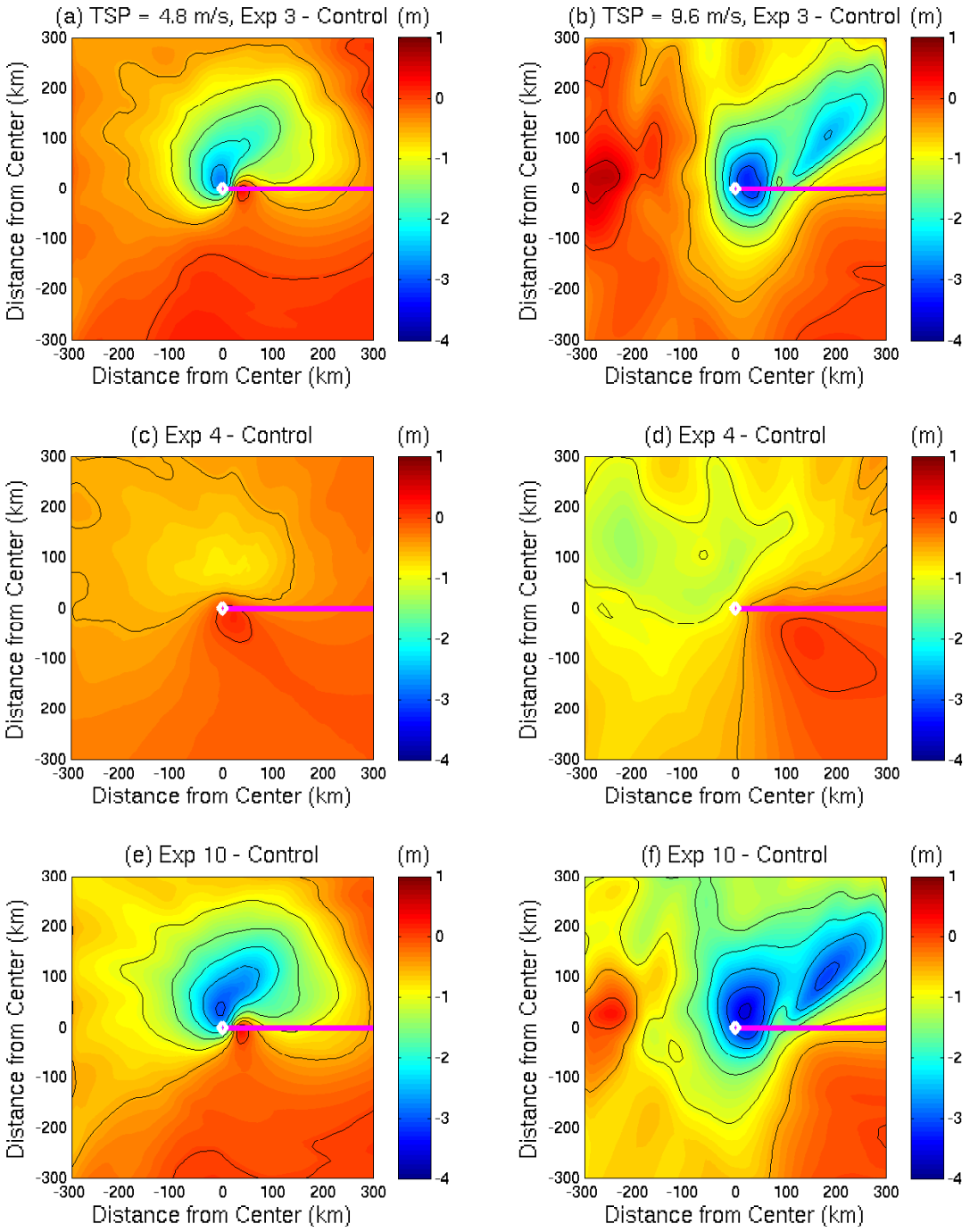

Figure 15: Significant wave height differences (m) (Current experiment - Control) (contours every 0.5 m) after 72 hours for moving TC with TSP = 4.8 m/s (left column) and TSP = 9.6 m/s (right column): Experiment 3 (a) and (b); Experiment 4 (c) and (d); Experiment 10 (e) and (f)

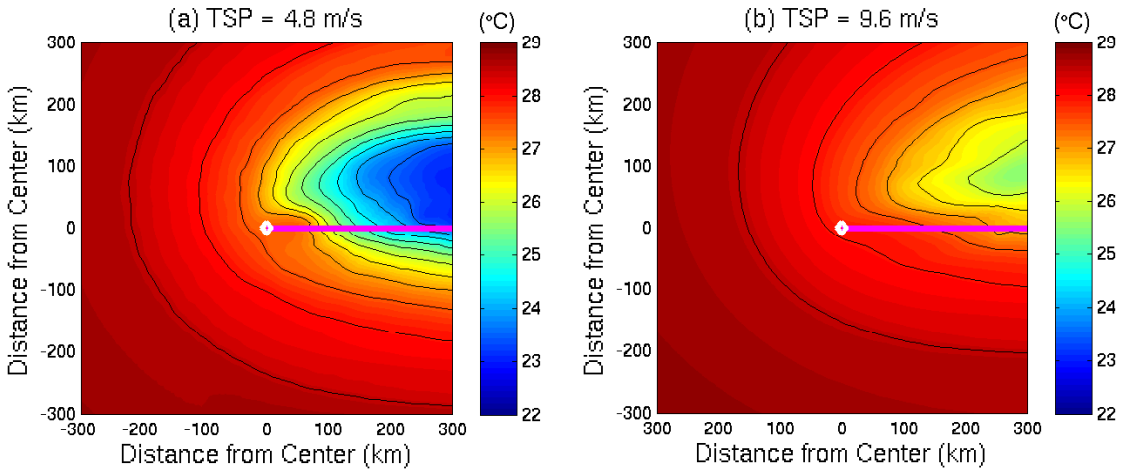

Figure 16: Control Experiment SST (contours every $0.5°C$) after 72 hours for moving TC with TSP= (a) 4.8 m/s and (b) 9.6 m/s

Since the storm occurs in the northern hemisphere, the Coriolis effect causes the ocean currents to be to the right of the wind forcing. This means that to the right of the storm track, the Coriolis effect and wind rotation are in the same direction, while to the left of the storm track they work against each other. The cooling is reduced for Experiment 2 (Figure 18 a and b), Experiment 7 (Figure 18 c and d), Experiment 8 (Figure 18 e and f), Experiment 9 (Figure 18 g and h), and in Experiment 10 (Figure 18 i and j). While the change in cooling is not the same for the modified wind stress experiments and the wave momentum flux budget experiments ($\vec{\tau}_c = \vec{\tau}_{air} - \vec{\tau}_{diff}$), it is difficult to determine which effect has a larger impact on the temperature (especially for the hurricane with a western translation speed of 9.6 m/s).

In the case of the 4.8 m/s hurricane, the maximum cooling reduction is larger for the wave momentum flux budget Experiment 7 and the contours are slightly different from the modified wind stress Experiment 2 but the reduction in cooling is still very similar. Both experiments actually have a slight increase in cooling in different bands as well. This includes localized regions along the storm track.

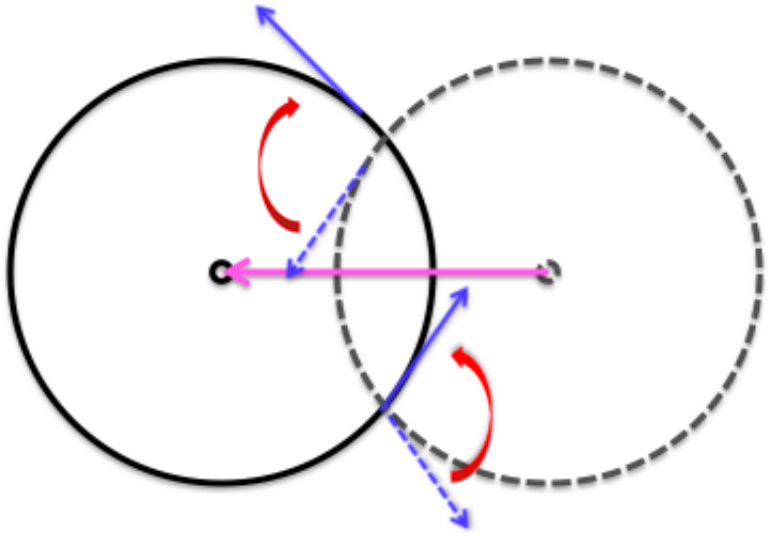

Figure 17: Resonance effect for a hurricane moving to the west along the magenta arrow. At the initial time (dashed circle), the wind direction at two selected points to the right and left of the storm center follows the dashed blue lines, but at the next timestep (solid line circle), the wind direction at those same locations has shifted to the solid blue arrows. The red arrows indicate the direction of the wind shift. Note: to the right of the storm track, the wind direction shifts to the right, but to the left of the storm track, it shifts to the left

For the 9.6 m/s hurricane, the differences are again very small, but the modified wind stress Experiment 2 has a slightly more reduced cold wake than the wave momentum flux Experiment 7. Experiment 2 has a larger region of cooling to the left of the storm track, but Experiment 7 has a region of increased cooling in front and to the right of the storm track.

The impact of including the Coriolis-Stokes forcing in the momentum flux into the ocean is similar in the moving storms to what it is for the stationary hurricane experiments. The cooling actually increases slightly (Figures 18 e and f). For the 4.8 m/s idealized hurricane, the cooling increases mostly along the storm track on both sides, slightly biased towards the right. This increase in SST cooling is due to an enhancement of upwelling near the storm center caused by the shift to the right of the ocean current in Experiment 8 (Figure 22). There are also a couple of bands where the cooling is reduced on both sides of the storm track.

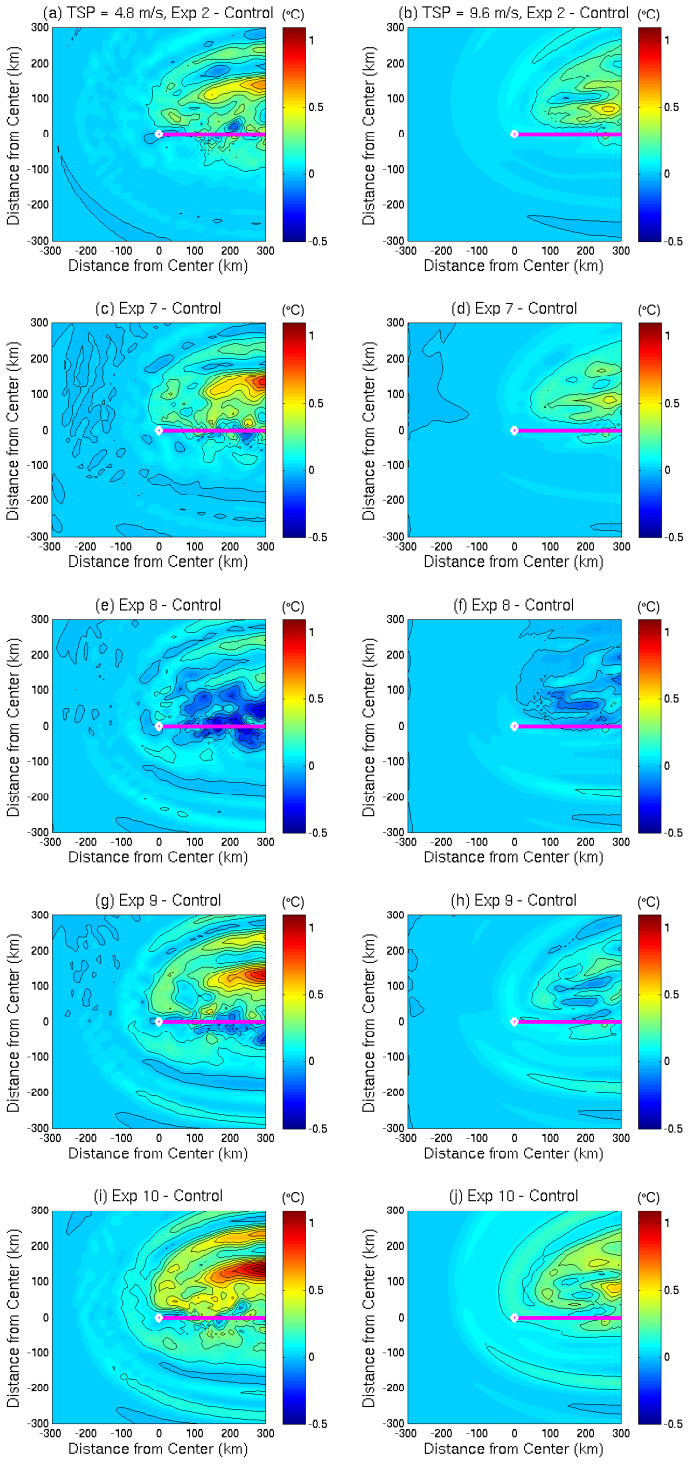

Figure 18: SST differences (Current Experiment - Control Experiment) (contours every $0.1°C$) after 72 hours for moving TCs with TSP = 4.8 m/s (left column) and TSP = 9.6 m/s (right column): Experiment 2 (a) and (b); Experiment 7 (c) and (d); Experiment 8 (e) and (f); Experiment 9 (g) and (h) ; Experiment 10 (i) and (j)

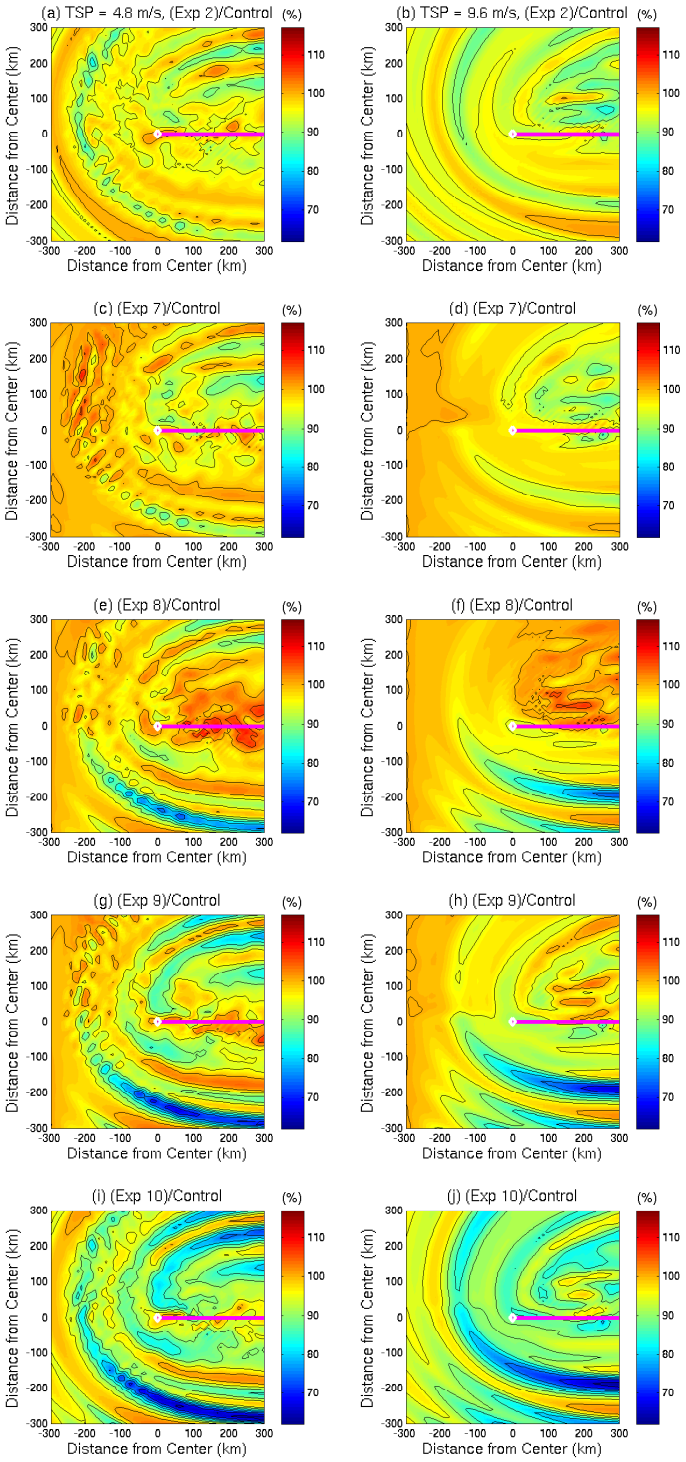

Figure 19: δSST ratios (Current Experiment/Control Experiment *100) (contours every 5 %) after 72 hours for moving TCs with TSP = 4.8 m/s (left column) and TSP = 9.6 m/s (right column): Experiment 2 (a) and (b); Experiment 7 (c) and (d); Experiment 8 (e) and (f); Experiment 9 (g) and (h) ; Experiment 10 (i) and (j)

The cooling increases almost exclusively to the right of the 9.6 m/s translating hurricane storm center with only a small band of increased cooling to the left and behind the storm. There is also a small segment of slightly reduced cooling to the left of the storm track. Furthermore, both the 4.8 m/s and the 9.6 m/s idealized hurricane versions of Experiment 8 have surface currents that vary more significantly from the control experiment (Figure 20 e and f) than the other experiments that alter the cold wake (Figure 20 a, b, c and d). On top of that, the surface current vector for Experiment 8 has a larger angle difference with the control experiment surface current vector than Experiments 2 and 7 do for both moving hurricanes (Figure 22).

The fully coupled Experiment 10 has the largest reduction of cooling for both moving tropical cyclones (Figure 18 i and j), although Experiment 9 is only slightly different. While the region of the largest difference with the control experiment for the 4.8 m/s hurricane corresponds to the maxima in Experiment 2 and Experiment 7, it also happens to be about in the same region where Experiment 8 has both a minimum and a local maximum. Several of the maxima for the 9.6 m/s hurricane Experiment 10 line up with maxima in Experiments 2, 7, and 8 in a similar matter. It is clear that the different components of the momentum flux into the ocean ($\vec{\tau}_{air}, \vec{\tau}_{diff},\ and\ \vec{\tau}_{cor}$) and the translation speed of the hurricane have important effects on the resulting cold wake.

What is also striking is that the changes in the cold wake from the control experiment to the other experiments are not uniform. Instead, they occur in different bands of local minima and maxima. These minima and maxima are a reflection of the non-uniform changes to the ocean surface currents ($\vec{U}_c$) (Figure 20).

The surface currents are significantly larger in the right rear quadrant than any of the other 3 quadrants (Figure 14) due to the resonance effect illustrated

in Figure 17. This differs from the significant wave height, but resembles the sea surface temperature distribution. As with the sea surface temperature, the higher translation speed leads to even smaller values to the left of the storm track.

Experiment 8 has currents that differ from the control experiment (Figure 20 e and f) much more than Experiment 2 (Figure 20 a and b) and Experiment 7 (Figure 20 c and d). However, the surface current magnitude differences show a different result (Figure 21). Experiment 2 and Experiment 7 have large sections where the current magnitude is reduced, along with smaller regions with larger surface current magnitudes than the control. Experiment 8 tends to slightly increase the surface current magnitude especially behind the storm center. Along and in front of the storm center, the surface current magnitude is larger than the control. Experiment 9 and especially the fully coupled Experiment 10 both have surface currents that consistently have a smaller magnitude than the control to the right of the storm track. As with the sea surface temperature and magnitude of the surface current vector differences, the surface current magnitude differences form banded structures.

Experiment 9 has surface current differences with the control experiment very similar to Experiment 8 for both the 4.8 m/s and 9.6 m/s translating hurricanes. But, the magnitudes of these differences are slightly larger and the surface current vectors for Experiment 9 are to the right of the control experiment for both moving idealized hurricanes (Figure 22).

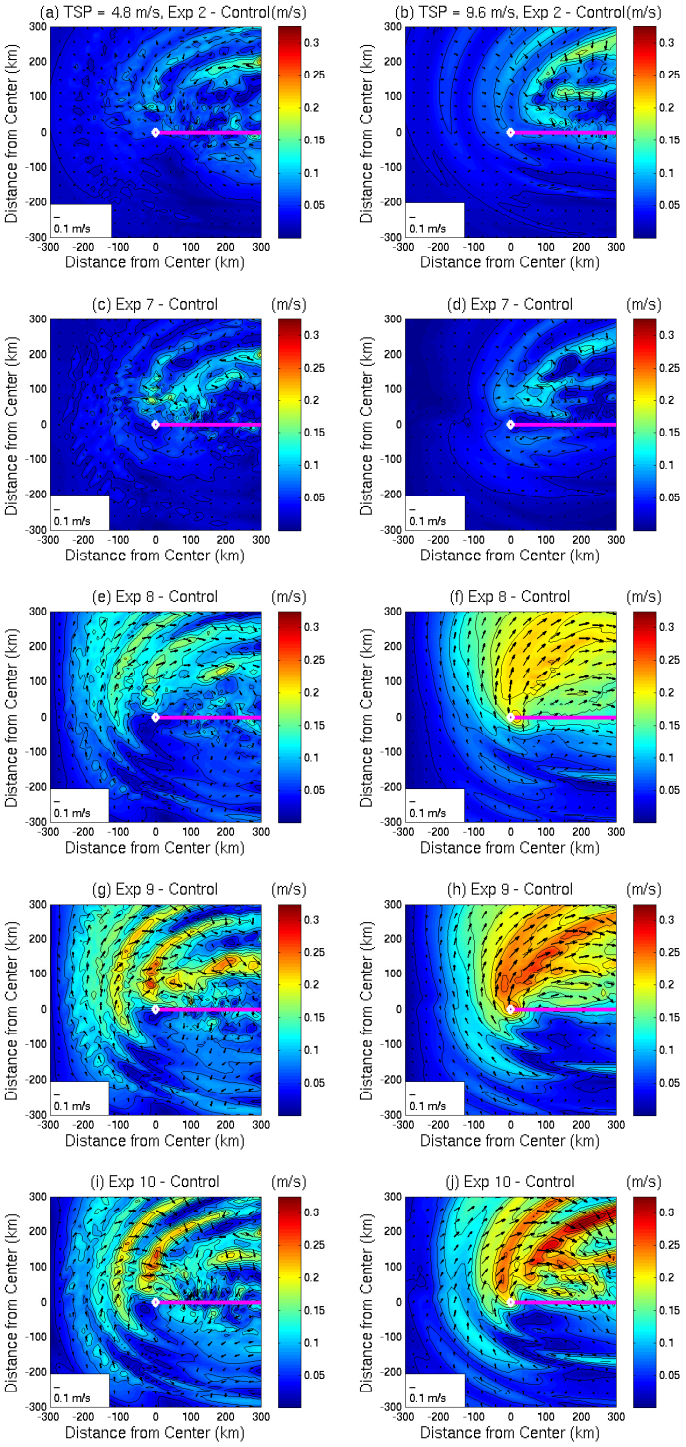

Figure 20: Surface current differences (m/s) (Current experiment - Control) (contours every 0.025 m/s) after 72 hours for moving TCs with TSP= 4.8 m/s (left column) and 9.6 m/s (right column): Experiment 2 (a) and (b); Experiment 7 (c) and (d); Experiment 8 (e) and (f); Experiment 9 (g) and (h); Experiment 10 (i) and (j)

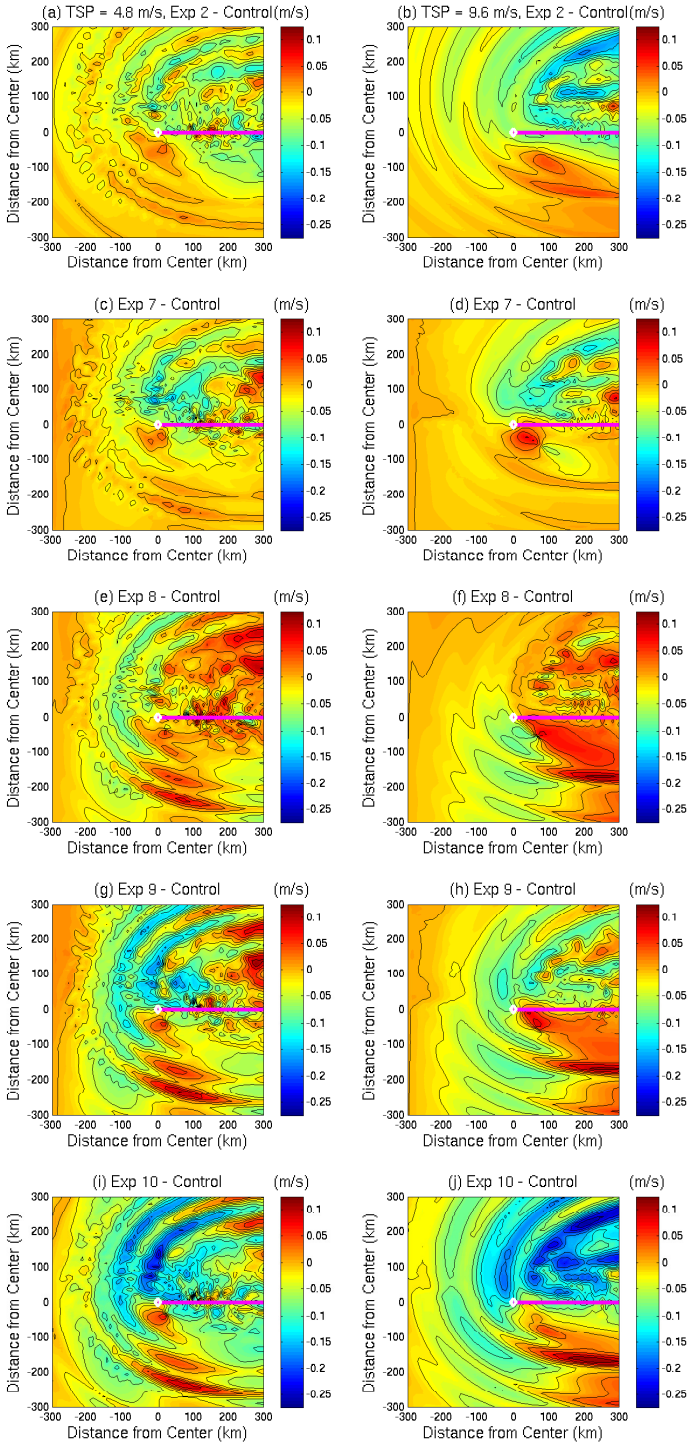

Figure 21: Surface current magnitude differences (m/s) (Current experiment - Control) (contours every 0.025 m/s) after 72 hours for moving TCs with TSP= 4.8 m/s (left col.) and 9.6 m/s (right col.): Experiment 2 (a) and (b); Experiment 7 (c) and (d); Experiment 8 (e) and (f); Experiment 9 (g) and (h); Experiment 10 (i) and (j)

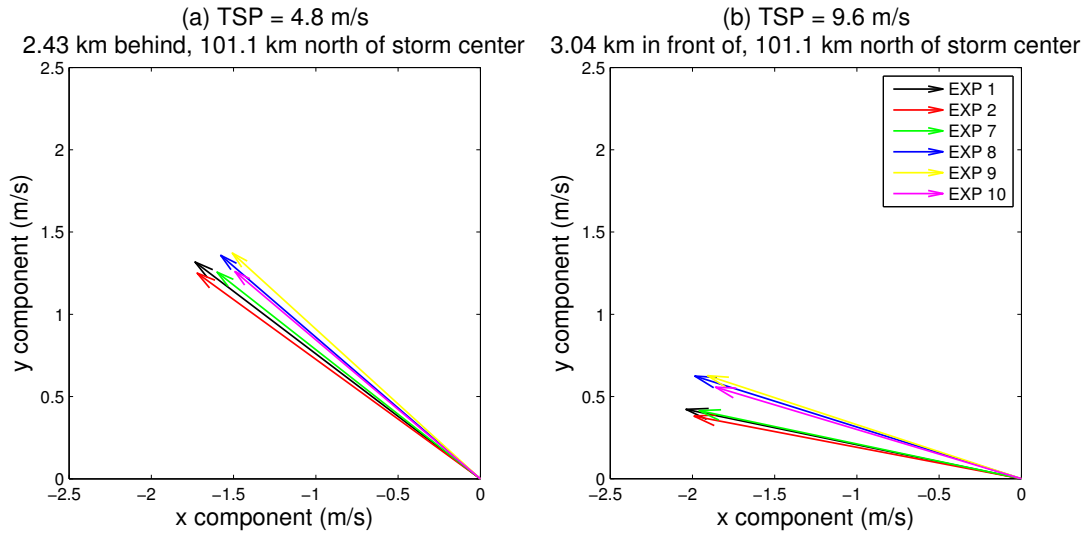

Figure 22: Surface current vectors (m/s) after 72 hours for moving TCs: TSP= (a) 4.8 m/s and (b) 9.6 m/s

The direction of the surface current vector shown in Figure 22 is largely broken into two different groups: experiments with the Coriolis-Stokes forcing included, and those without it. Experiments with the Coriolis-Stokes forcing included are consistently to the right of the experiments without the Coriolis-Stokes forcing. This, along with the surface current magnitude differences indicates that the Coriolis-Stokes forcing primarily alters the direction of the surface currents and has a much smaller impact on the magnitude.

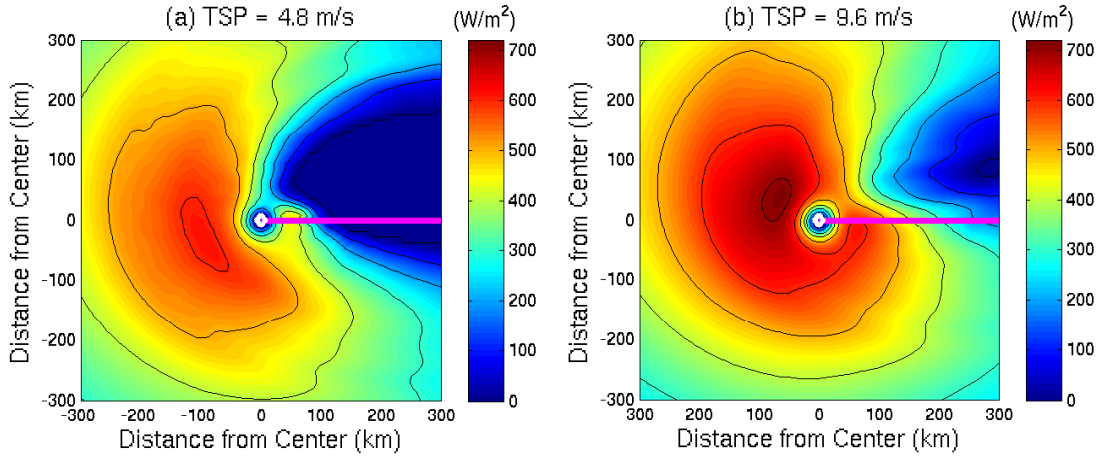

Figure 23: Control Experiment latent heat flux (contours every 100 W/m^2) after 72 hours for moving TC with TSP= (a) 4.8 m/s and (b) 9.6 m/s

In order to measure the potential effect of the changes in SST and surface currents on hurricane intensity in different experiments we calculate the latent heat flux into the atmosphere. The flux is calculated assuming a fixed horizontally homogenous atmosphere with 10-m air temperature of $25°C$, 95% relative humidity, and a fixed atmospheric pressure of 980 hPa. These values are similar to those used in (Cione and Uhlhorn, 2003). The latent heat flux, H_L is computed by

$$H_L = \rho L_v C_e U(q_{sst} - q_A) \tag{28}$$

where ρ is the air density, U is the 10-m wind speed, C_e is the dimensionless coefficient of moisture exchange at 10 m, L_v is the latent heat of vaporization, and q_{SST} and q_A are the saturation mixing ratios at the SST and the air temperature respectively.

There is a strong latent heat flux out of the ocean ahead of the idealized hurricanes. However, the latent heat flux is very small in the cold wake region and even goes to zero in the case of the 4.8 m/s translating hurricane (Figure 23 a). Given the strong cooling in the case of the 4.8 m/s hurricane (Figure 16 a), it is not surprising to see there is no latent heat flux in this region. As the ocean temperature cools, eventually, it might drop below the air temperature (assumed to be $25.5°C$ everywhere in these simplified experiments). Colder, dry air suppresses the latent heat flux. The 9.6 m/s hurricane latent heat flux has a larger maximum and is strongest in the front right quadrant (Figure 23 b). But, even to the left of the storm (in front of, alongside, and behind the storm center) the 9.6 m/s hurricane has a larger latent heat flux.

For all 4.8 m/s hurricane experiments, the latent heat flux is suppressed in a large section of the cold wake as noted above. Thus, the sensitivity experiments are not different from the Control in this section. Experiment 2 increases the latent heat flux into the atmosphere more so to the right of the storm track than the left,

over a larger region for the 9.6 m/s hurricane than the 4.8 m/s hurricane (Figure 24 a and b). There are also segments of reduced latent heat flux, especially in the front right quadrant for both storms. Experiment 7 alters the latent heat flux in a similar manner to Experiment 2, but it does not have the reduction in front of the storm center or even in small, localized regions behind or alongside it (Figure 24 c and d). Experiment 8 has section of the largest reduction of the latent heat flux (Figure 24 e and f). The 4.8 m/s hurricane even has regions where the magnitudes of latent heat flux increases are larger than its reductions. Experiment 9 tends to mostly increase the latent heat flux (especially to the right of the storm track) for the 4.8 m/s hurricane, but its 9.6 m/s counterpart has a more complicated impact (Figure 24 g and h). While the 9.6 m/s Experiment 9 increases the latent heat flux over a larger geographic range than it reduces it, the magnitudes of the increases and reductions are comparable. Experiment 10 has the largest increases in the latent heat flux and for both hurricanes; these increases are considerably larger to the right of the storm track (Figure 24 i and j). For all experiments, the changes in latent heat flux for the 9.6 m/s hurricane are further behind the storm center than the 4.8 m/s hurricane.

Hurricanes receive their energy from the latent heat flux occurring close to the storm center more than the latent heat flux in the cold wake region. Thus, the changes in the latent heat flux for the 4.8 m/s translating hurricane are actually more important to hurricane formation and development than the 9.6 m/s translating hurricane latent heat flux changes. An enhanced latent heat flux indicates a potential strengthening of tropical cyclones, while a reduced latent heat flux may lead to weaker hurricanes.

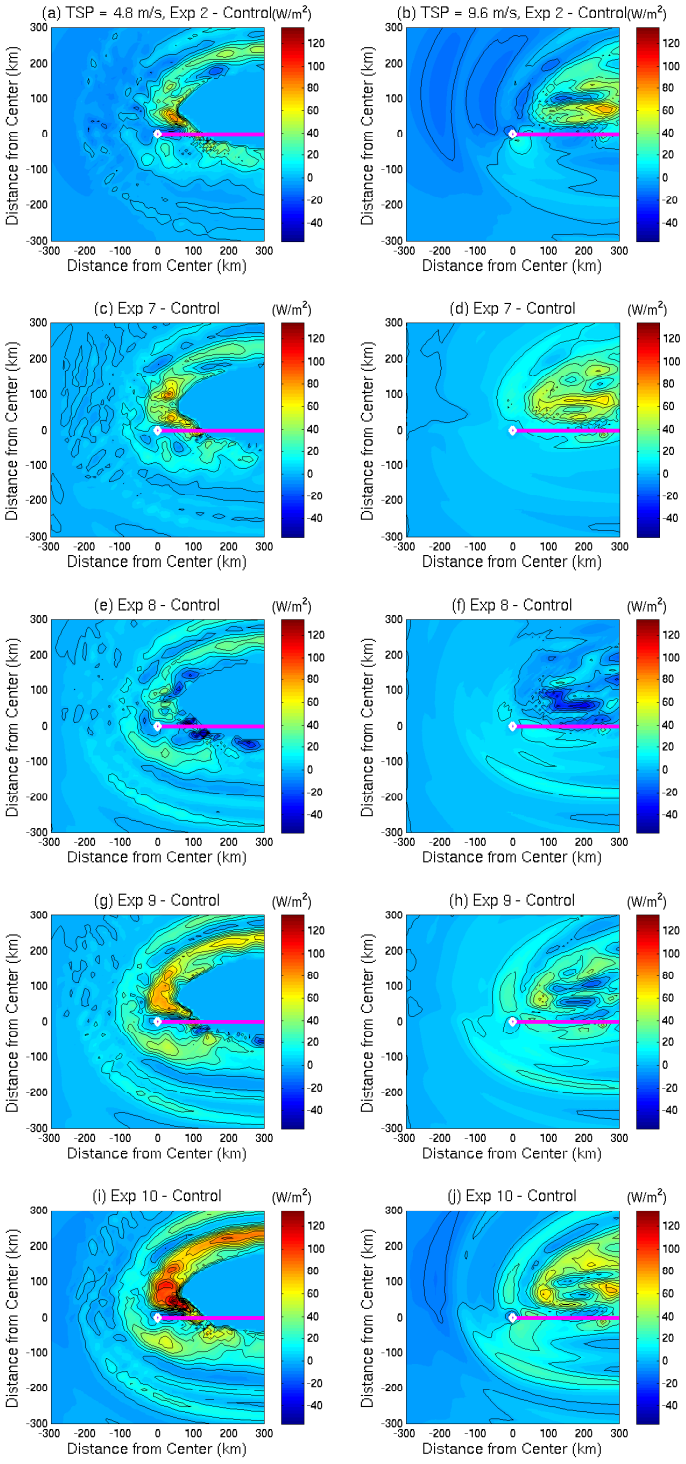

Figure 24: Latent heat flux differences (W/m^2) (Current experiment - Control) (contours every 10 W/m^2) after 72 hours for moving TCs with TSP= 4.8 m/s (left column) and 9.6 m/s (right column): Experiment 2 (a) and (b); Experiment 7 (c) and (d); Experiment 8 (e) and (f); Experiment 9 (g) and (h); Experiment 10 (i) and (j)

CHAPTER 4

Hurricane Irene (2011)

4.1 Background

Hurricane Irene was the first hurricane to make landfall over the United States since Ike had over Texas nearly 3 years earlier in September 2008. It began as a tropical wave that moved away from western Africa on August 15, 2011. Just before August 21 at 0000 UTC, the tropical wave had organized and strengthened into Tropical Storm Irene 120 nautical miles east of Martinique and it reached hurricane status over Puerto Rico just after 0535 UTC on August 22. Hurricane Irene reached its peak intensity of 105 $knots$ (approximately 54 m/s) as a Category 3 Hurricane on the 24th at 1200 UTC with the storm centered between Mayaguana and Grand Inagua in the Bahamas. From there, it translated west-northwest before the subtropical ridge steering it shifted eastward and Irene moved in a north-northeastern direction. It briefly made landfall near Cape Lookout, North Carolina on August 27 1200 UTC with an intensity of 75 $knots$ (38.6 m/s) and later reached New Jersey close to Atlantic City on August 28 0935 UTC. The high winds in the right front quadrant remained over the ocean while Irene moved across New Jersey and New York, sparing both states from greater damage. Irene's status changed to extra-tropical on August 29 0000 UTC with the center close to the New Hampshire/Vermont border before it was finally absorbed by a frontal system over Northeastern Canada on August 30 0600 UTC (Avila and Cangialosi, 2011).

Despite Hurricane Irene being directly responsible for 49 total deaths across the Dominican Republic, Haiti, and the eastern United States, it was not responsible for any over the Bahamas when it reached peak intensity. From North Carolina northward, it damaged homes, felled trees and caused widespread power outages. Parts of the Chesapeake Bay experienced storm surge and heavy rain

in Pennsylvania and New Jersey led to major flooding. New York City did not have massive damage due to the strongest winds remaining to the east, but it did experience problems caused by storm surge. However, inland New York state along with New England (especially central and southern Vermont) suffered from catastrophic flooding (Avila and Cangialosi, 2011).

4.2 Results

The Coupled Ocean Wave Model was run from August 22, 2011 at 1200 UTC to 1800 UTC on August 27. Wind forcing was specified based on the TCVitals file shown in Table 3. Unlike the idealized hurricanes, the ocean bathymetry is important for real hurricanes. When a hurricane, such as Irene, passes over land boundaries it causes a rapid decay of significant wave height (H_s) and the wave momentum flux budget ($\vec{\tau}_{diff}$). Along her pass, Hurricane Irene also interacted with a major ocean current, the Gulf Stream. To avoid these complications, we selected the integration time where the hurricane was over the open ocean (Figure 25). We will analyze the results at 0600 UTC on August 26. At this time, Hurricane Irene was translating northward at a speed of 5.7 m/s.

The wind stress ($\vec{\tau}_{air}$) and in turn the momentum flux into the ocean ($\vec{\tau}_c$) for the control experiment is continuous and larger to the right of the storm track (Figure 26). Experiment 2 modifies the momentum flux into the ocean slightly to the right and behind the storm center (Figure 27 b), while Experiment 7 alters it by a larger vector magnitude but over a smaller geographic area in front of the storm (Figure 27 d). Experiment 8 modifies the flux mostly along the edge of the front right quadrant (Figure 27 f). Both Experiment 9 and Experiment 10 have larger changes in the vectors of the momentum flux into the ocean than each of the individual effect experiments do. However, Experiment 9 modifies the flux vectors more in front of the storm (Figure 27 h), while Experiment 10 also alters the flux

vectors along the storm track in the rear right quadrant (Figure 27 j).

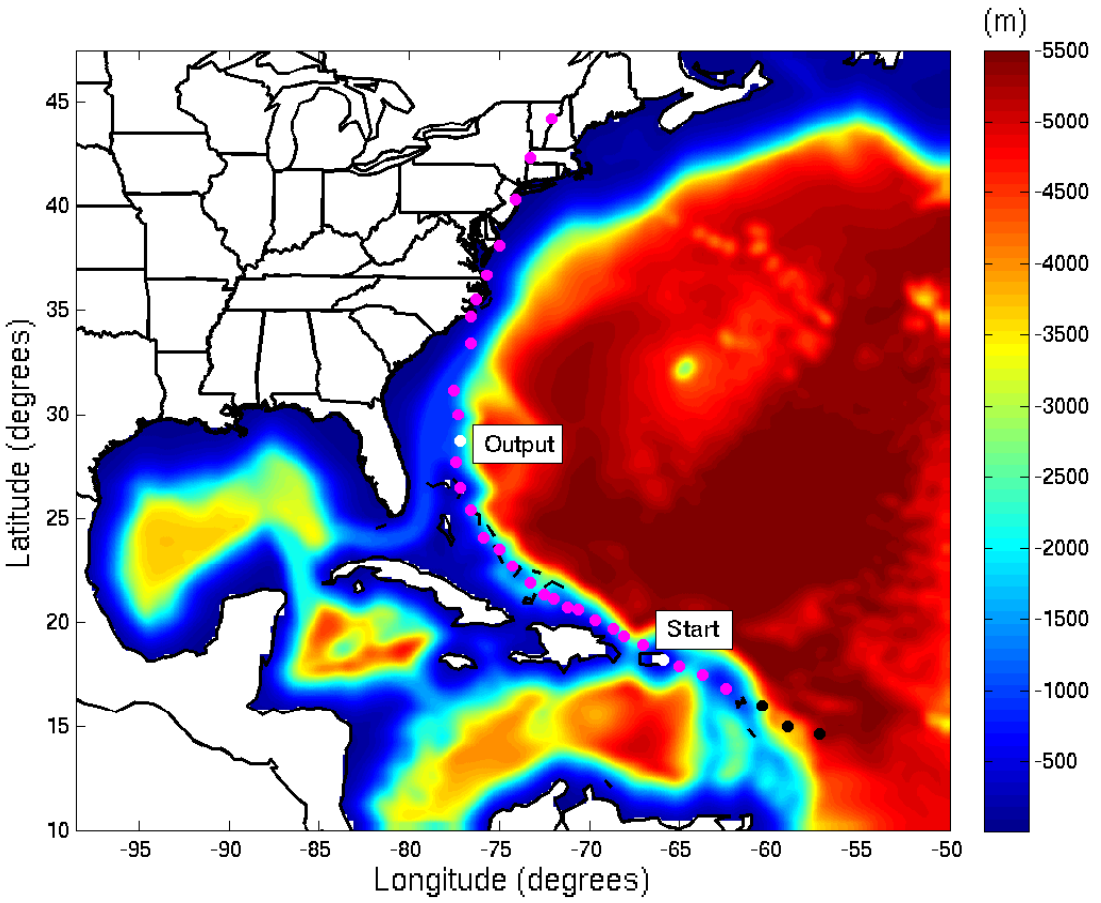

Figure 25: Storm track for Hurricane Irene with coupled model starting on August 22, 2011 at 12:00 UTC and output 90 hours later on August 26, 2011 at 06:00 UTC on top of Atlantic Ocean bathymetry

Experiment 2 reduces the air-sea momentum flux in the right rear quadrant along the storm track and not far from the storm center (Figure 28 b). It also slightly increases the flux into the ocean to the left of the storm, but this can be attributed to the Gulf Stream. Experiment 7 reduces the momentum flux into the ocean by a larger magnitude than Experiment 2, but only in a small region surrounding the storm center with a bias to the right side (Figure 28 d). It increases the flux into the ocean in the right rear quadrant. But, this occurs along the Bahamas where the wave momentum flux budget rapidly decays. Experiment

8 slightly increases the flux into the ocean to the right and slightly behind the storm center, while it also reduces the flux to the left of and slightly in front of the eye (Figure 28 f). Experiment 9 reduces the flux by a larger magnitude than any of the individual component experiments, but this is mostly confined to a small region near the storm center (Figure 28 h). The Fully Coupled Experiment 10 reduces the flux by the largest magnitude of all the experiments, and does so much more to the right of the storm than to the left, both just in front of and behind the storm center (Figure 28 j).

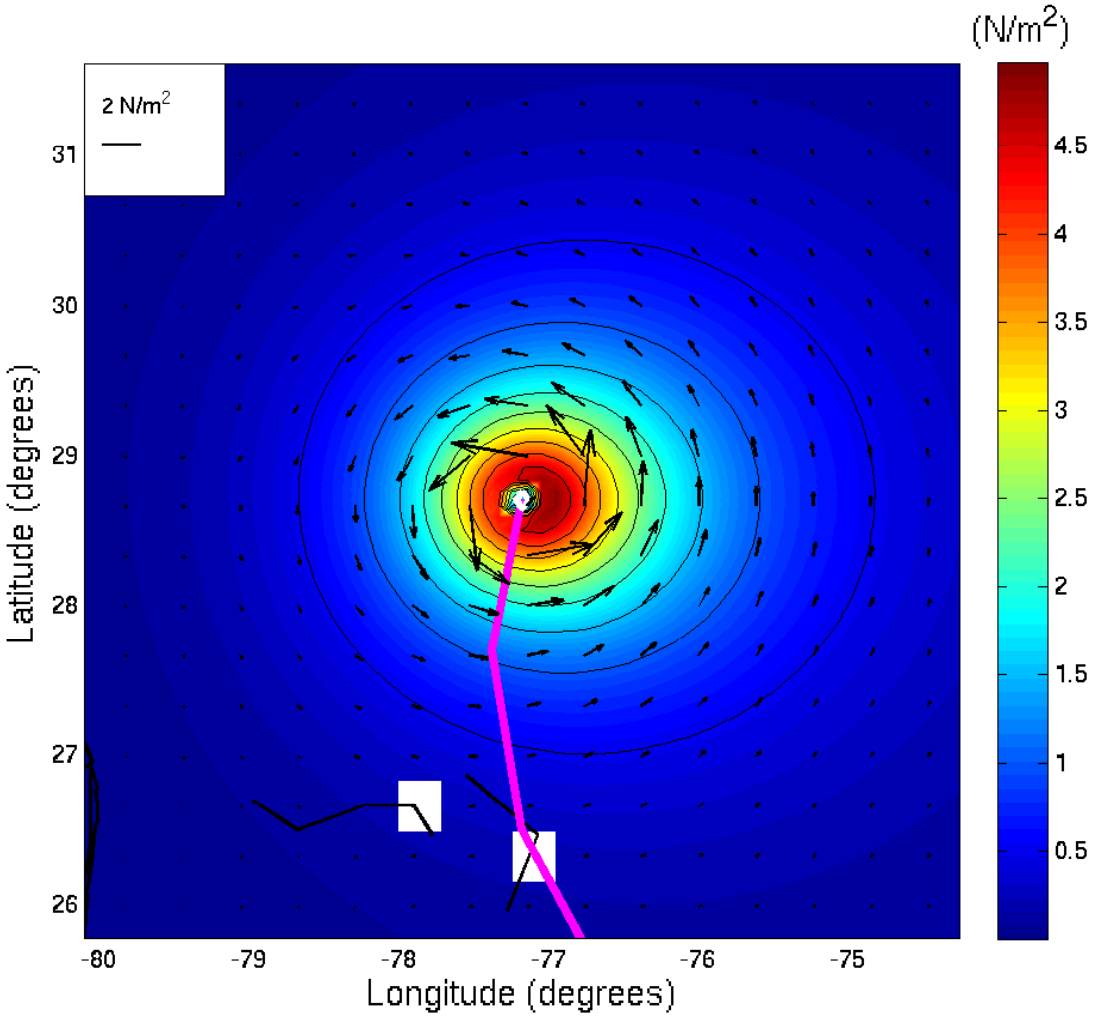

Figure 26: Control Experiment momentum flux into the ocean ($\vec{\tau}_c$) for Irene on August 26, 2011 at 06:00 UTC (contours every 0.5 N/m^2)

Table 3: Best track of Hurricane Irene, central pressure, environmental pressure, maximum wind speed (MWS), radii with wind speed of 18 m/s, 26 m/s, and the maximum in all quadrants (NE, SE, SW, and NW) of a hurricane from the message files provided by the National Hurricane Center.

Date/time	Position		Cen. pr.	Env. pr.	Max Wind speed	Radius (km)								
							18 m/s				26 m/s			
(UTC)	lat ($°N$)	lon ($°W$)	(hPa)	(hPa)	(m/s)	Max	NE	SE	SW	NW	NE	SE	SW	NW
22/1200	18.9	67.0	990	1010	36	28	241	111	111	167	74	46	37	65
1800	19.3	68.1	988	1010	36	28	297	111	74	167	74	56	37	46
23/0000	19.7	68.7	981	1010	44	28	297	130	74	167	111	56	37	93
0600	20.1	69.7	978	1010	44	28	334	222	222	241	167	111	111	130
1200	20.6	70.6	978	1008	44	28	334	222	222	241	167	111	111	130
1800	20.7	71.2	977	1006	41	37	334	222	167	241	139	111	74	111
24/0000	21.1	72.0	969	1006	41	37	334	334	167	278	130	130	74	139
0600	21.3	72.5	965	1008	49	37	334	334	167	278	130	130	74	130
1200	21.9	73.3	957	1008	51	28	334	278	167	278	167	111	83	148
1800	22.7	74.3	954	1008	54	28	334	297	185	278	185	130	93	148
25/0000	23.5	75.0	952	1008	54	56	408	334	185	278	185	167	93	148
0600	24.1	75.9	950	1008	51	56	408	334	185	241	185	148	93	130
1200	25.4	76.6	950	1008	51	56	463	371	185	259	185	185	93	130
1800	26.5	77.2	950	1008	49	56	463	371	232	278	204	185	93	130
26/0000	27.7	77.4	946	1008	51	56	463	371	232	297	204	185	93	139
0600	28.7	77.2	942	1010	49	19	463	371	241	324	232	195	139	139
1200	30.0	77.3	947	1010	46	74	463	371	241	324	232	195	139	139
1800	31.2	77.5	951	1012	44	74	463	417	259	324	259	232	148	167
27/0000	33.4	76.6	952	1012	41	111	417	417	259	259	232	232	167	139
0600	33.4	76.6	952	1012	41	111	417	417	259	259	232	232	167	139
1200	34.7	76.6	952	1012	39	83	417	417	278	232	232	232	167	111
1800	35.5	76.3	950	1012	39	83	389	389	278	232	222	222	148	111

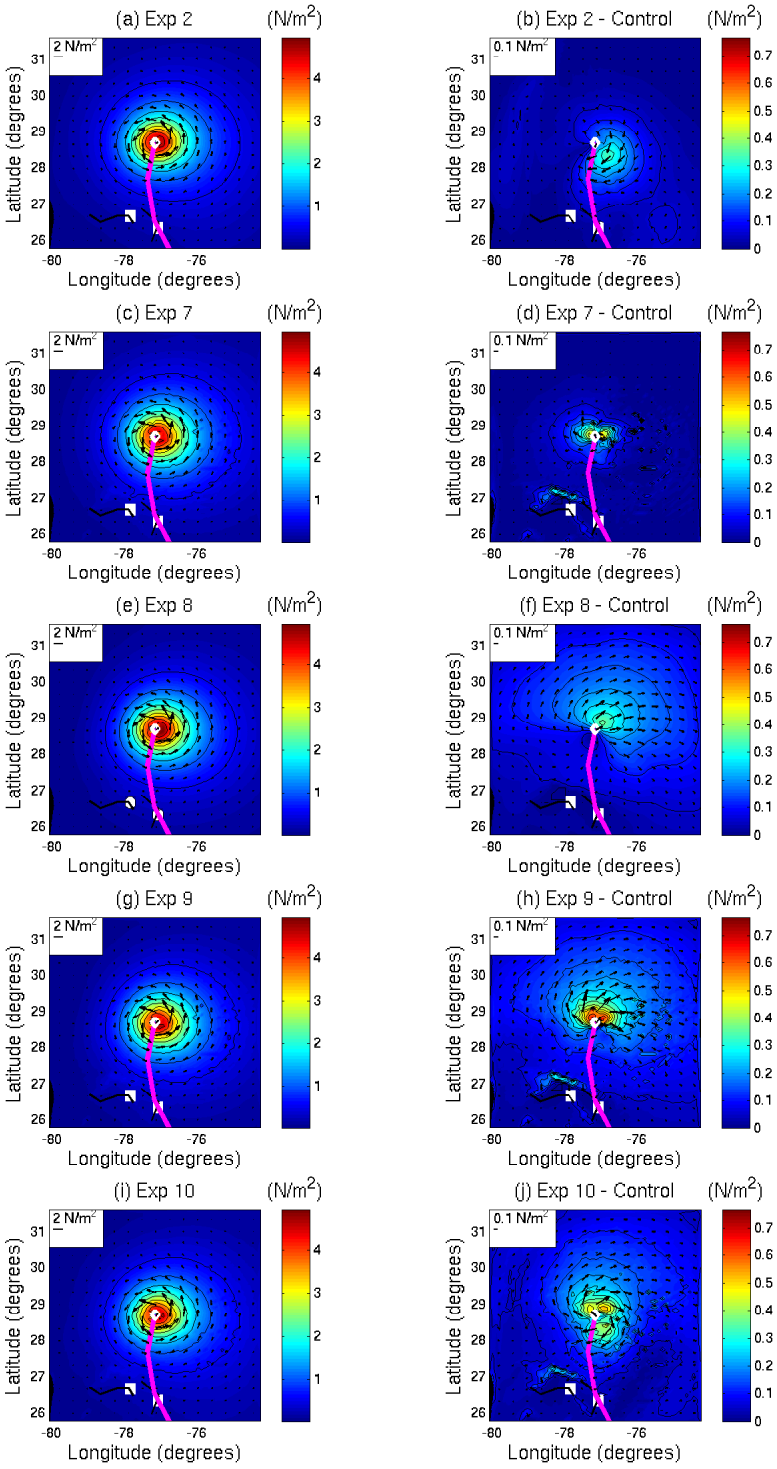

Figure 27: Momentum flux into the ocean $\vec{\tau}_c$ (left col.) and differences (Current experiment - Control) (right col.) for Irene: Experiment 2 (a) and (b); Experiment 7 (c) and (d); Experiment 8 (e) and (f); Experiment 9 (g) and (h); Experiment 10 (i) and (j) on August 26, 2011 at 06:00 UTC (contours every 0.5 N/m^2) and (difference contours every 0.05 N/m^2)

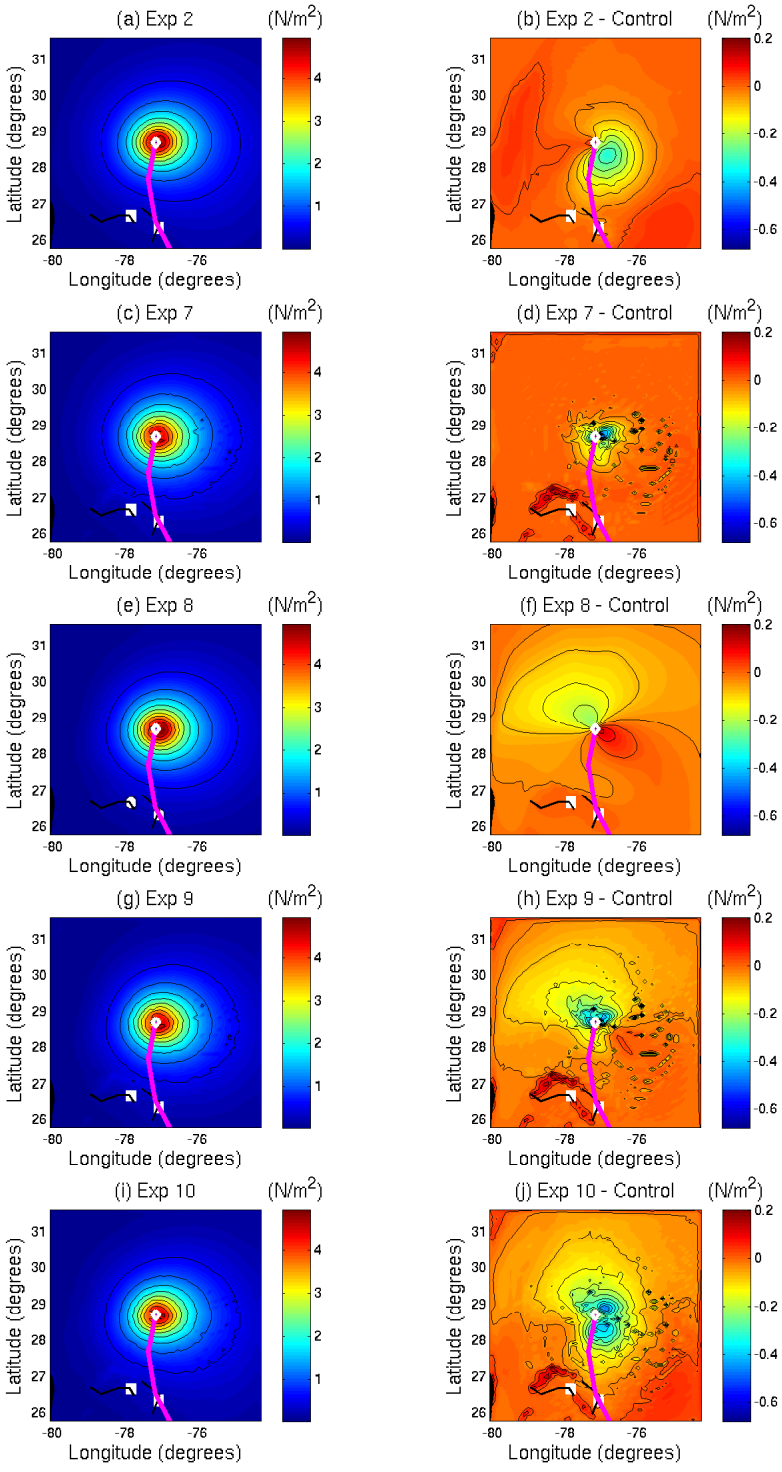

Figure 28: Momentum flux into the ocean $\vec{\tau}_c$ (left col.) and magnitude differences (Current experiment - Control) (right col.) for Irene: Experiment 2 (a) and (b); Experiment 7 (c) and (d); Experiment 8 (e) and (f); Experiment 9 (g) and (h); Experiment 10 (i) and (j) on August 26, 2011 at 06:00 UTC (contours every 0.5 N/m^2) and (difference contours every 0.05 N/m^2)

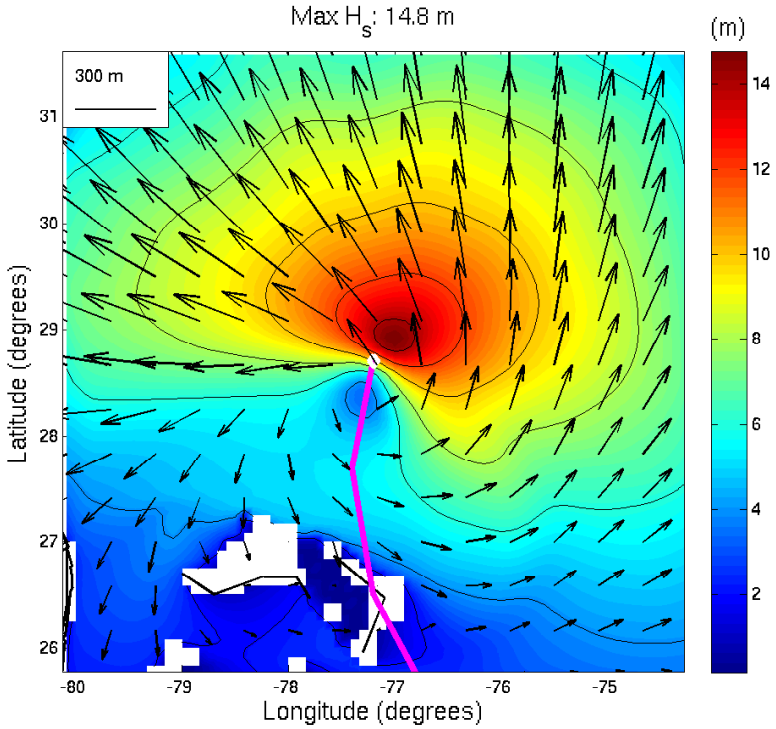

Figure 29: Control Experiment significant wave height (m) for Hurricane Irene on August 26, 2011 at 06:00 UTC (contours every 2 m)

The different components of the coupled model are investigated by examining the Significant Wave Height (H_s), sea surface temperature (SST), and surface currents ($\vec{U_c}$). As expected, the Significant Wave Height for Hurricane Irene is largest in the right front quadrant and smallest in the left rear quadrant (Figure 29). Also consistent with the idealized hurricanes, only experiments in which currents at depth $L/(4 * \pi)$ are passed to the wave equation and/or the wind forcing the wave model is modified by the surface currents have a wave field that differs from the control experiment. Passing currents to the wave equation (Figure 30 b) has a much larger impact on the surface waves; the maximum significant wave height is reduced by 3.5 m. Adjustment of the wind forcing on the wave model by including surface currents has a smaller effect; the maximum significant wave height is slightly decreased in the front of the storm, but slightly increased to behind and to the right of the storm center. (Figure 30 d).

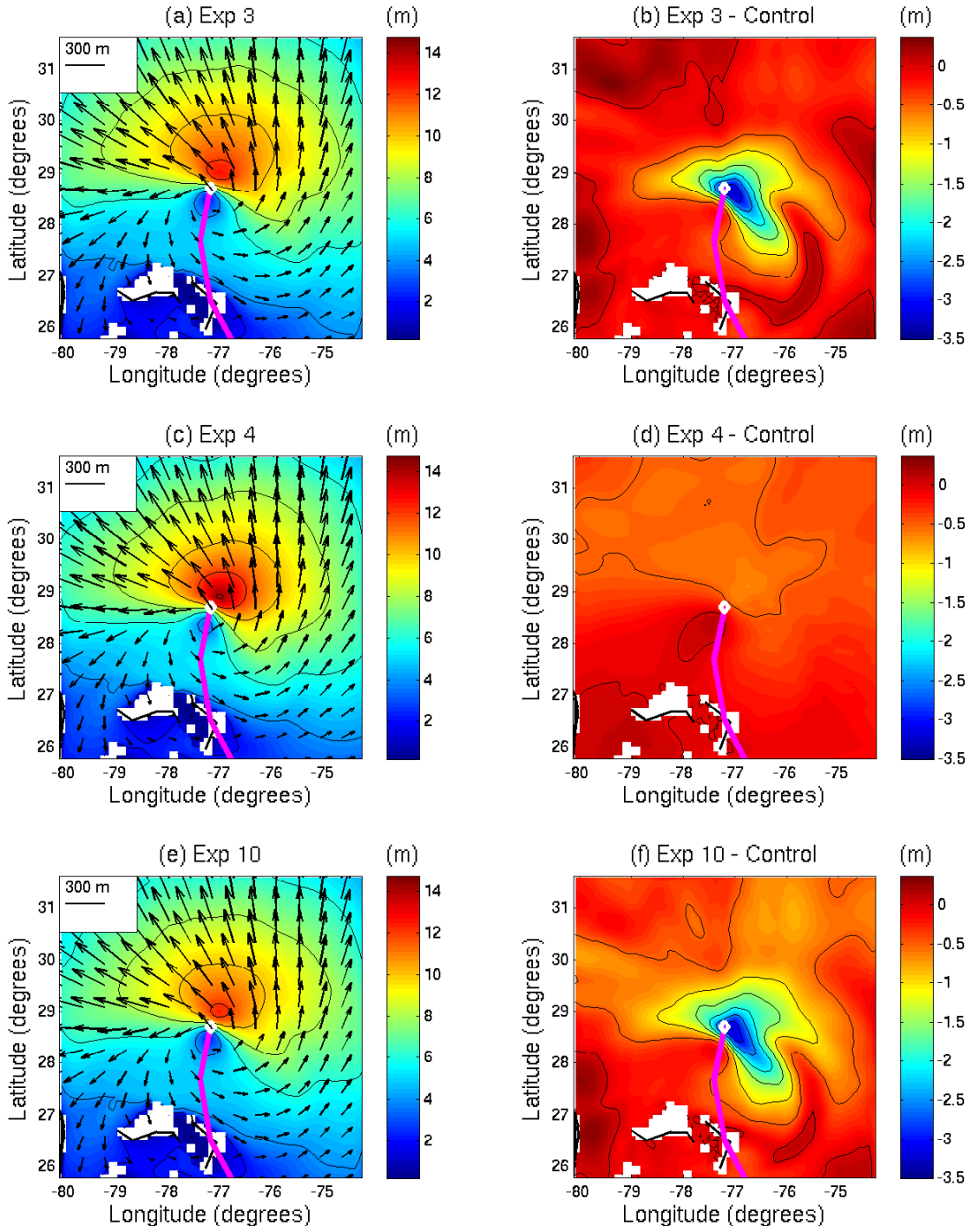

Figure 30: Significant wave height (m) (left column) and differences (m) (Current experiment - Control) (right column) for Irene: Experiment 3 (a) and (b); Experiment 4 (c) and (d); Experiment 10 (e) and (f) on August 26, 2011 at 06:00 UTC (wave contours every 2 m) and (difference contours every 0.5 m)

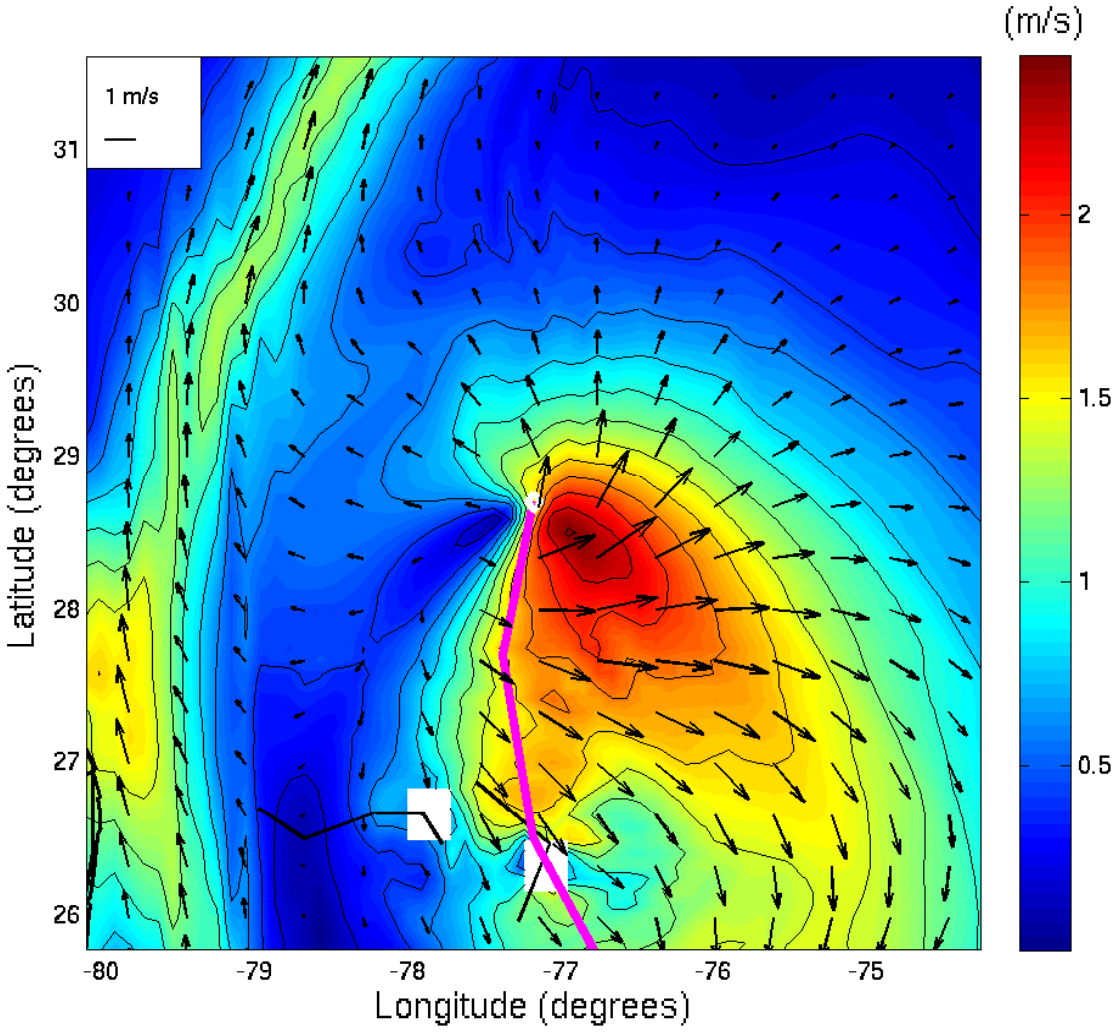

Figure 31: Control Experiment surface currents (m/s) for Irene on August 26, 2011 at 06:00 UTC (contours every 0.2 m/s)

Hurricane Irene drives ocean currents that are much stronger to the right of the storm track than to the left (Figure 31). The background Gulf Stream is clearly visible to the left of the storm track.

Surface current vectors and their differences are shown in Figure 32. Experiment 2 modifies the surface currents in the right rear quadrant (Figure 32 b), while Experiment 7 modifies them by a larger magnitude in a small region just to the right of the storm center and at several locations near the Bahamas islands behind the hurricane (Figure 32 d). Experiment 8 changes the surface currents across a

larger area to the right of the storm track (Figure 32 f). This change in the surface currents is more due to the Coriolis effect altering the direction of the currents than their magnitude. Experiment 9 and Experiment 10 have surface currents differing the most from the control experiment. Experiment 9 modifies the currents primarily in the right front quadrant of the storm (Figure 32 h). Experiment 10 has a larger region of modified currents just to the right of the eye, but also has discretized modifications behind it near the Bahamas (Figure 32 j).

Surface current magnitudes and their differences are shown in Figure 33. Experiment 2 clearly reduces the currents in the right rear quadrant (Figure 33 b), but Experiment 7 reduces them by a larger magnitude just to the right of the storm center and near the Bahamas along the storm track (Figure 33 d). It also slightly increases the current magnitude along two regions to the left of the storm track also near the Bahamas. Unique among the individual effects, Experiment 8 reduces the current magnitude in front of and to the left of the storm center (Figure 33 f). Even though Experiment 9 modifies the current vectors over a larger area than Experiment 10, it has a smaller impact on the magnitude (Figure 33 h). Experiment 10 reduces the surface current magnitude in the right rear quadrant along the storm track and in a couple of banded structures farther to the right (Figure 33 j).

Hurricane Irene has produced a clear cold wake in the right rear quadrant (Figure 34 a) coinciding with the region of largest surface currents (Figure 31). Also visible is the warm water of the Gulf Stream current to the west. This provides a clear contrast that better illustrates the effect of Irene on the SST just north of the Bahamas.

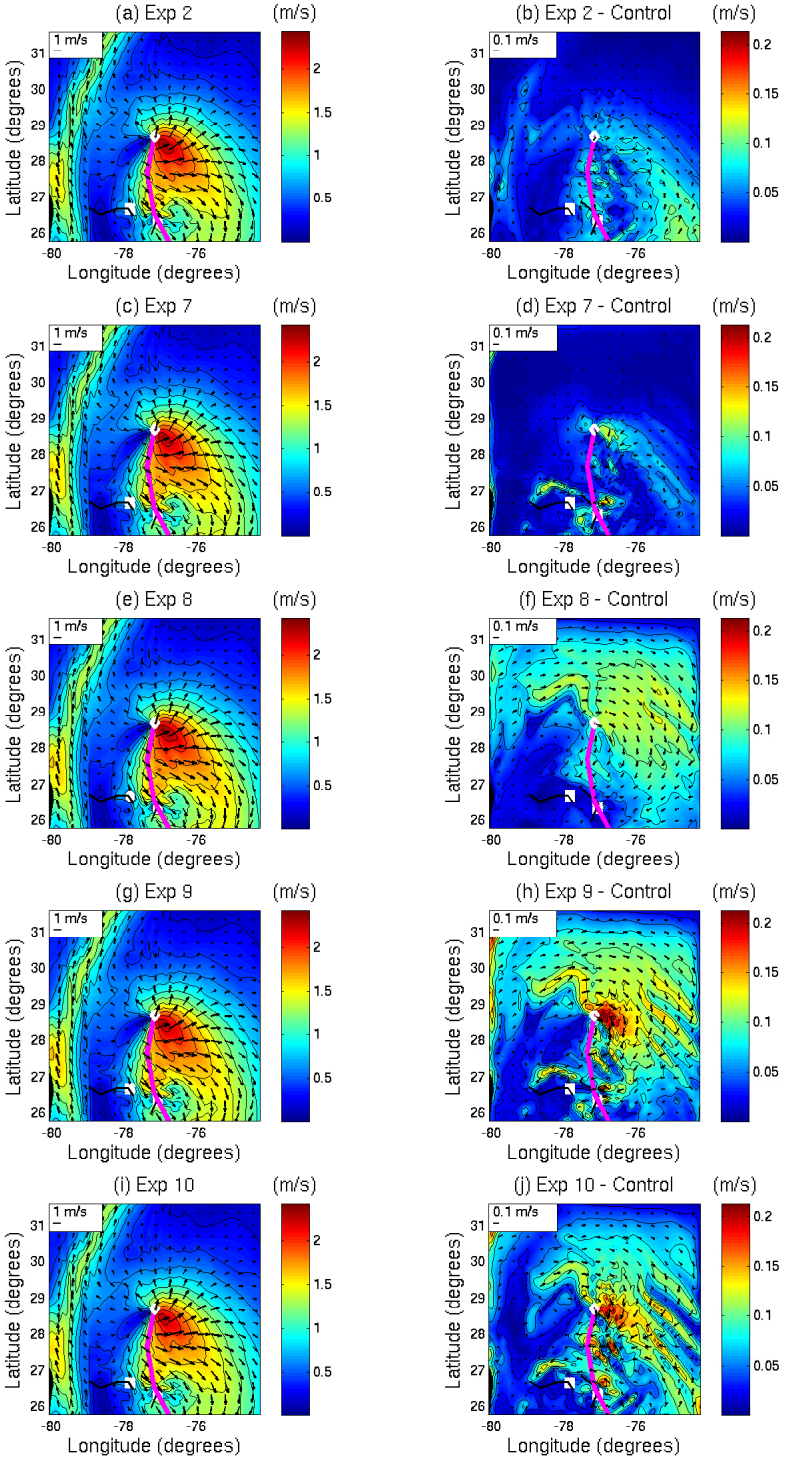

Figure 32: Surface current (left col.) and differences (Current experiment - Control) (right col.) for Irene: Experiment 2 (a) and (b); Experiment 7 (c) and (d); Experiment 8 (e) and (f); Experiment 9 (g) and (h); Experiment 10 (i) and (j) on August 26, 2011 at 06:00 UTC (contours every 0.2 m/s) and (difference contours every 0.025 m/s)

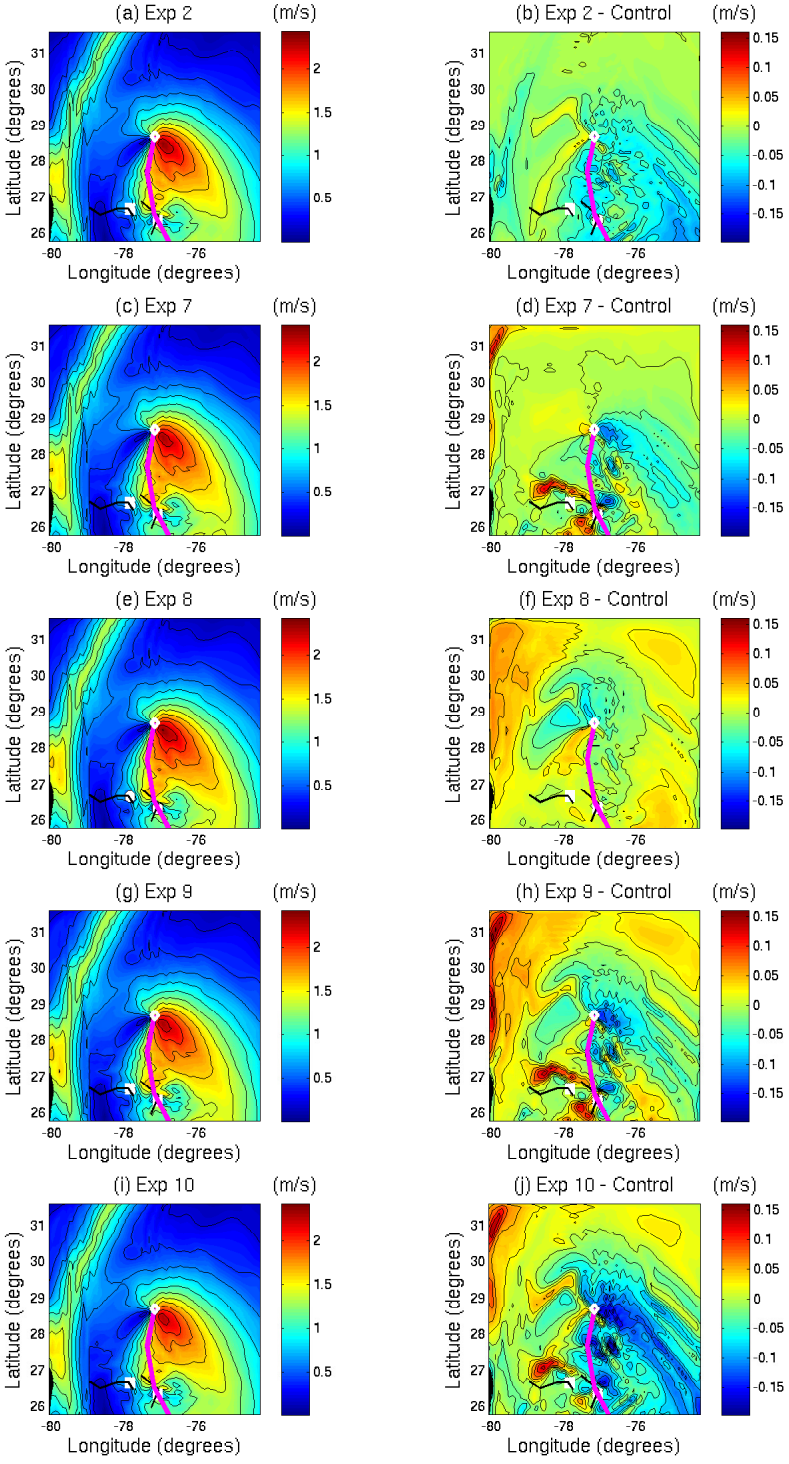

Figure 33: Surface current magnitude (left col.) and differences (Current experiment - Control) (right col.) for Irene: Experiment 2 (a) and (b); Expriment 7 (c) and (d); Experiment 8 (e) and (f); Experiment 9 (g) and (h); Experiment 10 (i) and (j) on August 26, 2011 at 06:00 UTC (contours every 0.2 m/s) and (difference contours every 0.025 m/s)

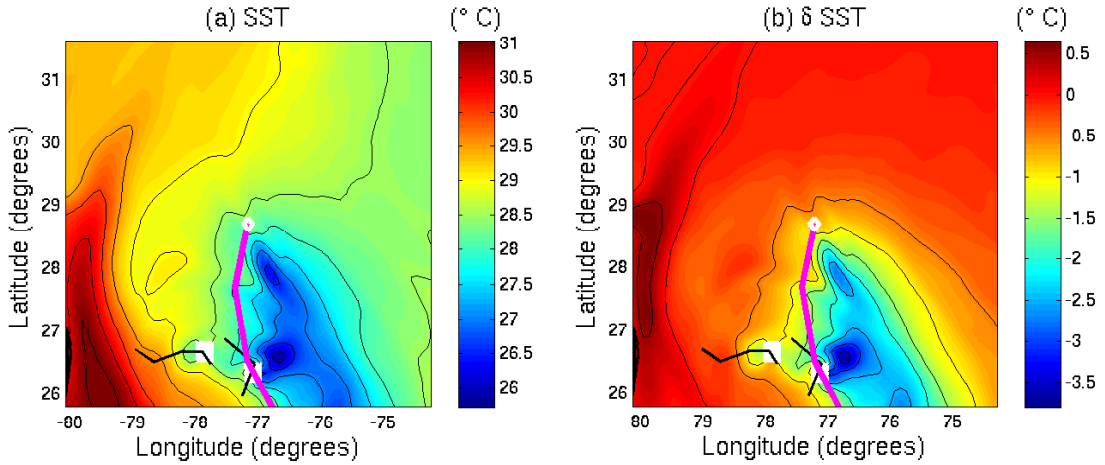

Figure 34: Control Experiment (a) SST and (b) $\delta SST = SST(output) - SST(24\ hours\ earlier)$ for Irene on August 26, 2011 at 06:00 UTC (contours every 0.5 $°C$)

The cooling is clearly reduced in Experiment 2 (Figure 35 b) and Experiment 7 (Figure 35 d). Consistent with the idealized hurricanes, both have regions where the cooling increases slightly: Experiment 2 in a small streak to the left of the storm track and just behind the storm center and Experiment 7 in several discretized regions along the storm track. Experiment 8 clearly increases the cooling to the right of the storm track (Figure 35 f), although the magnitude of this augmentation is less than similar regions in Experiment 7. This leads to an interesting dynamic of an area of increased cooling next to one with decreased cooling in Experiment 9 and the Fully Coupled Experiment 10. Experiment 9 has a large section of increased cooling along the storm track on both sides (Figure 35 h), but Experiment 10 mostly reduces the surface temperature in the right rear quadrant, with a maximum to the right and behind the storm center alongside a small patch of increased cooling (Figure 35 j).

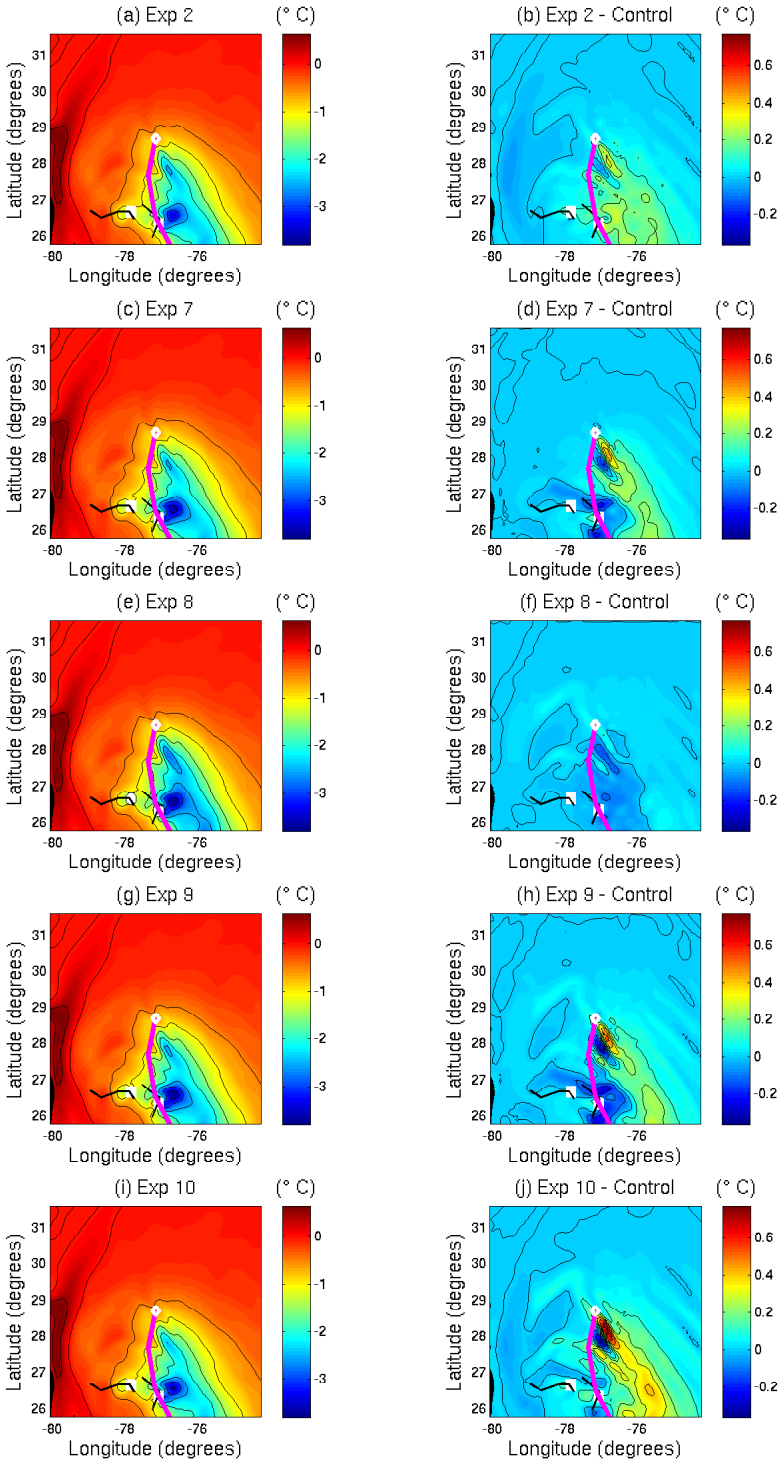

Figure 35: δSST (left column) and differences (Current Experiment - Control Experiment) (right column) for Irene: Experiment 2 (a) and (b); Experiment 7 (c) and (d); Experiment 8 (e) and (f); Experiment 9 (g) and (h); Experiment 10 (i) and (j) on August 26, 2011 at 06:00 UTC (contours every $0.5°C$) and (difference contours every $0.1°C$)

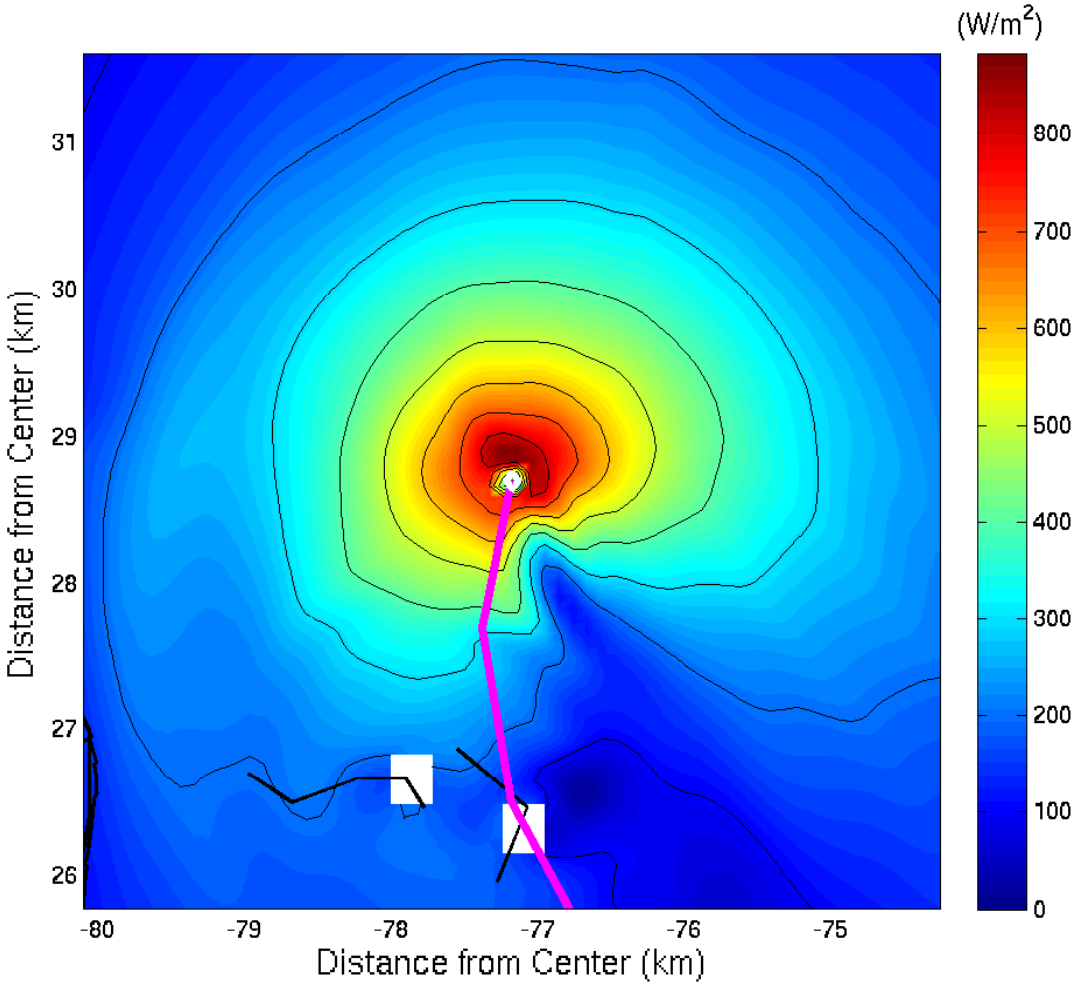

Figure 36: Control Experiment latent heat flux (contours every 100 W/m^2) for Irene on August 26, 2011 at 06:00 UTC

The Hurricane Irene latent heat flux calculations are done the same way as the idealized hurricane latent heat flux calculations in Chapter 3. The maximum estimated latent heat flux reaches about 850 W/m^2 in front of the storm (Figure 36). In the left rear quadrant of the storm over the cold wake, the flux is significantly reduced. Experiment 2 has alternating regions of increased and reduced latent heat flux into the atmosphere near the storm center (Figure 37 b). It also increases the latent heat flux in the right rear quadrant (along the cold wake) and to the left of the storm track (along the Gulf Stream). Experiment 7 also leads to alternating regions of increased and reduced latent heat flux near the storm center (Figure 37

d), but the magnitude of the increase is larger than the Experiment 2 maximum enhanced latent heat flux. The latent heat flux is reduced in Experiment 8 along the storm track and to the right, but to a smaller magnitude than Experiment 7, and the small section of increased latent heat flux is small in both geographic size and in magnitude (Figure 37 f). Experiment 9 has two neighboring regions of latent heat flux increases and reductions to the right and slightly behind the storm center with greater magnitude than Experiments 2, 7, and 8 (Figure 37 h). The latent heat flux is also reduced slightly in small localized regions along the storm track. The magnitudes of neighboring small sections of increased and reduced latent heat flux are slightly larger for Experiment 10 (Figure 37 j) than Experiment 9. Also, like Experiment 2, there is a larger section of slightly increased latent heat flux in the right rear quadrant and to the left of the storm track along the Gulf Stream.

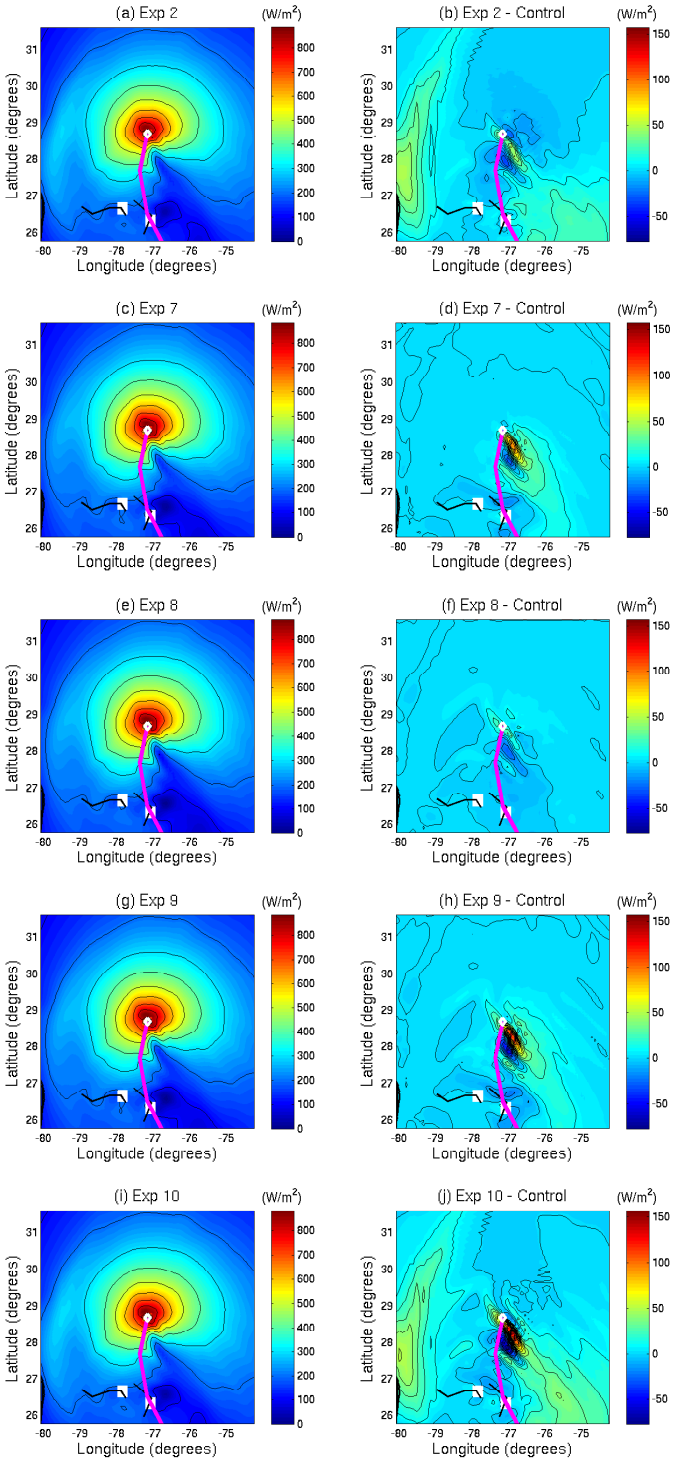

Figure 37: Latent heat flux (left column) (contours every 100 W/m^2) and differences (Current experiment - Control) (contours every 10 W/m^2): Experiment 2 (a) and (b); Experiment 7 (c) and (d); Experiment 8 (e) and (f); Experiment 9 (g) and (h); Experiment 10 (i) and (j) for Irene on August 26, 2011 at 06:00 UTC

CHAPTER 5

Hurricane Sandy (2012)

5.1 Background

Hurricane Sandy was a late season Atlantic Ocean basin Hurricane that began as a tropical wave moving off of western Africa on October 11, 2012. By 1200 UTC on October 22, it had become organized enough to be a tropical depression and reached hurricane status 48 hours later centered 80 nautical miles south of Kingston, Jamaica. It rapidly intensified after it passed over Jamaica and became a major hurricane (Category 3) with maximum sustained winds of 100 $knots$ (51.4 m/s) when it made landfall on Cuba at 0525 UTC on October 25. Hurricane Sandy weakened slightly over Cuba and then even more so afterwards as a result of a strong southwesterly wind shear. Shortwave ridging in the western Atlantic and a negatively titled upper level trough slowed Sandy and changed its trajectory from north-northeast to north-northwest towards the Bahamas. By 0000 UTC on October 27, it had weakened below hurricane strength, but the size had dramatically increased: the average radii of its tropical storm force winds were nearly double the radii of when it made landfall in Cuba as a hurricane. Sandy changed direction again to the northeast and sped up in advance of a mid-tropospheric trough over the central United States and regained hurricane status on October 27 at 1200 UTC. However, an anomalous blocking pattern over the North Atlantic prevented Sandy from moving out to sea and it strengthened again because of baroclinic forcing, a low vertical wind shear from the midtropospheric trough, and passage over warm Gulf Stream water. The trough also caused Hurricane Sandy to accelerate in a northwestern direction where it moved into a region with a cold air mass and cooler waters, thus weakening before making landfall at 2330 UTC on October 29 near Brigantine, New Jersey. Over land, Sandy slowed and turned

west-northwest, before eventually merging with a low-pressure area over eastern Canada on November 1 or 2 (Blake et al., 2013).

Hurricane Sandy was directly responsible for 147 total deaths and with 72 of those occurring in the U.S., it was the deadliest U.S. hurricane outside of southern states since Hurricane Agnes in 1972. It was also responsible for at least 87 indirect deaths. Across the entire east coast, water levels rose with the highest storm surges occurring in New Jersey, New York, and Connecticut which included setting new storm tide records in New York City. Rhode Island and Massachusetts also experienced large storm surges and even New Hampshire and Maine recorded large storm surges. Torrential rainfall affected parts of Cuba, Jamaica and Hispaniola, while Mid-Atlantic States also experienced heavy rainfall. (Blake et al., 2013)

5.2 Results

The sensitivity experiments for Hurricane Sandy were conducted using the TCVitals data in Table 4 beginning on October 24 at 1800 UTC and ending on October 30 at 0000 UTC. For most of its duration, it had a lower wind speed than either Hurricane Irene or the idealized hurricanes, but was a larger storm. We analyzed the results on October 29 at 0000 UTC (Figure 38) when the storm was located over the open ocean and away from the Gulf Stream that would skew the wave momentum flux into the ocean ($\vec{\tau}_{diff}$). Hurricane Sandy was moving northeast at 6.2 m/s at that time.

As in other experiments discussed above, the Coupled Model sensitivity experiments for Hurricane Sandy are analyzed through investigation of the significant wave height (H_s), sea surface temperature (SST), ocean surface currents ($\vec{U}_c$), and momentum flux into the ocean ($\vec{\tau}_c$). The momentum flux into the ocean for the Hurricane Sandy control experiment is equivalent to the wind stress and is demonstrably larger to the right of the storm track. It does not have a particularly large

magnitude, but the size of the storm is very large (Figure 39). Experiment 8 (Figure 40 f) changes the momentum flux into the ocean ($\vec{\tau}_c$) vectors more than either Experiment 2 or 7 (Figure 40 b and d). Finally, Experiment 9 modifies the flux into the ocean vectors over the largest area and to the greatest vector difference magnitude (Figure 40 h). Experiment 10 has an unusual section to the right of the storm track where the flux into the ocean is only slightly altered from Experiment 1 (Figure 40 j).

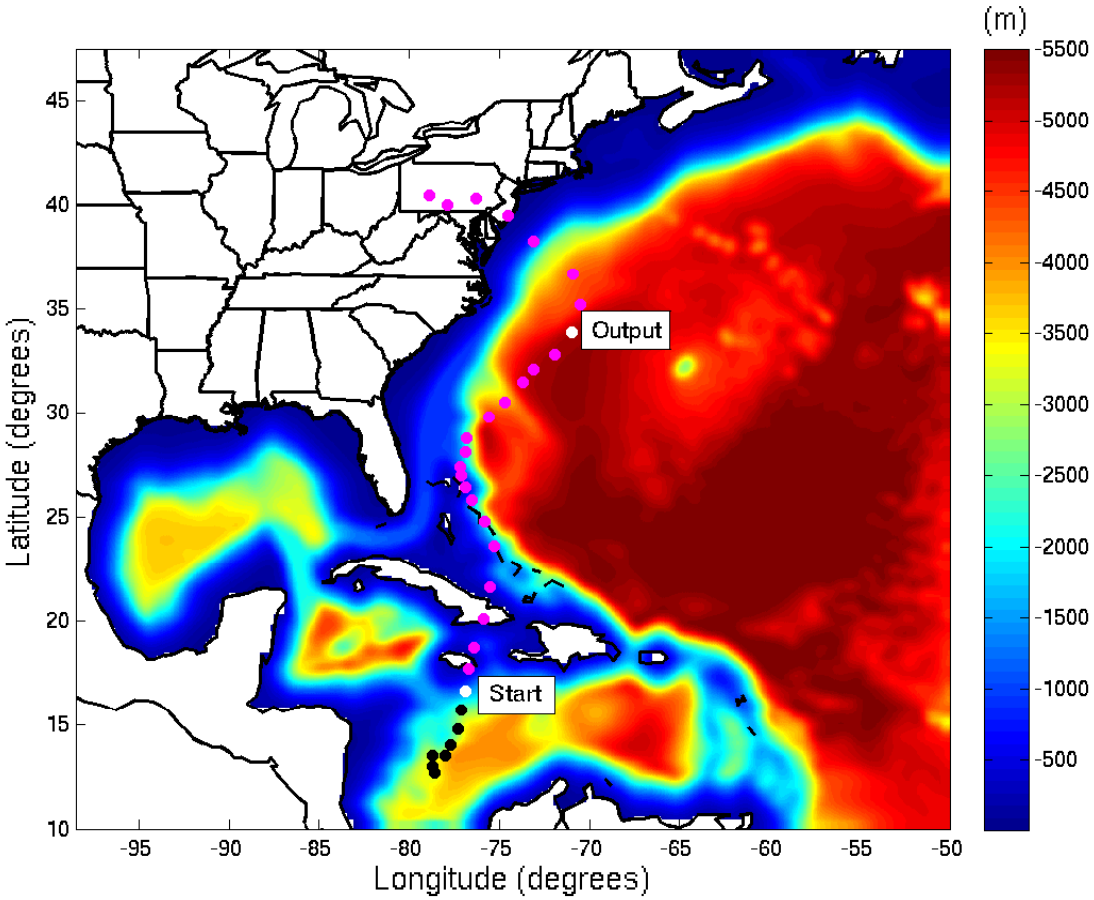

Figure 38: Storm track for Hurricane Sandy with coupled model starting on October 24, 2012 at 18:00 UTC and output 102 hours later on October 29, 2012 at 00:00 UTC on top of Atlantic Ocean bathymetry

Table 4: Best track of Hurricane Sandy, central pressure, environmental pressure, maximum wind speed, radii with wind speed of 18 m/s, 26 m/s, and the maximum in all quadrants (NE, SE, SW, and NW) of a hurricane from the message files provided by the National Hurricane Center.

Date/time	Position		Cen. pr.	Env. pr.	Max Wind speed	Radius (km)								
							18 m/s				26 m/s			
(UTC)	lat ($°N$)	lon ($°W$)	(hPa)	(hPa)	(m/s)	Max	NE	SE	SW	NW	NE	SE	SW	NW
24/1800	17.7	76.7	973	1005	36	46	204	222	130	111	93	111	74	74
25/0000	18.7	76.4	964	1005	41	28	204	222	130	111	93	111	74	74
0600	20.1	75.9	954	1005	49	19	204	222	130	111	93	111	74	74
1200	21.6	75.5	966	1005	46	37	204	222	130	111	93	111	74	74
1800	23.6	75.3	963	1005	46	37	334	334	130	334	93	93	74	56
26/0000	24.8	75.8	965	1007	44	37	334	334	130	334	130	111	74	111
0600	25.8	76.5	968	1006	39	56	445	334	148	371	167	93	93	130
1200	26.4	76.9	970	1008	36	56	445	334	167	371	185	148	111	130
1800	27.0	77.1	971	1008	33	56	445	334	167	371	185	148	111	185
27/0000	27.4	77.2	969	1008	33	111	667	334	204	500	185	148	111	222
0600	28.1	76.9	969	1008	31	130	723	371	297	519	NA	NA	130	241
1200	28.8	76.8	956	1008	33	139	723	371	352	519	NA	NA	241	241
1800	29.8	75.6	961	1006	33	139	834	500	445	519	NA	NA	278	241
28/0000	30.5	74.7	960	1006	33	167	834	500	445	519	NA	NA	278	297
0600	31.5	73.7	960	1006	33	167	834	500	500	519	NA	278	278	NA
1200	32.1	73.1	960	1006	33	167	834	556	556	500	NA	278	371	278
1800	32.8	71.9	952	1006	33	222	834	556	556	500	NA	278	371	278
29/0000	33.9	71.0	950	1004	33	222	834	667	667	500	278	278	371	278
0600	35.2	70.5	950	1004	36	185	778	612	667	500	278	278	371	278
1200	36.7	70.9	946	1004	41	204	778	612	741	500	278	278	371	278
1800	38.3	73.1	940	1004	41	204	778	686	741	371	315	278	371	278
30/0000	39.5	74.5	946	1006	36	148	778	686	556	297	278	278	278	NA

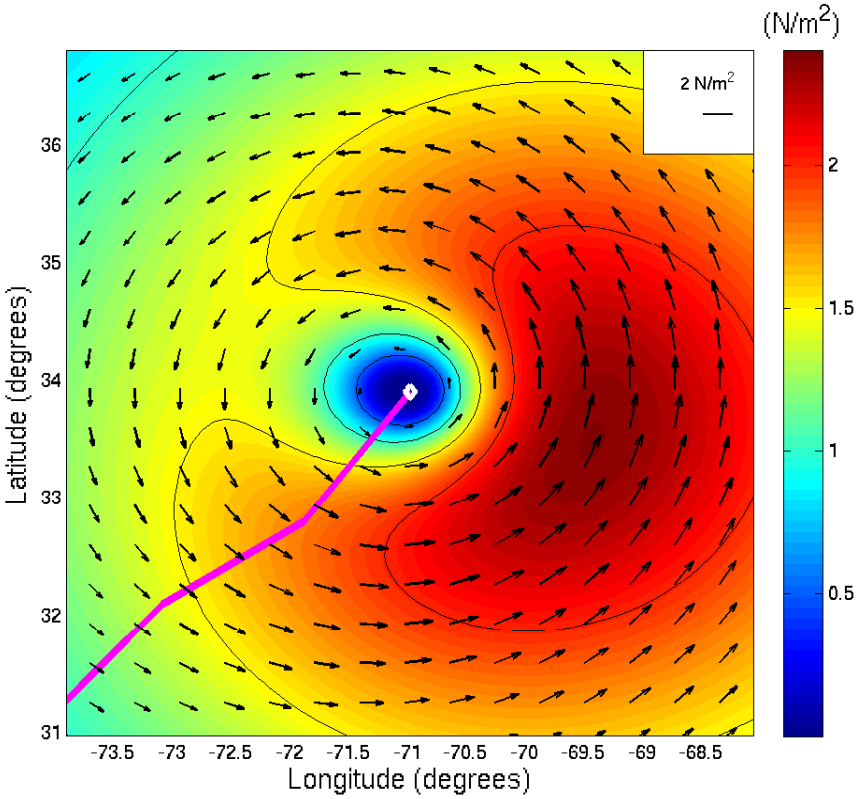

Figure 39: Control Experiment momentum flux into the ocean ($\vec{\tau_c}$) for Sandy on October 29, 2012 at 00:00 UTC (contours every 0.5 N/m^2)

Experiment 2 slightly weakens the flux into the ocean to the right of the storm center (Figure 41 b). Experiment 7 reduces the flux by a slightly larger magnitude (Figure 41 d) and over a larger area to the right of the storm center than Experiment 2. Once again, Experiment 8 slightly increases the flux into the ocean to the right of the hurricane eye, but moderately reduces it in front of the storm (Figure 41 f). The magnitude of reduction is larger for Experiment 9 than the preceding experiments. However, the reduction is mostly in the right front quadrant, while the flux increases close to and to the right of the storm center (Figure 41 h). The fully coupled Experiment 10 consistently decreases the air-sea momentum flux over the largest area and magnitude of all the sensitivity experiments. The largest reduction in magnitude is confined to the right frontal quadrant (Figure 41 j).

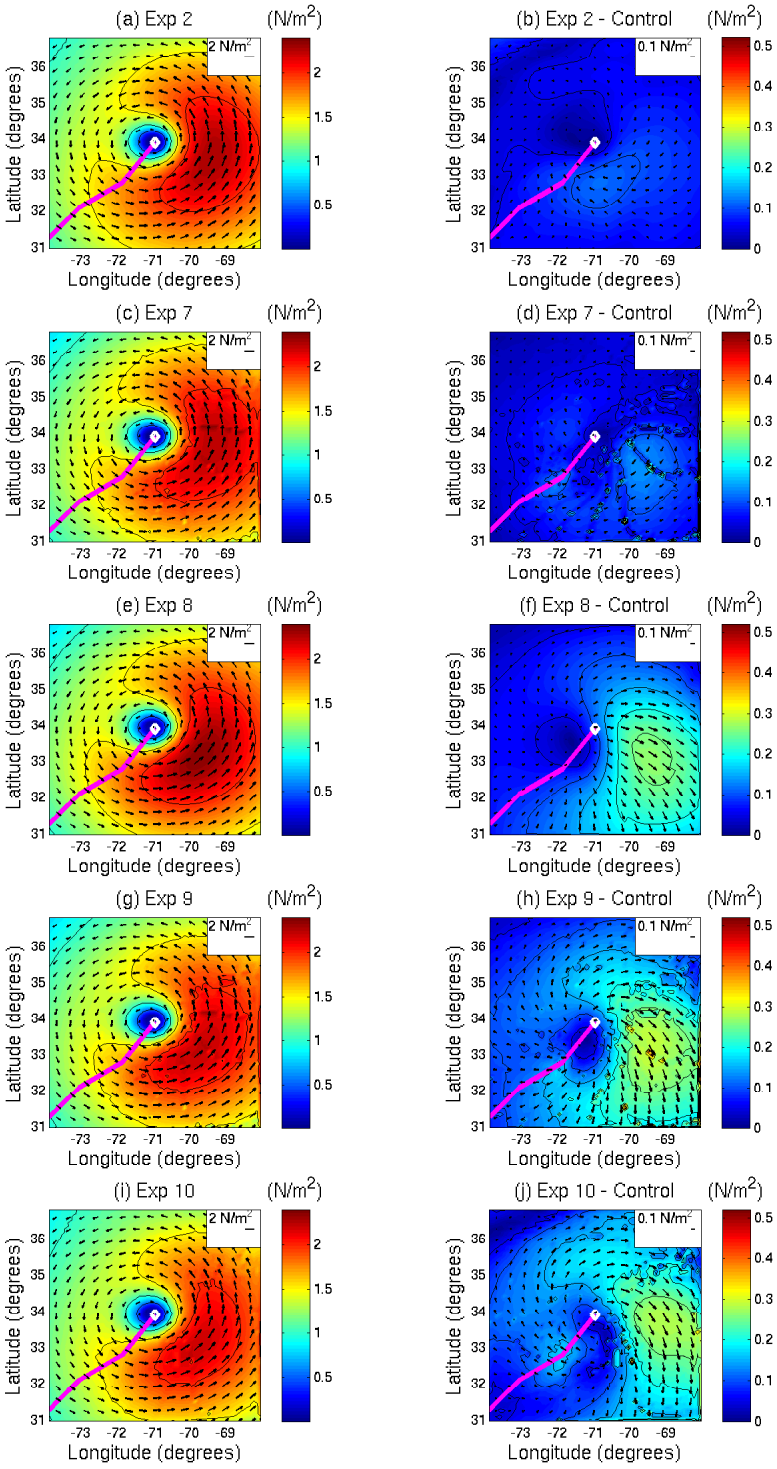

Figure 40: Momentum flux into the ocean $\vec{\tau}_c$ (left col.) and differences (Current experiment - Control) (right col.) for Sandy: Experiment 2 (a) and (b); Experiment 7 (c) and (d); Experiment 8 (e) and (f); Experiment 9 (g) and (h); Experiment 10 (i) and (j) on October 29, 2012 at 00:00 UTC (contours every 0.5 N/m^2) and (difference contours every 0.05 N/m^2)

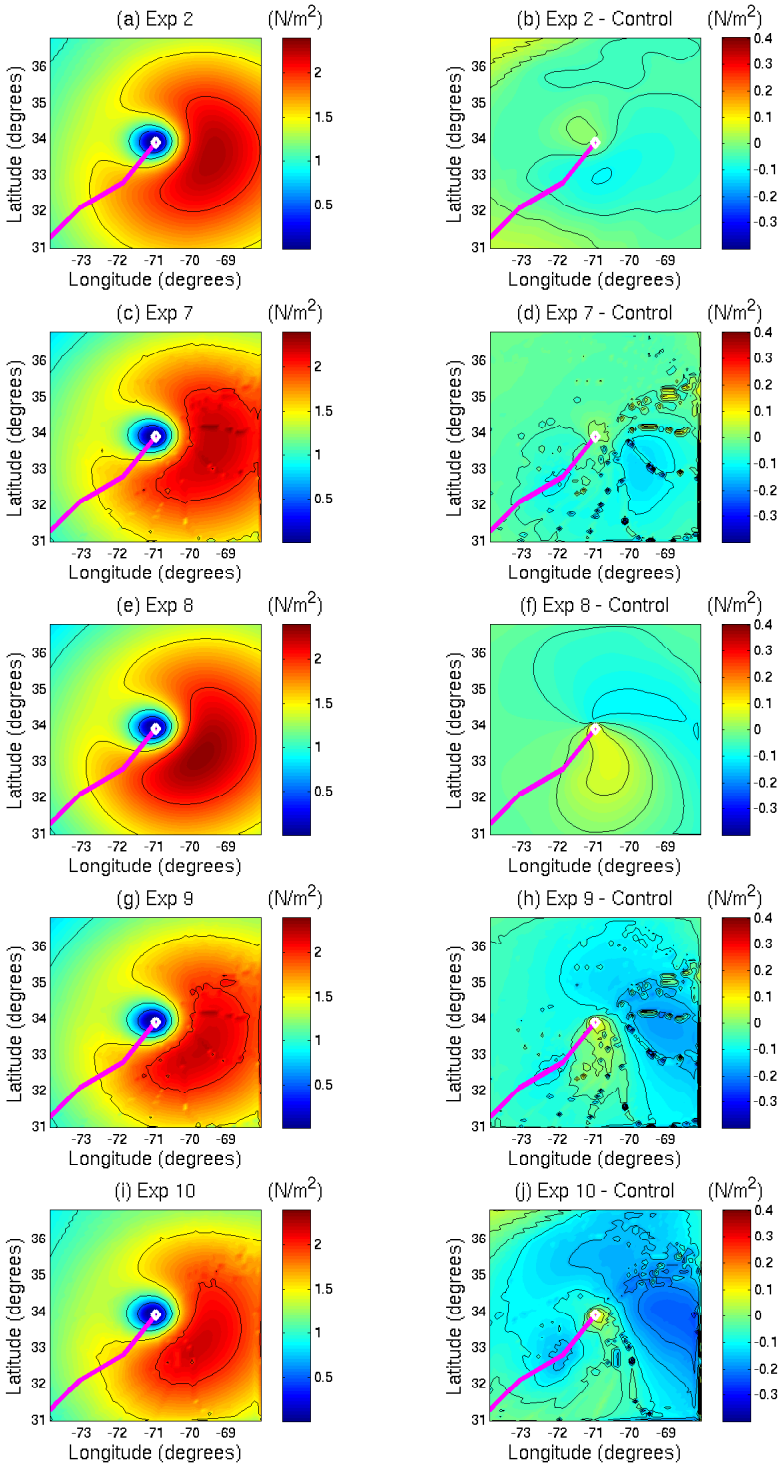

Figure 41: Momentum flux into the ocean $\vec{\tau}_c$ (left col.) and magnitude differences (Current experiment - Control) (right col.) for Sandy: Experiment 2 (a) and (b); Experiment 7 (c) and (d); Experiment 8 (e) and (f); Experiment 9 (g) and (h); Experiment 10 (i) and (j) on October 29, 2012 at 00:00 UTC (contours every 0.5 N/m^2) and (difference contours every 0.05 N/m^2)

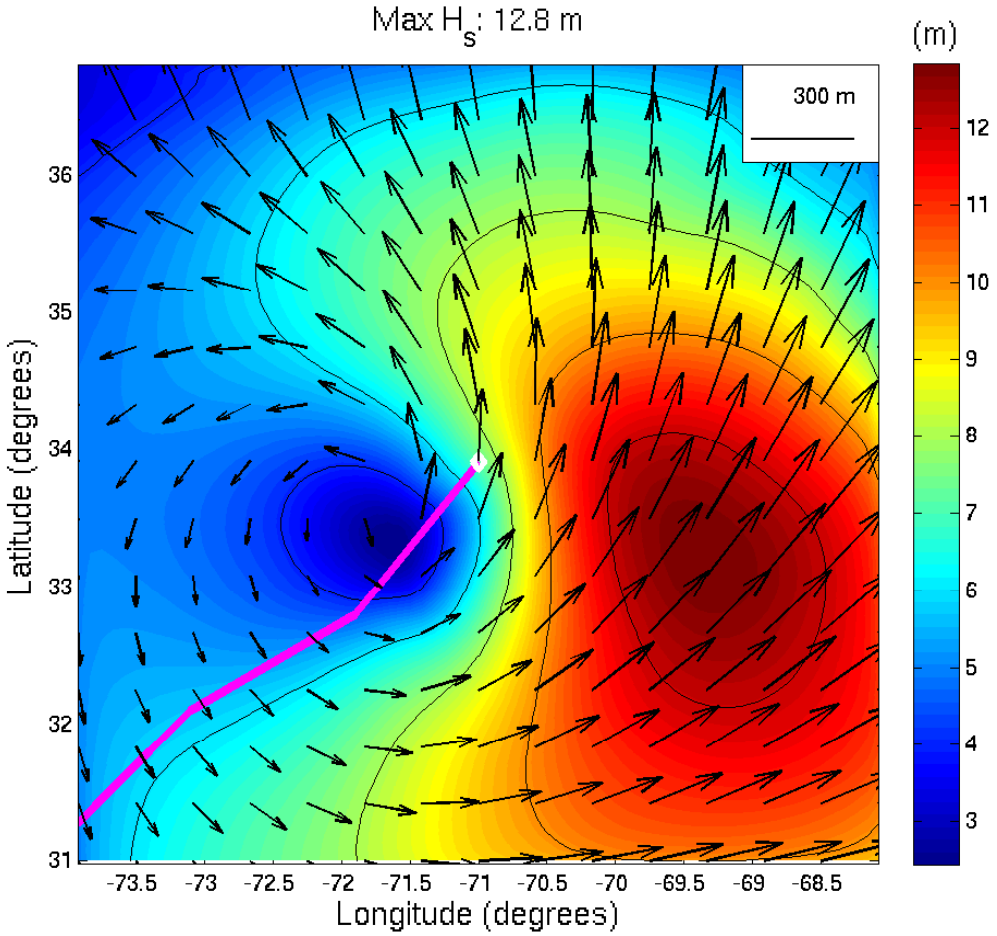

Figure 42: Control Experiment significant wave height (m) for Hurricane Sandy on October 29, 2012 at 00:00 UTC (contours every 2 m)

In response to the large size of Sandy (RMW at output time = 222 km as opposed to 19 km for Irene and 70 km for the idealized hurricanes), the geographic size of the wave field is also larger (Figure 42). Consistent with Hurricane Irene and the idealized hurricanes, the wave field only differs from the control when the currents at depth $L/(4 * \pi)$ are passed to the wave equation and/or the surface currents modify the wind forcing the wave model. Also as with previous hurricanes, Experiment 3 alters the significant wave height much more than Experiment 4 (Figure 43 b and d respectfully). As in Hurricane Irene, the maximum reduction of the significant wave height for Experiment 10 is comparable to Experiment 3.

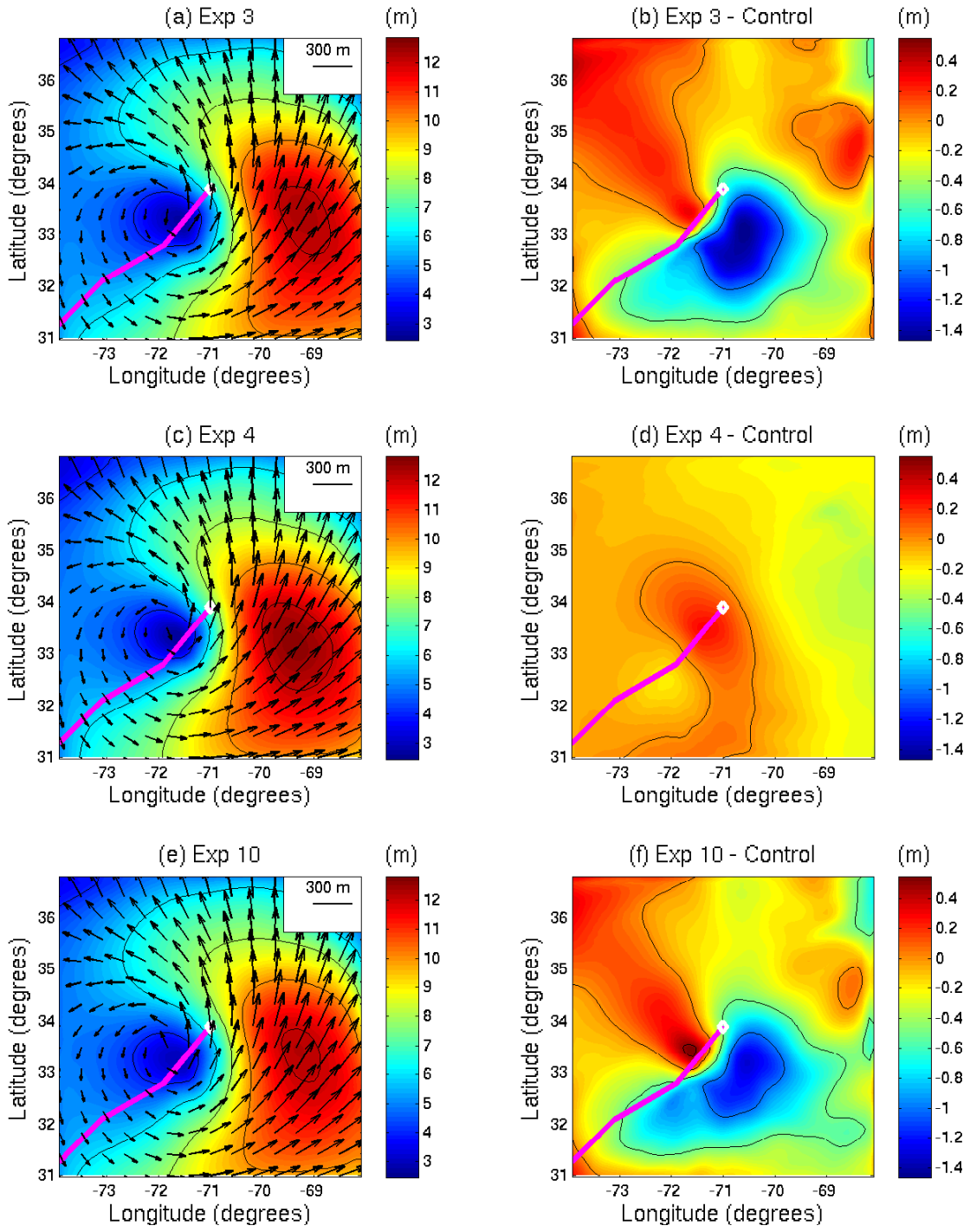

Figure 43: Significant wave height (m) (left column) and differences (m) (Current experiment - Control) (right column) for Sandy: Experiment 3 (a) and (b); Experiment 4 (c) and (d); Experiment 10 (e) and (f) on October 29, 2012 at 00:00 UTC (wave contours every 2 m) and (difference contours every 0.5 m)

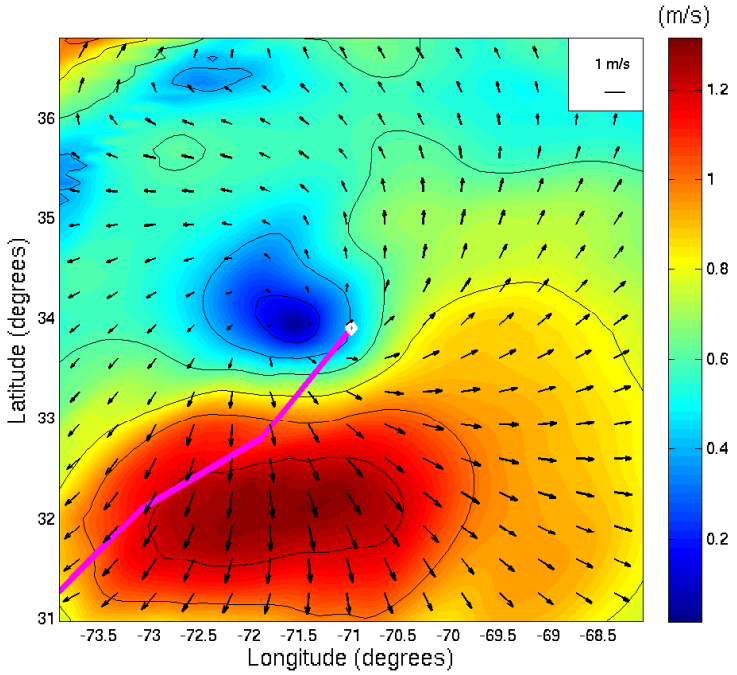

Figure 44: Control Experiment surface currents (m/s) for Sandy on October 29, 2012 at 00:00 UTC (contours every 0.2 m/s)

Consistent with Irene and the idealized hurricanes, Sandy has strong currents to the right of the storm track (Figure 44). But the magnitude of the Gulf Stream current to the northwest is comparable. Figure 45 shows the surface current vectors and their differences in different experiments and Figure 46 shows the magnitude of the surface currents and their differences in different experiments. Experiment 8 alters the surface current vectors more than either Experiment 2 or 7. However, Experiments 2 and 7 both alter the surface current magnitude more than Experiment 8 does. Experiment 2 reduces the surface current magnitude to the right of the storm track, while Experiment 7 reduces it in a region to the right of the storm track. Experiment 8 increases the surface current magnitude in two localized regions: one along the storm track, and the other well to the right of it. This leads to Experiments 9 and 10 having current magnitude differences with the Control Experiment with localized regions of increased and decreased current magnitudes (Figure 45 h and j; Figure 46 h and j).

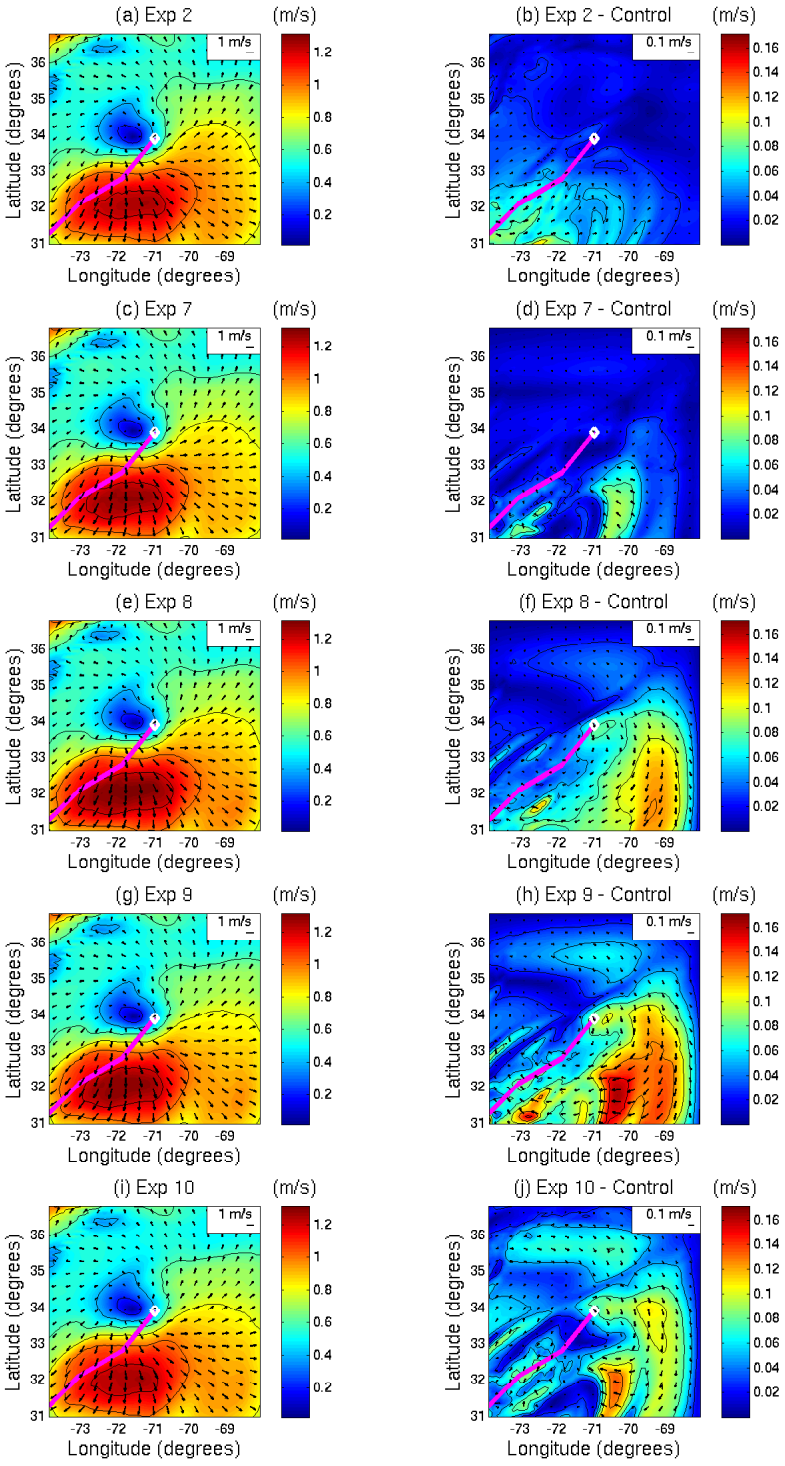

Figure 45: Surface current (left col.) and differences (Current experiment - Control) (right col.) for Sandy: Experiment 2 (a) and (b); Experiment 7 (c) and (d); Experiment 8 (e) and (f); Experiment 9 (g) and (h); Experiment 10 (i) and (j) on October 29, 2012 at 00:00 UTC (contours every 0.2 m/s) and (difference contours every 0.025 m/s)

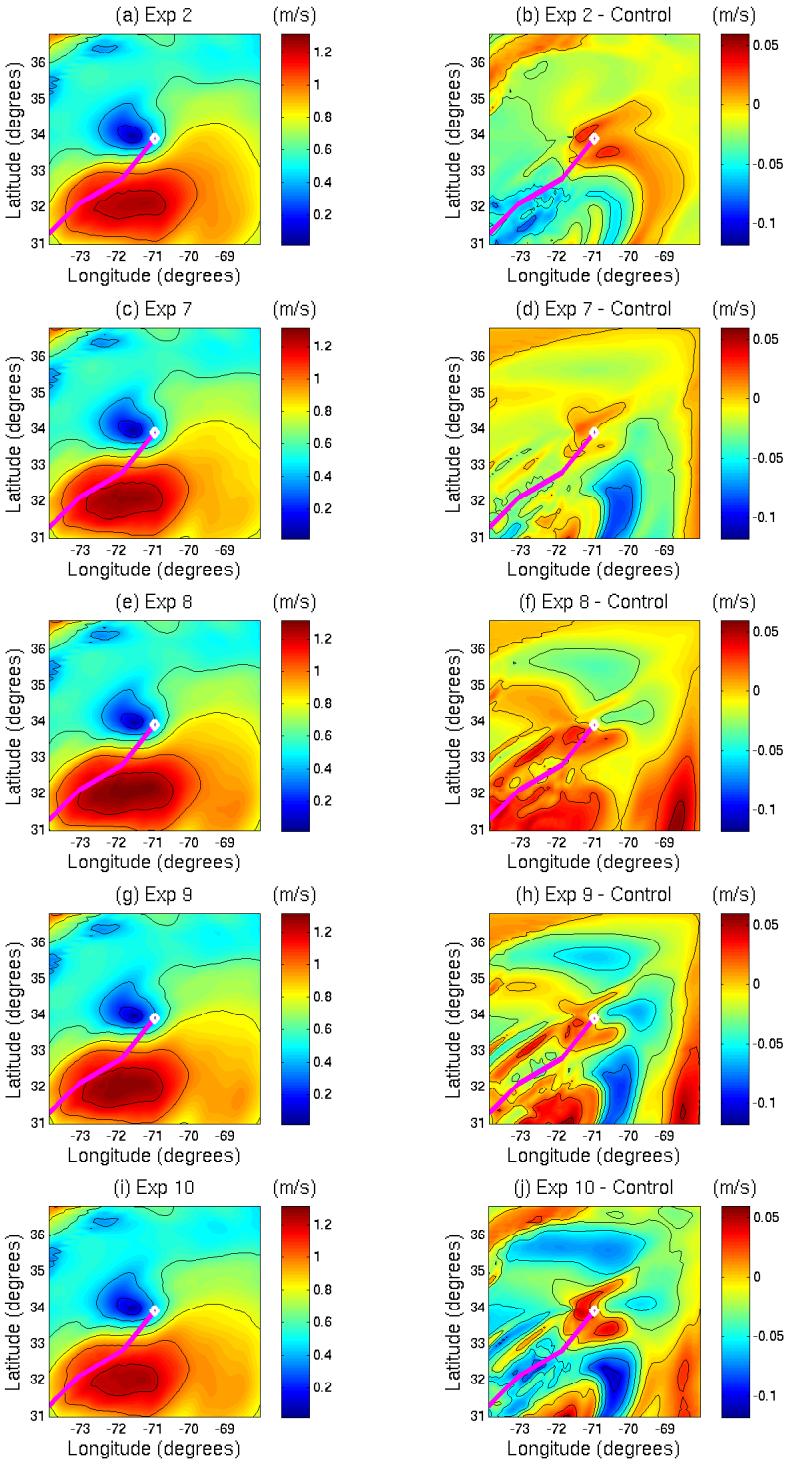

Figure 46: Surface current (left col.) and magnitude differences (Current experiment - Control) (right col.) for Sandy: Experiment 2 (a) and (b); Experiment 7 (c) and (d); Experiment 8 (e) and (f); Experiment 9 (g) and (h); Experiment 10 (i) and (j) on October 29, 2012 at 00:00 UTC (contours every 0.2 m/s) and (difference contours every 0.025 m/s)

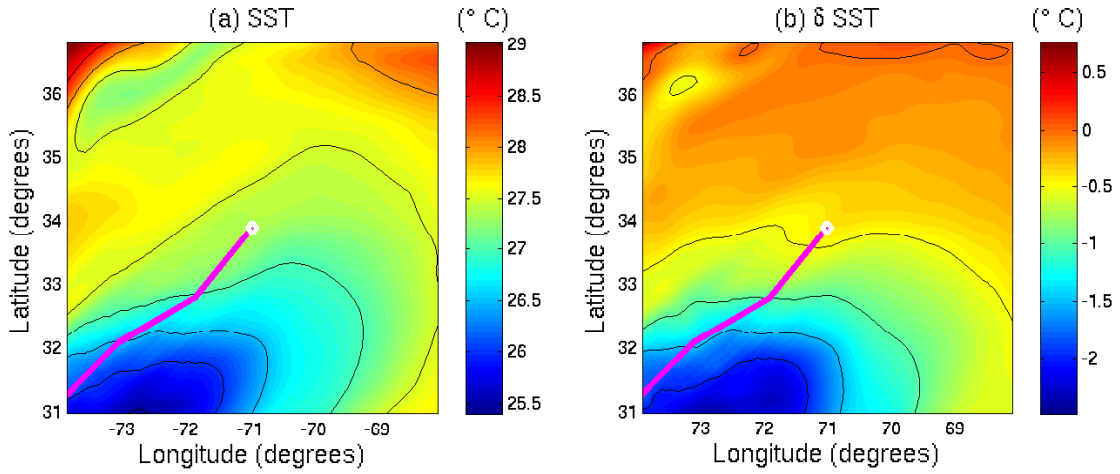

Figure 47: Control Experiment (a) SST and (b) $\delta SST = SST(output) - SST(24\ hours\ earlier)$ for Sandy on October 29, 2012 at 00:00 UTC (contours every $0.5°C$)

There is a marked cooling in the ocean surface temperature following Hurricane Sandy primarily to the right of the storm (Figure 47). The relatively short proximity of the Gulf Stream to the left of the storm did not effect this cooling.

Experiment 2 and Experiment 7 have a comparable impact on the cold wake (Figure 48 b and d respectfully). While the area over which the cooling is reduced is similar, Experiment 2 reduces it over a slightly larger area. Experiment 7 has a small region of increased cooling near the storm track. However, there is a section along the Gulf Stream where Experiment 2 actually increases the cooling (similar to the pattern seen along the Florida Current with Hurricane Irene). Experiment 8 has an uneven effect on the cooling. Along alternating streaks, it slightly increases or decreases the cooling from the control experiment. This leads to a rather complex change in cooling for Experiment 9 and for Experiment 10, but overall the cooling the largely reduced.

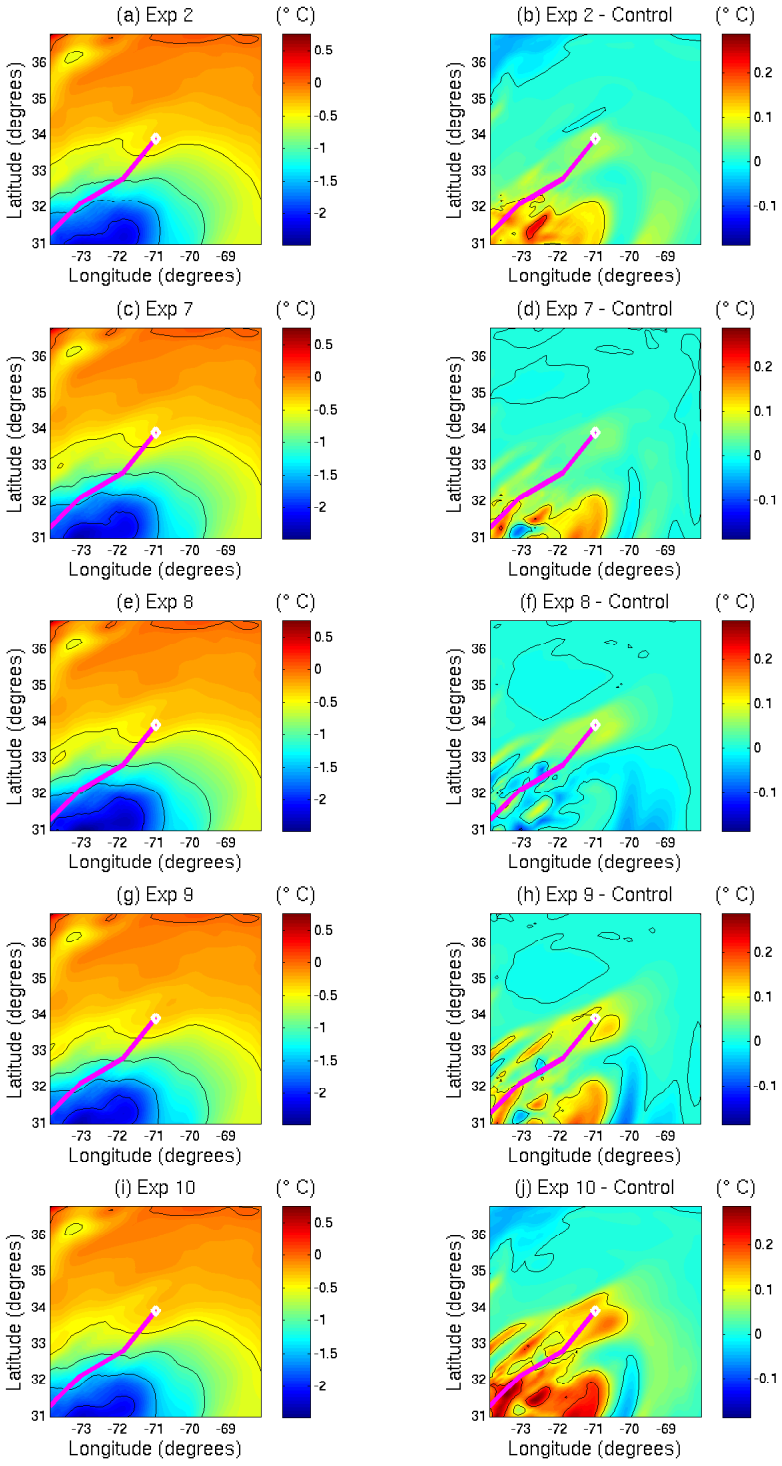

Figure 48: δSST (left column) and differences (Current Experiment - Control Experiment) (right column) for Sandy: Experiment 2 (a) and (b); Experiment 7 (c) and (d); Experiment 8 (e) and (f); Experiment 9 (g) and (h); Experiment 10 (i) and (j) on October 29, 2012 at 00:00 UTC (contours every $0.5°C$) and (difference contours every $0.1°C$)

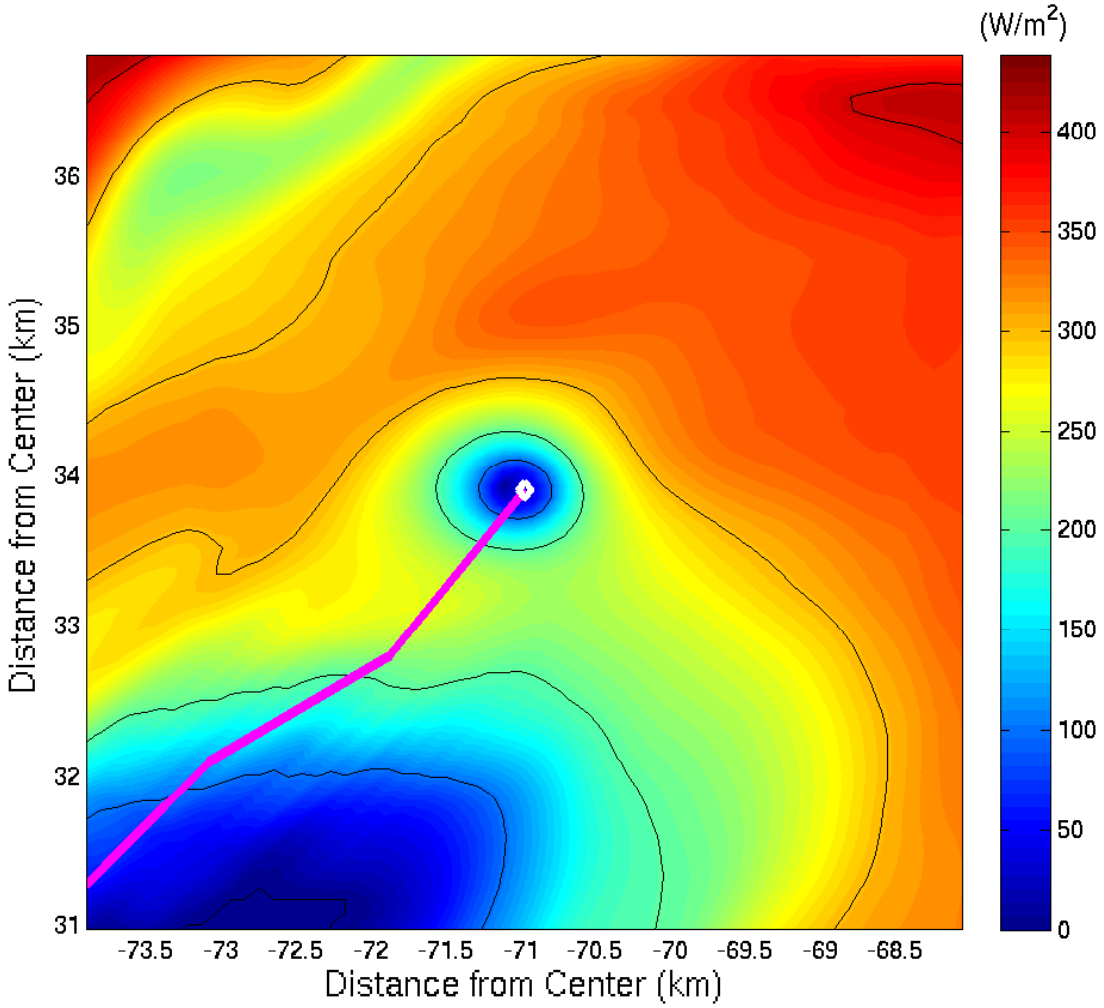

Figure 49: Control Experiment latent heat flux (contours every 100 W/m^2) for Sandy on October 29, 2012 at 00:00 UTC

The Hurricane Sandy latent heat flux calculations are done the same way as the Hurricane Irene latent heat flux calculations in Chapter 4 and the idealized hurricane latent heat flux calculations in Chapter 3. There is a large section of a significant increase of latent heat flux into the atmosphere primarily in the right frontal quadrant (Figure 49). In the left frontal quadrant, there is another small segment of the latent heat flux increase corresponding to the Gulf Stream. As with previous experiments, the latent heat flux is inhibited in the cold wake region. However, Hurricane Sandy is unique in that there is a large segment of suppressed

latent heat flux into the atmosphere around the storm center. This may be due to the larger size of Hurricane Sandy as well as the relatively low wind speed.

The latent heat flux is increased in the right rear quadrant mostly in the cold wake region, but also further to the right (Figure 50 b) in Experiment 2. This is primarily due to the reduction of cooling in the cold wake. There is also a second region of increased latent heat flux in the left frontal quadrant corresponding to the Gulf Stream. However, over most of the area in front of the storm, the latent heat flux is slightly reduced from the Control Experiment. Experiment 7 increases the latent heat flux in a similar manner to Experiment 2 (Figure 50 d). Experiment 8 reduces the latent heat flux in a larger segment in the right rear quadrant, but also in different patches along the storm track (Figure 50 f). It also slightly increases the latent heat flux near the storm center and in a few smaller regions along the storm track. This leads to Experiment 9 mostly increasing the latent heat flux by a larger magnitude than Experiment 2, 7, or 8, but with a clear section of reduced heat flux in the rear right quadrant and small patches close to the storm track (Figure 50 h). The Fully Coupled Experiment 10 increases the latent heat flux by the largest magnitude and perhaps over the largest area of all the sensitivity experiments (Figure 50 j). However, it also has sections of reduced heat flux (including the area in front of the storm center and a portion to the right of the storm track). As with Experiment 2, the Gulf Stream influence on increasing the heat flux is clear in the upper left edge of the figure.

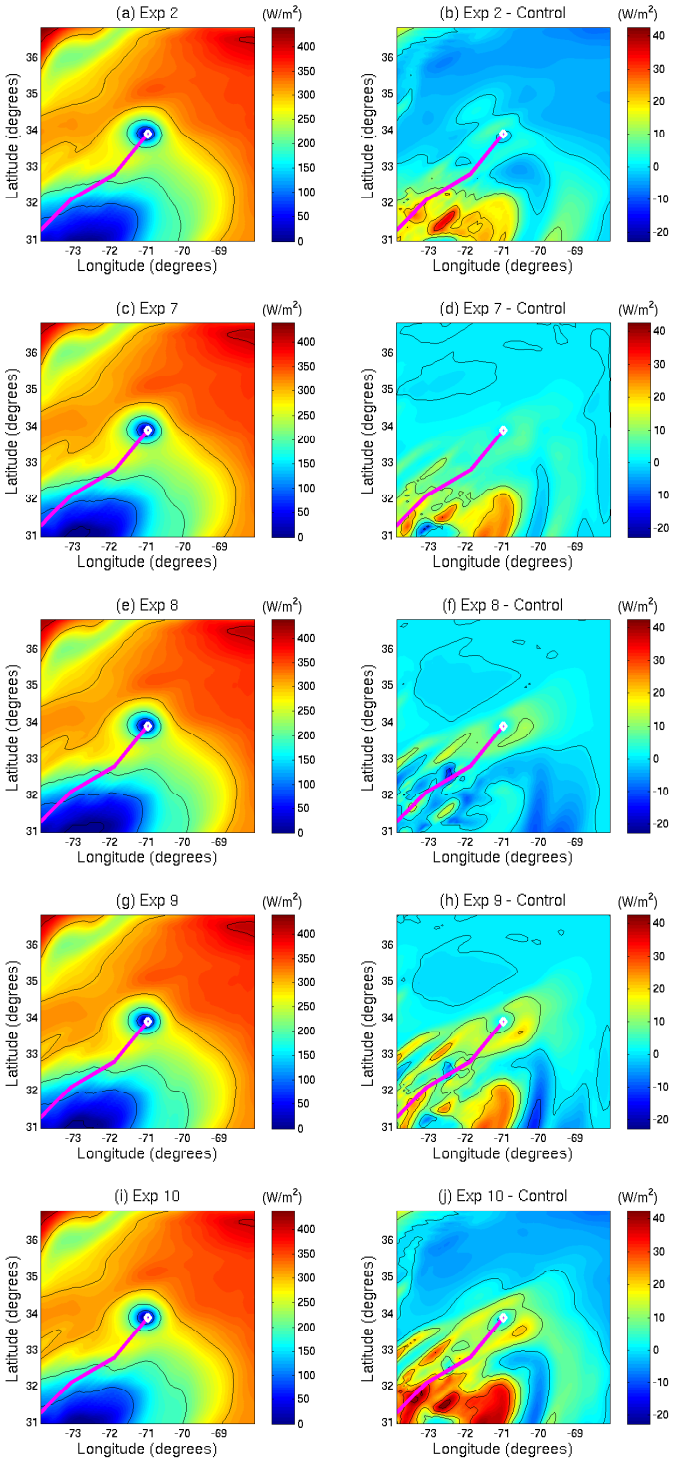

Figure 50: Latent heat flux (left column) (contours every 100 W/m^2) and differences (Current experiment - Control) (contours every 10 W/m^2): Experiment 2 (a) and (b); Experiment 7 (c) and (d); Experiment 8 (e) and (f); Experiment 9 (g) and (h); Experiment 10 (i) and (j) for Sandy on October 29, 2012 at 00:00 UTC

CHAPTER 6

Conclusions

This study sought to develop a fully coupled ocean-wave model to enhance understanding of the air-sea momentum flux budget in tropical cyclones and as a result, improve models of the cold wake. The ocean model component used is the Princeton Ocean Model (POM) with a 1/12 degree resolution and 23 half sigma levels. It calculates the ocean temperature and currents driven by a prescribed wind stress interpolated from hurricane message files generated by the National Hurricane Center. The wave model used is Wave Watch 3.14 and also has a 1/12 degree resolution. It uses a prescribed wind speed based on the same hurricane message file and calculates the momentum flux lost to or gained from a growing or decaying wave field and the momentum flux modified by Coriolis-Stokes forcing. In the coupled model, the ocean currents are used in the wave model and the wind stress calculations.

Results of idealized and real hurricane simulations demonstrate clearly that the altered wind stress (by including the ocean current effect), wave momentum flux budget, and Coriolis-Stokes forcing significantly alter the momentum flux into the ocean currents and in turn the cold wake. While the wave momentum flux budget and reduced wind stress decrease the surface cooling, the Coriolis-Stokes forcing may lead to increased surface cooling. It is also shown that these three effects can alter the latent heat flux that fuels hurricanes.

6.1 Wave Field

In the idealized and real hurricane experiments, passing the currents to the wave equation reduces the significant wave height more than subtracting the surface current in the wind forcing. There are two different effects from the currents

being passed to the wave equation: the modulation of the wavenumber and in turn the wave action due to spatial variation of the currents, and the currents adjusting the wave propagation speed. Given the relatively strong wind forcing, it is more likely that the wave packet propagation speed being adjusted by the currents is the more important effect. Since the currents are in the same direction as the wind, the waves will propagate faster, thus causing them to be in the high wind regions for a shorter period of time, reducing the wave height.

Combining the faster wave packets with reduced wind would be expected to lead to the smallest wave fields (as it did for both the idealized and real hurricanes). For the idealized experiments, the reductions in wave height are larger for the faster hurricane translation speed. The larger waves are likely a result of the higher hurricane translation speed being closer to the wave group velocity ($\vec{C}_g$), leading to the larger waves remaining under the high wind region of the hurricane for longer time. For the stationary hurricane and 4.8 m/s translating hurricane, the waves are able to "outrun" the hurricane, and thus the wind duration is shorter. Hurricane Irene and Hurricane Sandy both have translation speeds in between the 4.8 m/s and 9.6 m/s translating idealized hurricanes: 5.7 m/s and 6.2 m/s respectively. However, the translation speed and direction varies for real hurricanes along with the radius of maximum wind and maximum wind speed. Thus, comparing the significant wave height for the idealized hurricane experiments with the real hurricane experiments requires some care. Hurricane Irene has a similar maximum wind speed (MWS) to the idealized experiments and a translation speed slightly closest to the 4.8 m/s translating idealized hurricane. However, it also has a much smaller radius of maximum wind (RMW) at the output (19 km) than the idealized hurricanes. This works against the larger translation speed and slightly higher maximum wind speed. The surface currents generated by Irene are much larger

than the background currents during the output time to the right of and close to the storm track and have a similar magnitude and distribution as the moving idealized hurricanes. Hence, its wave field and difference plots are similar to the idealized experiments and closer to the 4.8 m/s hurricane.

Hurricane Sandy has a much larger radius of maximum wind (222 km) and a significantly lower maximum wind speed (33 m/s) than Irene and the idealized hurricanes, and its translation speed is slightly higher than Irene's. The increase in translation speed effects helps to counteract the weaker wind forcing on the waves. To the right of the storm track, the translation speed, wind speed, and waves are all in the same direction, so there is a resonance wind forcing there. Since the waves tend to move at a faster speed than the hurricanes, a greater translation speed will lead to the largest waves being in the high wind region for a longer period of time. However, for higher winds, there are also larger currents that further reduce the time that the large waves are in the high wind region.

6.2 Currents and Surface Cooling

The wave field is important to the momentum flux into the ocean because it affects the momentum flux lost to or gained from the wave field growing or decaying ($\vec{\tau}_{diff}$) and introduces the additional Coriolis-Stokes forcing ($\vec{\tau}_{cor}$).

Both the moving and stationary idealized hurricanes show the same general trends from adjusting the momentum flux into the ocean currents ($\vec{\tau}_c$). When the wave momentum flux ($\vec{\tau}_{diff}$) is included in the calculation of the momentum flux into the ocean ($\vec{\tau}_c$), there is an overall reduction in cooling with some small, localized regions of slightly increased cooling. But, the Coriolis-Stokes forcing alters the surface current vectors more than the modified wind stress or the wave momentum flux budget primarily by shifting the direction of the surface currents to the right as opposed to altering the magnitude. This leads to an increased

divergence of ocean surface currents, which in turn leads to cooler water near the storm track due to enhanced upwelling.

The momentum flux into the currents ($\vec{\tau}_c$) to the right of the storm track, and the currents themselves increase with the translation speed. In fact, the stationary hurricane also has the smallest magnitude reductions in the air-sea momentum flux, while the 4.8 m/s translating hurricane has the largest reductions of the idealized hurricanes. For the stationary hurricane, the largest difference between the control flux and the fully coupled flux is approximately 0.5 N/m^2. The difference is about 0.65 and 0.9 N/m^2 for the 4.8 and 9.6 m/s translating hurricanes respectfully.

As the translation speed increases, the surface cooling decreases. The change in surface temperature between the output and initial conditions for the control (δSST) is over 9°C for the stationary hurricane, nearly 6.5°C for the 4.8 m/s hurricane, and about 3.5°C for the 9.6 m/s hurricane. The maximum reductions of cooling in the fully coupled experiments are approximately 0.75, 1.25, and 0.5°C for the stationary, 4.8, and 9.6 m/s translating hurricanes respectively. This indicates that for the idealized hurricanes, reducing the duration of the wind is more important to surface cooling than the changes in the momentum flux resulting from the various sensitivity experiments.

Hurricane Irene and Hurricane Sandy show more complicated responses to changes in the momentum flux into the ocean. For both hurricanes, the modified wind stress and wave momentum flux tend to decrease the cooling to the right of the storm track. However, there are also sections of increased cooling for Experiment 7 (Wave momentum flux budget experiment) for Irene and Sandy. The increased cooling for Irene overlaps with local maximum current vector differences with the control experiment. The increased cooling for Sandy also occurs along a section of localized maximum current vector differences from the control experiment. The

modified wind stress also has some sections of increased cooling for both hurricanes, but they are due to the background Gulf Stream current. Coriolis-Stokes forcing also increases the cooling near the storm track for Hurricane Irene due to increased upwelling. But, for Hurricane Sandy, the increased cooling due to the Coriolis-Stokes forcing occurs in regions more displaced from the storm track along with two small, localized sections along the track. This is due to the large modification of the surface currents in Experiment 8 for Hurricane Sandy mostly occurring away from the storm track.

Results from the real hurricanes suggest that changing the surface currents will alter the cold wake by either changing the turbulent mixing or increasing or decreasing the surface divergence and in turn the resulting upwelling. However, the turbulent mixing process is not uniform or linear. The greatest increases and reductions in cooling do not necessarily align directly with the regions of the largest surface current alterations. This points to the importance of subsurface currents, the nonlinearity of turbulent mixing, and the effect of upwelling resulting from a divergence of surface currents. Both Irene and Sandy also show that the surface current magnitude has a greater impact on the cold wake than changes in the current direction.

Despite the differences in the Irene and Sandy simulations, general results from both are consistent with those of the idealized hurricanes. The wave momentum flux budget tends to reduce surface cooling while the Coriolis-Stokes forcing tends to slightly enhance it. Cooling usually increases slightly along the storm track, but warming in the cold wake occurs slightly farther from the storm track with the distances and patterns varying with the specific storms. A faster tropical cyclone tends to have higher winds, larger waves, and a weaker cold wake. The exact role of the ocean currents is not obvious and requires further analysis. In addition to

the surface currents, the vertical current profile and upwelling all affect turbulent mixing. For the real hurricanes, the background currents are also important.

6.3 Latent Heat Flux

The latent heat flux is the primary mechanism behind hurricane maintenance/intensification. It tends to be largest where the difference between the sea surface temperature (SST) and the air temperature is the largest. For simplicity, the air temperature is assumed to be spatially uniform in each of these experiments for both the idealized and real hurricanes. Thus, the flux is smallest in the cold wake and largest in front of the storms. Since the 4.8 m/s translating hurricane has a greater cold wake than the 9.6 m/s hurricane, it also has a more suppressed latent heat flux in the right rear quadrant. It also has less latent heat reach the atmosphere in front of the storm than the faster moving hurricane does. The modified wind stress and the wave momentum flux budget (which both reduce the cold wake) increase the latent heat flux into the atmosphere from the control, while the Coriolis-Stokes forcing (which increases the magnitude of the cold wake) reduces the latent heat flux into the atmosphere. The net impact of the two wave momentum flux components more closely resembles the wave momentum flux budget difference than the Coriolis-Stokes forcing, but does demonstrate the impact of both (more so for the 9.6 m/s hurricane). Once again, the fully coupled experiment has the largest difference from the control of all of the sensitivity experiments, proving the importance of all effects working simultaneously to in some areas increase the latent heat flux, while reducing it in others.

Since the SST is larger in front of Hurricane Irene than Hurricane Sandy, it is no surprise that the latent heat flux in front of Irene is also larger than its counterpart in Sandy. Also, the magnitudes of Irene's cold wake reductions are larger than Sandy's, explaining the greater changes in the latent heat flux.

LIST OF REFERENCES

Avila, L. and Cangialosi, J. (2011). Tropical cyclone report hurricane irene (al092011) 21-28 august 2011. Technical Report AL092011, National Hurricane Center, Miami, FL.

Bender, M., Ginis, I., Tuleya, R., and Marchok, T. (2007). The operational gfdl coupled hurricane-ocean prediction system and a summary of its performance. *Monthly Weather Review*, 135:3965–3989.

Blake, E., Kimberlain, T., Berg, R., Cangialosi, J., and II, J. B. (2013). Tropical cyclone report hurricane sandy (al182012) 22 29 october 2012. Technical Report AL182012, National Hurricane Center, Miami, FL.

Cione, J. and Uhlhorn, E. W. (2003). Sea surface temperature variability in hurricanes: Implications with respect to intensity change. *Monthly Weather Review*, 131:1783–1796.

Fan, Y., Ginis, I., and Hara, T. (2009). The effect of wind-wave-current interaction on air-sea momentum fluxes and ocean response in hurricanes. *Journal of Physical Oceanography*, 39(4):1019–1034.

Fan, Y., Ginis, I., and Hara, T. (2010). Momentum flux budget across the air-sea interface under uniform and tropical cyclone winds. *Journal of Physical Oceanography*, 40(10):2221–2242.

Ginis, I. and Dikinov, K. Z. (1989). Modeling of the typhoon virginia (1978) forcing on the ocean. *Soviet Meteorology and Hydrology*, 7:53–60.

Hasselmann, K. (1970). Wave-driven inertial oscillations. *Geophysical Fluid Dynamics*, 1:463–502.

Holland, G. (1980). An analytic model of the wind and pressure profiles in hurricanes. *Monthly Weather Review*, 108:1212–1218.

Jacob, S. D., Shay, L. K., Mariano, A. J., and Black, P. G. (2000). The 3d oceanic mixed layer response to hurricane gilbert. *Journal of Physical Oceanography*, 30:1407–1429.

Kurihara, Y., Tuleya, R. E., and Bender, M. A. (1998). The gfdl hurricane prediction system and its performance in the 1995 hurricane season. *Monthly Weather Review*, 126:1306–1322.

Mellor, G. (2004). *Users Guide for A Three-Dimensional, Primitive Equation, Numerical Ocean Model (June 2004 Version)*. Princeton, New Jersey, United States of America.

Moon, I., Ginis, I., Hara, T., Tolman, H., Wright, C., and Walsh, E. (2003). Numerical simulation of sea surface directional wave spectra under hurricane wind forcing. *Journal of Physical Oceanography*, 33:1680–1706.

Morey, S. L., Bourassa, M. A., Dukhovskoy, D. S., and O'Brien, J. J. (2006). Modeling studies of the upper ocean response to a tropical cyclone. *Ocean Dynamics*, 56:594–606.

Phillips, O. M. (1977). *Dynamics of the Upper Ocean*. Cambridge University Press, Princeton, New Jersey, United States of America.

Pollard, R. T. (1970). Surface waves with rotation: An exact solution. *Journal of Geophysical Research*, 75:5895–5898.

Polton, J. A., Lewis, D. M., and Belcher, S. E. (2005). The role of wave-induced coriolis-stokes forcing on the wind-driven mixed layer. *Journal of Physical Oceanography*, 35:444–457.

Price, J. F. (1981). Upper ocean response to a hurricane. *Journal of Physical Oceanography*, 35:153–175.

Tallapragada, V., Bernardet, L., Gopalakrishnan, S., Liu, Q., Kwon, Y., Marchok, T., Sheinin, D., Tong, M., Trahan, S., Tuleya, R., Yablonsky, R., and Zhang, X. (2013). *Hurricane Weather Research and Forecasting (HWRF) Model: 2013 Scientific Documentation*.

Tolman, H. (2009). *User manual and system documentation of WAVEWATCH III version 3.14*. Camp Springs, Maryland, United States of America.

Wright, C. W., Walsh, E. J., Vandemark, D., Krabill, W. B., Garcia, A. W., Houston, S. H., Powell, M. D., Black, P. G., and Marks, F. D. (2001). Hurricane directional wave spectrum spatial variation in the open ocean. *Journal of Physical Oceanography*, 31:2472–2488.

Yablonsky, R. M. and Ginis, I. (2009). Limitation of one-dimensional ocean models for coupled hurricane-ocean model forecasts. *Monthly Weather Review*, 137:4410–4419.

Young, I. R. (1988). Parametric hurricane wave prediction model. *Journal of Waterway, Port, Coastal, and Ocean Engineering*, 114:637–652.

Young, I. R. (2003). A review of the sea state generated by hurricanes. *Marine Structures*, 16:201–218.

Young, I. R. and Burchell, G. P. (1996). Hurricane generated waves as observed by satellite. *Ocean Engineering*, 23:761–776.

BIBLIOGRAPHY

Avila, L. and Cangialosi, J., "Tropical cyclone report hurricane irene (al092011) 21-28 august 2011," National Hurricane Center, Miami, FL, Tech. Rep. AL092011, Dec. 2011.

Bender, M., Ginis, I., Tuleya, R., and Marchok, T., "The operational gfdl coupled hurricane-ocean prediction system and a summary of its performance," *Monthly Weather Review*, vol. 135, pp. 3965–3989, 2007.

Blake, E., Kimberlain, T., Berg, R., Cangialosi, J., and II, J. B., "Tropical cyclone report hurricane sandy (al182012) 22 29 october 2012," National Hurricane Center, Miami, FL, Tech. Rep. AL182012, Feb. 2013.

Cione, J. and Uhlhorn, E. W., "Sea surface temperature variability in hurricanes: Implications with respect to intensity change," *Monthly Weather Review*, vol. 131, pp. 1783–1796, 2003.

Fan, Y., Ginis, I., and Hara, T., "The effect of wind-wave-current interaction on air-sea momentum fluxes and ocean response in hurricanes," *Journal of Physical Oceanography*, vol. 39, no. 4, pp. 1019–1034, 2009.

Fan, Y., Ginis, I., and Hara, T., "Momentum flux budget across the air-sea interface under uniform and tropical cyclone winds," *Journal of Physical Oceanography*, vol. 40, no. 10, pp. 2221–2242, 2010.

Ginis, I. and Dikinov, K. Z., "Modeling of the typhoon virginia (1978) forcing on the ocean," *Soviet Meteorology and Hydrology*, vol. 7, pp. 53–60, 1989.

Hasselmann, K., "Wave-driven inertial oscillations," *Geophysical Fluid Dynamics*, vol. 1, pp. 463–502, 1970.

Holland, G., "An analytic model of the wind and pressure profiles in hurricanes," *Monthly Weather Review*, vol. 108, pp. 1212–1218, 1980.

Jacob, S. D., Shay, L. K., Mariano, A. J., and Black, P. G., "The 3d oceanic mixed layer response to hurricane gilbert," *Journal of Physical Oceanography*, vol. 30, pp. 1407–1429, 2000.

Kurihara, Y., Tuleya, R. E., and Bender, M. A., "The gfdl hurricane prediction system and its performance in the 1995 hurricane season," *Monthly Weather Review*, vol. 126, pp. 1306–1322, 1998.

Mellor, G., *Users Guide for A Three-Dimensional, Primitive Equation, Numerical Ocean Model (June 2004 Version)*, Princeton, New Jersey, United States of America, June 2004.

Moon, I., Ginis, I., Hara, T., Tolman, H., Wright, C., and Walsh, E., "Numerical simulation of sea surface directional wave spectra under hurricane wind forcing," *Journal of Physical Oceanography*, vol. 33, pp. 1680–1706, 2003.

Morey, S. L., Bourassa, M. A., Dukhovskoy, D. S., and O'Brien, J. J., "Modeling studies of the upper ocean response to a tropical cyclone," *Ocean Dynamics*, vol. 56, pp. 594–606, 2006.

Phillips, O. M., *Dynamics of the Upper Ocean*. Princeton, New Jersey, United States of America: Cambridge University Press, 1977.

Pollard, R. T., "Surface waves with rotation: An exact solution," *Journal of Geophysical Research*, vol. 75, pp. 5895–5898, 1970.

Polton, J. A., Lewis, D. M., and Belcher, S. E., "The role of wave-induced coriolis-stokes forcing on the wind-driven mixed layer," *Journal of Physical Oceanography*, vol. 35, pp. 444–457, 2005.

Price, J. F., "Upper ocean response to a hurricane," *Journal of Physical Oceanography*, vol. 35, pp. 153–175, 1981.

Tallapragada, V., Bernardet, L., Gopalakrishnan, S., Liu, Q., Kwon, Y., Marchok, T., Sheinin, D., Tong, M., Trahan, S., Tuleya, R., Yablonsky, R., and Zhang, X., *Hurricane Weather Research and Forecasting (HWRF) Model: 2013 Scientific Documentation*, Aug. 2013.

Tolman, H., *User manual and system documentation of WAVEWATCH III version 3.14*, Camp Springs, Maryland, United States of America, May 2009.

Wright, C. W., Walsh, E. J., Vandemark, D., Krabill, W. B., Garcia, A. W., Houston, S. H., Powell, M. D., Black, P. G., and Marks, F. D., "Hurricane directional wave spectrum spatial variation in the open ocean," *Journal of Physical Oceanography*, vol. 31, pp. 2472–2488, 2001.

Yablonsky, R. M. and Ginis, I., "Limitation of one-dimensional ocean models for coupled hurricane-ocean model forecasts," *Monthly Weather Review*, vol. 137, pp. 4410–4419, 2009.

Young, I. R., "Parametric hurricane wave prediction model," *Journal of Waterway, Port, Coastal, and Ocean Engineering*, vol. 114, pp. 637–652, 1988.

Young, I. R., "A review of the sea state generated by hurricanes," *Marine Structures*, vol. 16, pp. 201–218, 2003.

Young, I. R. and Burchell, G. P., "Hurricane generated waves as observed by satellite," *Ocean Engineering*, vol. 23, pp. 761–776, 1996.